4

RESULTS AND DISCUSSION

The present study titled **"Investigation of Biomass Derived Functional Carbon Electrodes from leaves of *Spathodea campanulata* and *Tecoma capensis* for Supercapacitors Applications,"** addresses the potential of using biomass precursors as sustainable sources for carbon-based electrodes. The study is structured into three phases, focusing on synthesis, physiochemical characterization, and electrochemical evaluation of the derived carbon materials.

4.1: Phase I: Synthesis of carbon materials (SPL/TCL) and nitrogen doped carbon from *Spathodea campanulata* and *Tecoma capensis* (SN/TN) Leaves

4.1.1 Biomass carbon from plant leaves precursors *Spathodea campanulata* (SPL) and *Tecoma capensis* (TCL)

4.1.2 N-doped carbon from synthesised biomass carbon – SN/TN

SPL 700
SPL 800
SPL 900
TCL 700
TCL 800
TCL 900

Biomass carbon

SN 700
SN 800
SN 900
TN 700
TN 800
TN 900

N-doped carbon

4.2: Phase II: Physiochemical and Morphological characterization of synthesized carbon materials-SPL/TCL/SN/TN

The synthesized carbon materials are characterized using the following techniques:

4.2.1 Fourier-Transform Infrared Spectroscopy (FT-IR)

4.2.2 X-ray Diffraction (XRD)

4.2.3 Raman Spectroscopy

4.2.4 Field Emission Scanning Electron Microscopy (FE-SEM)

4.2.5 Energy-Dispersive X-ray Spectroscopy (EDAX)

4.2.6 Transmission Electron Microscope (TEM)

4.2.7 Braeuer–Emmett–Teller (BET)

4.3: Phase III: Electrochemical characterization of SPL/TCL/SN/TN derived carbon materials for utilization of synthesized carbon materials in supercapacitor electrode applications

Electrochemical behaviour of the synthesized carbon electrode materials are performed using the following techniques:

4.3.1 Cyclic Voltammetry (CV)

4.3.2 Galvanostatic Charge and Discharge (GCD)

4.3.3 Electrochemical Impedance Spectroscopy (EIS)

4.1: Phase I

Synthesis of carbon materials (SPL/TCL) and nitrogen doped carbon from *Spathodea campanulata* and *Tecoma capensis* (SN/TN) Leaves

The carbon materials are prepared from selected waste biomass *Spathodea campanulata* (SPL) and *Tecoma capensis* (TCL) leaves through a carbonization process without any external activation.

Characterization of Raw powdered *Spathodea campanulata* (SPL) and *Tecoma capensis* (TCL) leaves

4.1.1.1. Phytochemical screening Analysis of SPL/TCL

A phytochemical screening analysis (Table 4.1) was used for identification of active phytochemical constituents present in leaves extracts of SPL and TCL. Preliminary phytochemical analysis for alkaloids, flavonoids, phenols, reducing sugar, saponins, steroids, tannins, terpenoids and Quinones were examined by standard procedures **(Harborne, 1998)**.

The results from Table 4.1 indicate the presence of nitrogen and oxygen rich compounds like flavonoids, alkaloids, saponins, steroids in the ethanolic extract of SPL and TCL **(Indurthy Kavya *et al.*, 2015, Nandha Kumar *et al.*, 2015**). The phytoconstituents present in the extract may be responsible for the intrinsic activation of the samples, leading to enhanced porosity and conductivity.

Table 4.1: Preliminary Phytochemical Constituents of the leaves extract of SPL/TCL

Phytochemical Tests		SPL	TCL
1.	Alkaloids	+	+
2.	Simple sugars	+	+
3.	Tannins	+	-
4.	Steroids	+	-
5.	Terpenoids	+	-
6.	Flavonoids	+	+
7.	Anthraquinones	+	+
8.	Phenols	+	-

\+ Presence – Absence

4.1.1.2. FT-IR spectrum of raw SPL/TCL leaves

FT- IR spectrum of aqueous extract of SPL leaves (Figure 4.1) indicates main peaks at 3222cm^{-1}, 2339 cm^{-1}, 1659 cm^{-1} and 692 cm^{-1}. A peak at 3222 cm^{-1} may be attributed to -OH stretching vibration. Peaks at 2339 cm^{-1} and 1659 cm^{-1} may be attributed to triple bond of nitrile group, C=O band of unsaturated aldehyde, while the peak at 692 cm^{-1} correspond to aromatic bending. These peaks occurred due to phytochemicals like steroids, flavonoids, cardiac glycosides, alkaloids, tannins, caffeic acid and flavanols present in *Spathodea campanulata* **(Ochieng, P. E *et al.,* 2015).**

The FT-IR spectral data of aqueous TCL in Figure 4.1 displays a peak at 2924 cm^{-1} may be due to stretching mode of aliphatic and aromatic C–H groups. A peak at 1628 cm^{-1} correspond to the stretching modes of carbonyl groups in ester or aldehyde and ketones or organic acids. A peak for C–O stretching mode is noted at 1443 cm^{-1}. The peaks at 1381 and 1327 cm^{-1} imply the presence of C–O–C stretch and a peak pertaining to C-O stretch is noticed at 1250 cm^{-1}. A band at 1065 cm^{-1} is due to the stretching mode of C–O. This indicates that TCL extract contains mixture of compounds i.e. terpenoids, flavonoids etc., in it that are capable of mimicking synthetic organic compounds **(Satapathy *et al.*, 2009).**

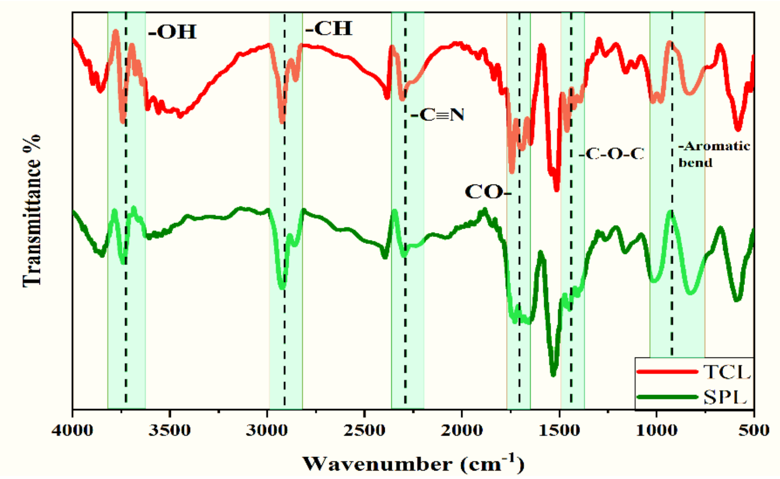

Figure 4.1: FT-IR Spectra of raw SPL and TCL leaves

Fourier Transform Infrared (FT-IR) spectroscopy analysis provides crucial insights into the functional groups present in the plant material, revealing the chemical composition and potential for carbon synthesis. The substantial carbon content, approximately 51.5% in the raw biomass, **(Lugo *et al.,* 2011)** indicates that these plant materials are rich in carbonaceous compounds, making them promising precursors for carbon electrode fabrication.

4.1.1.3. Selection of Carbonisation temperature

TGA Analysis for raw SPL/TCL

The raw plant powders of SPL/ TCL are subjected to thermogravimetric (TG) analysis to optimise the carbonisation temperatures for synthesising biomass carbons. TGA analysis allows identification of critical decomposition stages and temperature ranges where substantial mass loss occurs. The TGA curve in Figure 4.2 represents apparent degradation stages, first stage of weight loss comprising of 15 % mass loss as noticed at 105 °C, represents the evaporation of moisture from the surface of biomass. Second stage of mass loss constituting about 25 % occurred between 300- 600°C due to combustion organic components **(Lugo *et al.,* 2018).** No significant mass loss has been observed after 700°C in the third stage. The thermogravimetric analysis (TGA) results facilitate the selection of optimal pyrolysis temperatures (700°C, 800°C, 900°C), ensuring efficient biomass decomposition.

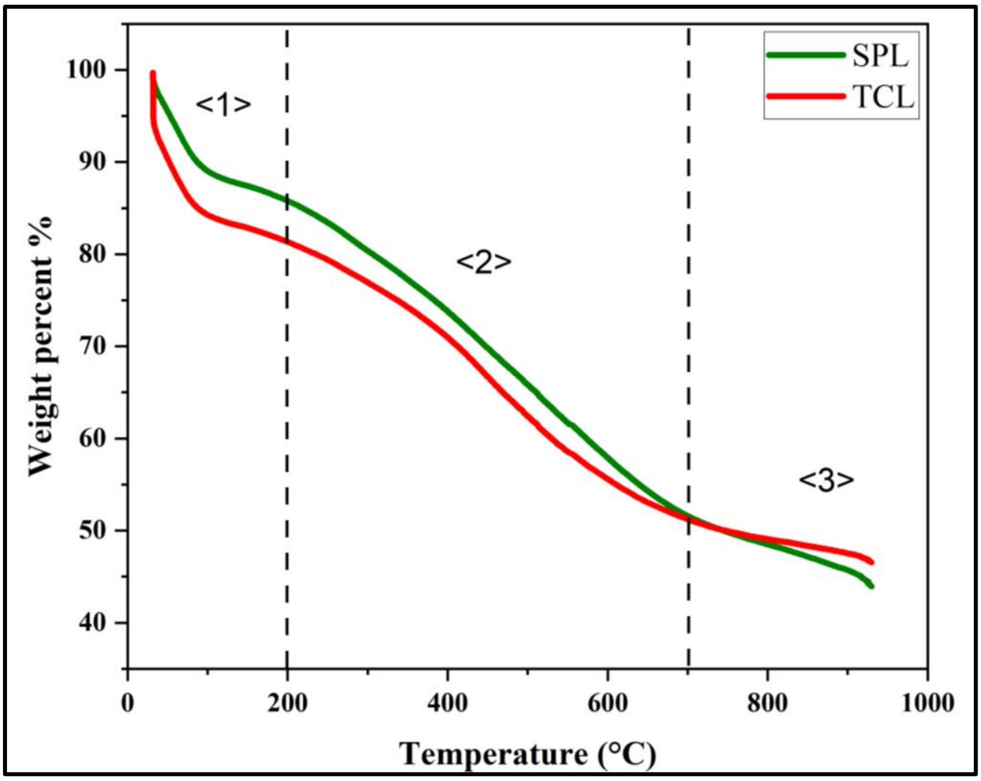

Figure 4.2: TGA Analysis of raw SPL and TCL leaves

4.1.1. Synthesis of Biomass carbon from selected plant materials:

The carbon materials are produced by direct carbonization process (pyrolysis method) without any external activation from selected waste biomass -*Spathodea campanulata* and *Tecoma capensis* leaves using the adopted experimental procedure **(Biswal *et al.*, 2013)**. The carbonized sample at 700°C, 800°C, and 900°C for *Spathodea campanulata* and *Tecoma capensis* leaves were designated as SPL-700, SPL-800, SPL-900 and TCL-700, TCL-800, TCL-900-respectively. The representation for the preparation of functional carbon from dried leaves is depicted in Figure 4.3. Nearly 10 g of biomass is taken, 8.2g of carbon (82%) yield is obtain after pyrolysis.

4.1.2 Synthesis of N-doped carbon from selected plant leaves precursors – SPL/TCL

The N- doped carbon was synthesised from SPL / TCL carbon materials as per the procedure adopted from **Anitha *et al*., 2016** and designated as SN-700, SN- 800 and SN-900. A schematic representation of the synthesis of doped carbon from biomass derived carbon is shown in Figure 4.4.

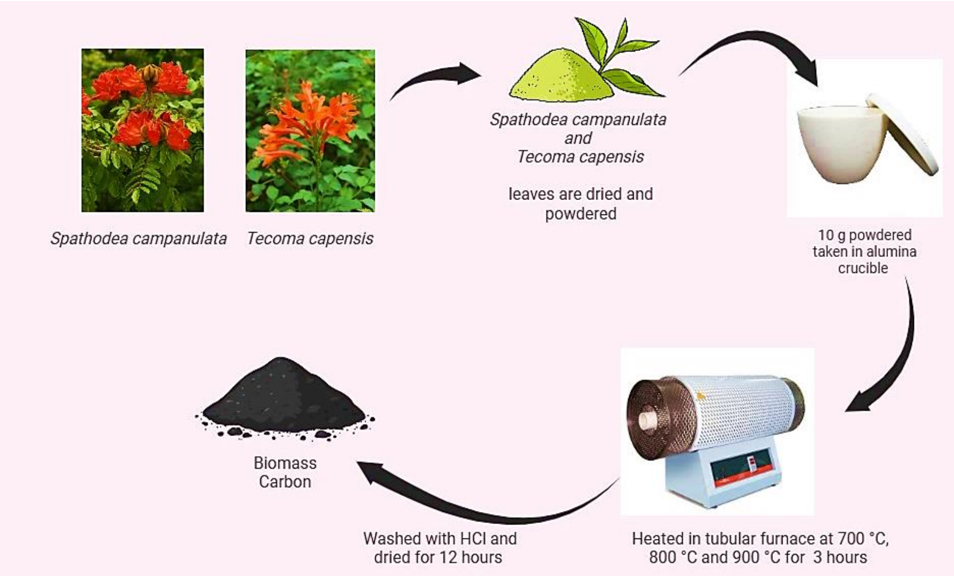

Figure 4.3: Synthesis of Biomass carbon from selected plant materials

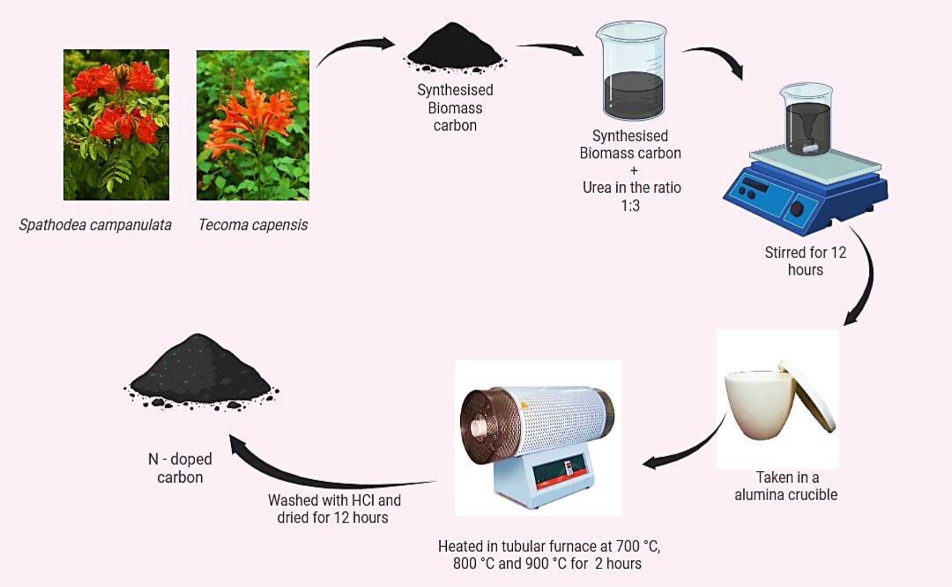

Figure 4.4: Synthesis of N-doped carbon from selected plant leaves precursors –SPL/TCL

4.2: Phase II Characterisation of Synthesised carbon materials

4.2.1 FT-IR Analysis of SPL/ TCL

The FT-IR profile for SPL/TCL are displayed in Figure 4.5 and tabulated in Table 4.2

SPL-700

The FT- IR spectrum (Figure:4.5) displays a notable absorption band at 1585 cm^{-1}, corresponding to N-O stretching and N-H bending vibrations. These peaks can be attributed to nitro compounds and amine groups, respectively, indicating the presence of nitrogen-containing functionalities within the carbon structure **(Gandhi *et al.*, 2014)**. The C=C bending vibration at 2920 cm^{-1} suggests the presence of aromatic or aliphatic double bonds, highlighting the complex carbon network formed during the carbonization process **(Jayappa *et al.,* 2020).** A band at 3731 cm^{-1} corresponding to O-H stretching vibration is indicative of the presence of hydroxyl groups, which are common in biomass-derived carbon materials and suggest the retention of some oxygen-containing functional groups from the original biomass **(Ojha *et al.*, 2022)**.

SPL-800

FT-IR spectrum of SPL -800 is depicted in Figure 4.5 and the spectral frequencies are listed in Table 4.2. The C=C bending vibration at 1453 cm^{-1} and C-O stretching at 1018 cm^{-1} highlights the presence of double bonds within the carbon network, which are essential for the material's structural properties **(Kangathara *et al.*, 2022)**. N-O stretching and N-H bending vibrations at 1593 cm^{-1} imply the presence of nitrogen-containing functional groups, maintaining the trend observed in SPL-700 **(Imaliza *et al.*, 2023)**. O-H stretching vibration is observed at 3682 cm^{-1} indicating the presence of hydroxyl groups. This corroborates the fact that similar oxygen-containing functionalities are also present as in SPL-700, albeit with slight variations due to different treatment conditions **(Ahmad *et al.*, 2022)**.

SPL-900

For SPL-900, C=C bending vibration at 1484 cm^{-1} reflects the presence of aromatic or aliphatic double bonds, crucial for the material's mechanical properties **(Ton *et al.*, 2024)**. N-O stretching and N-H bending vibrations are noticed at 1593 cm^{-1} , evidenced of nitrogen functionalities across different samples **(Neelaveni *et al.*, 2023)**.

O-H stretching vibration at 3692 cm^{-1} indicates that hydroxyl groups remain a significant component of the material's surface chemistry, even after extensive carbonization **(Aouini *et al.*, 2022)**.

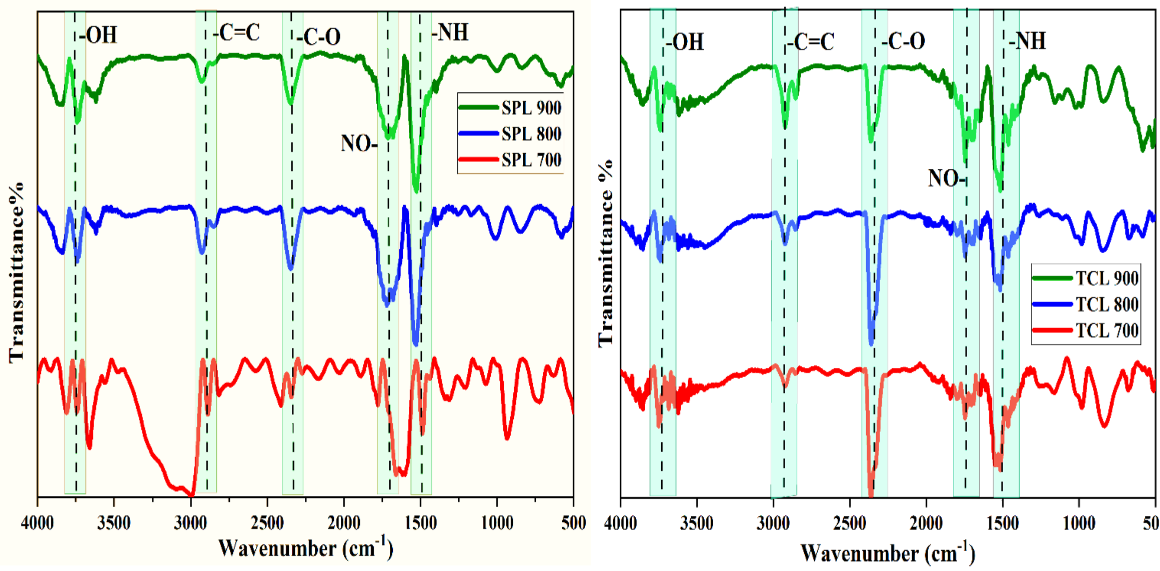

Figure 4.5: FTIR for SPL- 700, SPL- 800, SPL-900, TCL-700, TCL-800, TCL-900

TCL-700

The FT-IR spectrum of TCL-700 exhibits C=C bending vibration at 1465 cm^{-1} indicates the presence of double bonds, essential for maintaining the structural integrity of the carbon network **(Akinwunmi *et al.*, 2022).** The spectrum also implies an N-O stretching and N-H bending vibration at 1631 cm^{-1}, pointing to the presence of nitro compounds and amines, respectively. These functionalities are significant for the material's potential applications in adsorption and catalysis. An O-H stretching vibration at 3663 cm^{-1}, indicating the presence of hydroxyl groups, which are important for the material's hydrophilicity and reactivity **(Zhang *et al.*, 2013)**.

TCL-800

In TCL-800, C=C bending vibration at 1493 cm^{-1} reflects the presence of aromatic or aliphatic double bonds, important for the material's mechanical and thermal stability **(Aswini *et al.*, 2020)**. The N-O stretching and N-H bending vibrations at 1609 cm^{-1} suggest the presence of nitrogen-containing functional groups, which are crucial for the material's chemical reactivity **(Jayappa *et al.*, 2020)**. O-H stretching vibration at 3665 cm^{-1}, indicating the presence of hydroxyl groups similar to those in TCL-700.

TCL-900

The FT-IR spectrum of TCL-900 displays N-O stretching and N-H bending vibrations at 1601 cm^{-1} point to the presence of nitro compounds and amines, highlighting the material's potential for chemical functionality. The C=C bending vibration at 2882 cm^{-1} suggests the presence of aromatic or aliphatic double bonds, which contribute to the material's structural properties and thermal stability **(Pulit-Prociak *et al.*, 2023).** O-H stretching vibration at 3762 cm^{-1}, indicating a higher intensity of hydroxyl groups compared to other samples, which could be due to the specific treatment conditions **(Ebrahimi Naghani *et al.*, 2023)**.

Table 4.2: FTIR for SPL- 700, SPL- 800, SPL-900, TCL-700, TCL-800, TCL-900

Precursors						
Wavenumber (cm^{-1})						Assignment
SPL 700	SPL 800	SPL 900	TCL 700	TCL 800	TCL 900	
3731	3682	3692	3663	3665	3762	O-H stretching
1585	1593	1593	1631	1609	1601	N-O Stretching, N-H bending
2920	1018, 1453	1002, 1484	981,1465	1493	2882	C=C bending, C-O stretching

4.2.2 FT-IR Analysis of SN/TN

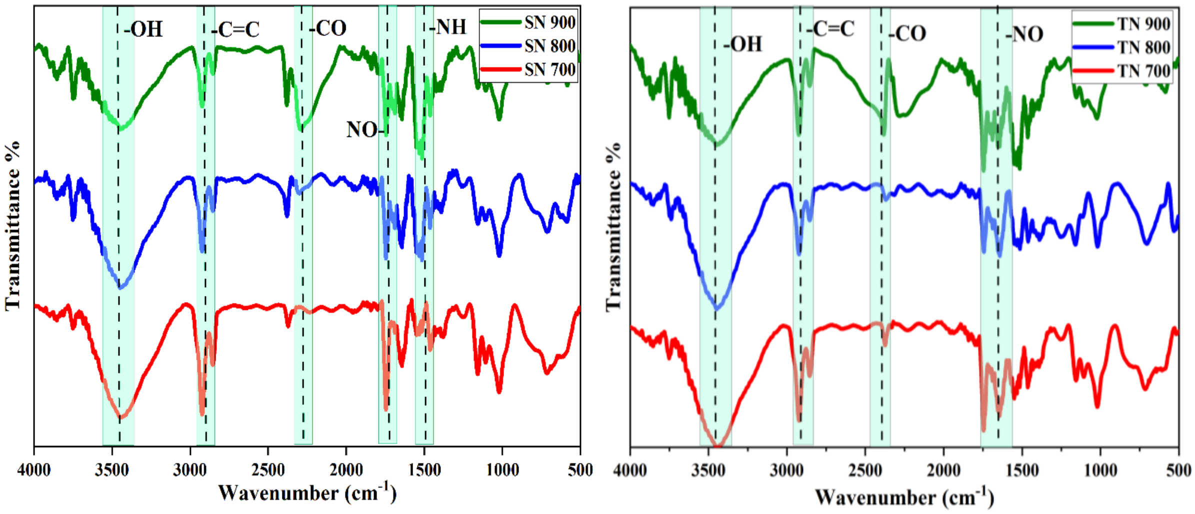

Figure 4.6: FTIR for SN- 700, SN- 800, SN-900, TN-700, TN-800, TN-900

SN-700

FT-IR spectrum of SN-700 (Figure 4.6) displays a peak at 1100 cm^{-1} that may be assigned to C-O stretching vibrations, suggesting the presence of aromatic structures within the carbon matrix **(Gabrienko *et al*., 2016)**. The peak at 1562 cm^{-1} is attributed to the N-O stretching vibration, indicating the presence of nitrogen-oxygen bonds, which are typical in nitrogen-doped carbon materials. Additionally, a prominent peak is noticed at 3731 cm^{-1}, which corresponds to O-H stretching vibration. This peak indicates the presence of hydroxyl groups on the surface of the carbon material, possibly due to adsorbed water or hydroxylated sites on the carbon surface **(Jiang *et al*., 2017& Zhang *et al*., 2022)**.

Table 4.3: FT-IR for SN- 700, SN- 800, SN-900, TN-700, TN-800, TN-900

N-Doped Carbon						
Wavenumber (cm^{-1})						**Assignment**
SN 700	**SN 800**	**SN 900**	**TN 700**	**TN 800**	**TN 900**	
3731	3556	3692	3663	3668	3762	O-H bond
1562	1593	1593	1531	1565	1532	N-O bond
1100	695	885	965	1095	885	C=C bending, C-O stretching

SN-800

For SN-800, a peak at 695 cm^{-1} may be assigned to C=C bending vibrations, suggesting that aromatic structures are also present in SN-800 **(Dovbeshko *et al*., 2020)**. The peak at 1593 cm^{-1} is associated with the N-O stretching vibration, confirming the presence of nitrogen-oxygen bonds within the sample. A peak at 3556 cm^{-1} corresponds to the O-H stretching vibration, indicates the presence of hydroxyl groups **(Zheng *et al*., 2023)**.

SN-900

FT-IR spectrum of SN-900 primarily comprised of peak at 885 cm^{-1} may be assigned to C=C bending vibrations, indicating aromatic structures within the carbon matrix **(Aziz *et al.*, 2017).** The peak at 1593 cm^{-1} is attributed to N-O stretching vibration, suggesting the presence of nitrogen-oxygen bonds. The peak 3692 cm^{-1}, corresponding to the O-H stretching vibration indicates the presence of hydroxyl groups (Cheng et al., 2017).

TN-700

The FT-IR spectrum for TN-700 exhibits a peak at 965 cm^{-1} assigned to C=C bending vibrations, suggests the presence of aromatic structures within the sample **(Pagacz-Kostrzewa *et al.*, 2022)**. The peak at 1531 cm^{-1} is associated with the N-O stretching vibration, confirming the presence of nitrogen-oxygen bonds. Additionally, the peak at 3663 cm^{-1}, corresponding to the O-H stretching vibration, indicates the presence of hydroxyl groups **(Spaltro *et al.*, 2024)**.

TN-800

For TN-800, the FT-IR spectrum displays a peak at 1095 cm^{-1} is assigned to C=C bending vibrations, C-O stretching, indicates the presence of aromatic structures **(Yuan *et al.*, 2015).** The peak at 1565 cm^{-1} is attributed to the N-O stretching vibration, suggesting the presence of nitrogen-oxygen bonds within the sample. A peak at 3668 cm^{-1}, corresponds to O-H stretching vibration, indicating the presence of hydroxyl groups **(Zheng *et al.*, 2022)**.

TN-900

The FT-IR spectrum of TN-900 shows a peak at 885 cm^{-1}, assigned to C=C bending vibrations, suggesting the presence of aromatic structures within the sample **(Sałdyka& Mielke, 2018)**. The peak at 1532 cm^{-1} is associated with the N-O stretching vibration, confirming the presence of nitrogen-oxygen bonds. A peak at 3762 cm^{-1}, corresponding to the O-H stretching vibration, indicating the presence of hydroxyl groups **(Kang & Wang, 2013)**.

Discussion from FT-IR

The FT-IR spectra of prepared carbon/ N- doped carbon samples reveal significant information about their chemical structures. The presence of O-H stretching, N-O stretching, N-H bending, and C=C bending vibrations provides insights into the functional groups and chemical interactions within these materials. These functional groups are essential for elucidating the material's properties and assessing its potential applications for energy storage systems.

4.2.2 XRD Analysis

4.2.2.1 XRD analysis of SPL/TCL

The XRD pattern of SPL/TCL are depicted in Figure 4.7& 4.8 and the corresponding 2θ values tabulated in Table 4.4.

SPL-700/800/900

The XRD spectra of SPL–700 show broad peaks at 2θ values of 24.6 and 43 respectively. Broad peaks are characteristic to amorphous structure which indicate short range order of the atoms in the material. X-ray diffraction patterns do not observe sharp peaks due to disordered graphitic nature as reflected in the indices plane of (002), (101) for amorphous graphite respectively **(Dai *et al.*, 2016).**

For SPL–800, XRD patterns exhibited broad peaks at 2θ values of 23.4 and 43.2. The presence of these broad peaks signifies that SPL-800 retains its amorphous structure which reflects the miller indices of (002) and (101) respectively. The slight shift in 2θ values compared to SPL-700 is local atomic variations but still in the amorphous graphite structure **(Lu *et al.*, 2019).**

The XRD pattern of SPL -900 shows broad peaks of 2θ values at 24.6 and 43.1 which are close to those of SPL-700 and SPL-800. It confirms that SPL 900 has also an amorphous graphite structure where broad peak patterns were obtained irrespective of the heating conditions which is reflected by the miller indices of (002) and (101) respectively. The persistence of broad peaks suggests the absence of long-range orderly arrangement in the sample material **(Moseenkov *et al.*, 2023).**

TCL-700/800/900

However, the XRD pattern for TCL-700 demonstrated more pronounced peaks at 2θ=23.7, 64 and 77.5 which correspond to miller indices of (002), (101) and (110) respectively which ascribed to the development of particular crystalline phases upon the treatment **(Ramazanov *et al.*, 2021).** Presence of multiple sharp peaks suggests the existence of a high level of crystallinity in TCL-700 which depicts properties of a crystalline structure representing that there is definite periodicity over long-range order in the arrangement of atoms.

For TCL-800, the XRD pattern depicts three sharp peaks at 43.9, 64.45 and 77.5. All sharp peaks suggest crystal nature as found in TCL-700. Clearly, these slight linear shifts in 2θ values and the presence of distinct sharp peaks indicate the formation of crystalline phases that are well defined and reflected by miller indices of (002), (101) and (110) respectively **(Nabiałek *et al.*, 2015)**

The XRD pattern of TCL-900 illustrates distinct peaks at 43.9, 64.6 and 77.5 indicating crystalline nature corresponding to miller indices of (002), (101) and (110) respectively. These peaks are similar to TCL-800 which indicates that even at elevated carbonization temperatures, the crystalline structure is sustained. Sharp defined peaks indicative of the presence of ordered crystalline phases which are require for certain electronic or mechanical properties **(Hoe *et al.*, 2018).**

The crystallite size of the synthesised carbon materials SPL/ TCL are calculated using Scherrer formula and tabulated in Table 4.4.

Table 4.4: XRD analysis of SPL- 700, SPL- 800, SPL-900,
TCL- 700, TCL- 800, TCL- 900

Precursors	2θ value	Inference	Nature	Crystallite Size (nm)
SPL-700	24.6, 43	Broad peak	Amorphous	0.71
SPL-800	23.4, 43.2	Broad peak	Amorphous	0.68
SPL-900	24.6, 43.1	Broad peak	Amorphous	0.51
TCL- 700	43.7, 64 , 77.5	Sharps peaks	Crystalline	6.53
TCL- 800	43.9, 64.45, 77.5	Three sharp peaks	Crystalline	14.67
TCL- 900	43.9, 64.6, 77.5	Sharp peaks	Crystalline	2.75

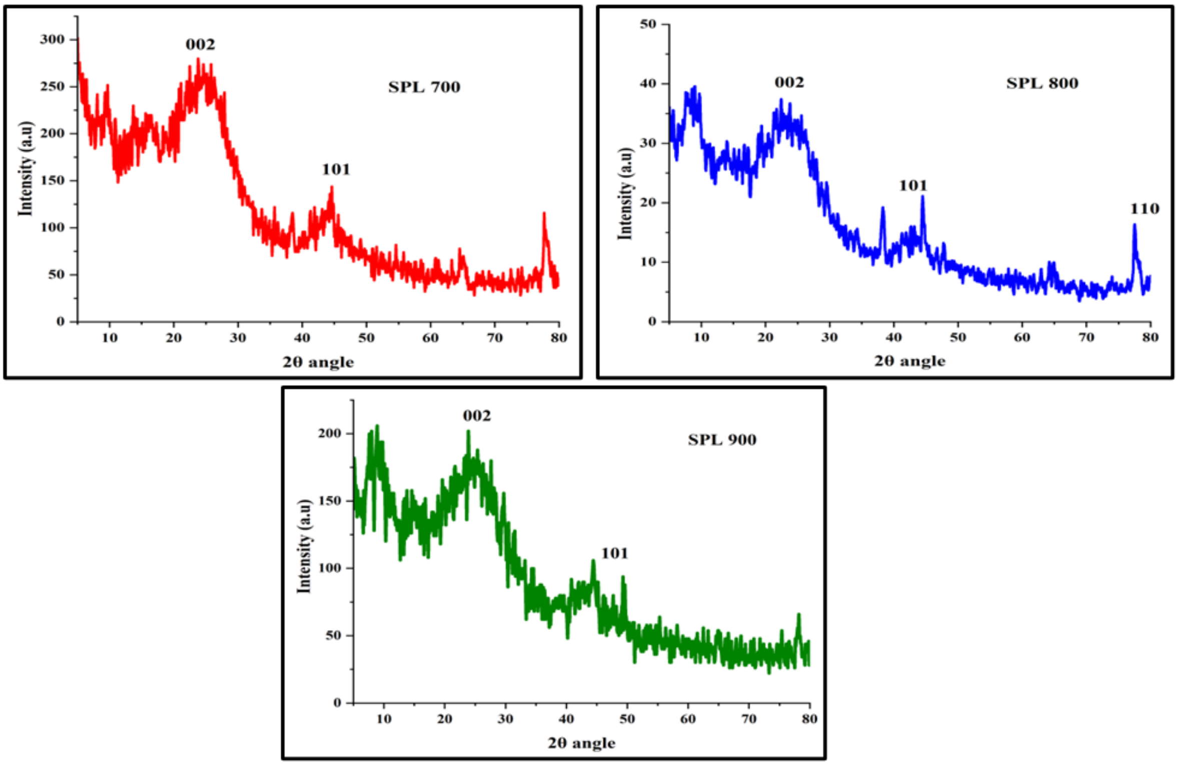

Figure 4.7: XRD Spectra for SPL- 700, SPL- 800, SPL-900

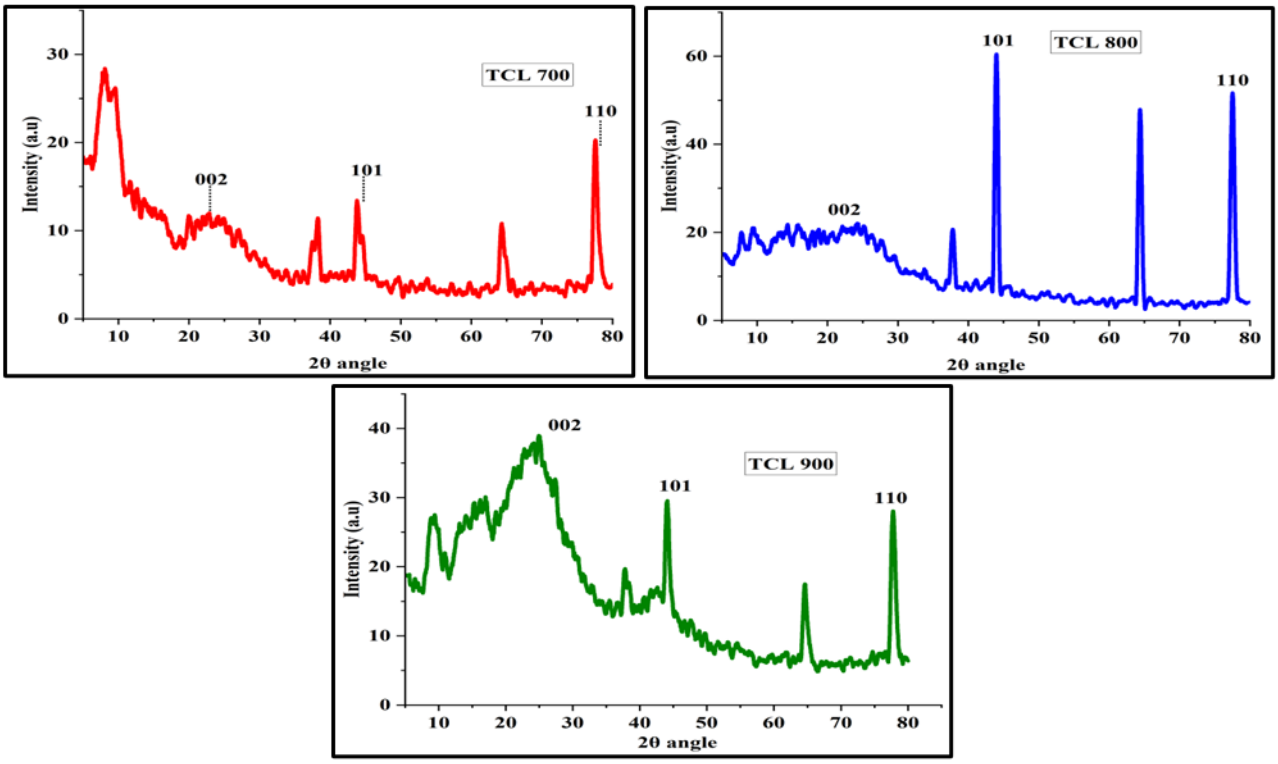

Figure 4.8: XRD Spectra for TCL- 700, TCL- 800, TCL-900

4.2.2.2 XRD analysis of SN/ TN

The XRD pattern of SN are depicted in Figure 4.9 and the corresponding 2θ values tabulated in Table 4.5.

SN-700/800/900

The XRD pattern of SN-700 shows broad peaks at 2θ values 24.2 and 43.8 which are attributed to miller indices of (002) and (100) respectively. Broad peaks are indicative of amorphous structures that define short-range atomic order. This indicates that SN-700 is a form of amorphous graphite which have short range atomic order and do not exhibit sharp peaks in diffraction patterns **(Ardiani *et al.*, 2020).**

For SN-800, the XRD pattern depicts in Figure 4.9 shows broad peaks at 2θ values of 23.4 and 43.2 which are reflected by the miller indices of (002) and (100) respectively. Presence of broad peaks indicates that SN-800 has also an amorphous graphite structure compared to SN 700, the shift in 2θ values may be attributed to local atomic environment variations but amorphous nature is retains **(Azuara-Tuexi*et al.*, 2023).**

The diffractogram of SN-900 shows peaks at around 24.6 and 43.1 which indicate by miller indices of (002) and (101) planes comparable to those revealed for SN-700 and SN-800.The presence of broad peaks over a different sample indicates that SN-900 possess amorphous graphite structure. The reappearance of the broad peaks indicates that there is no long- range order within the crystalline arrangement of this sample **(Shan *et al.*, 2024).**

The XRD pattern of TN are depicted in Figure 4.10 and the corresponding 2θ values tabulated in Table 4.5

TN-700/800/900

In contrast, the XRD pattern of TN-700 shows broad peaks at 2θ values of 43.7, 64 and 77.5 with respective miller indices (002), (013) and (100). However, these peaks have very low intensity represent that TN-700 possesses an amorphous graphite nature **(Firdaus *et al.*, 2023).**

For TN-800, the XRD pattern shows broad peaks around 43.9 and 77.5 with respective miller indices (002), (110). The broad nature of the peaks indicates an amorphous graphite structure which is consistent for TN-700. This variation specifies that the sample transformed from that specific phase to a more disordered structure.

Amorphous nature of TN-800 is also confirmed by the absence of sharp peaks **(Sutarsis *et al*., 2023).**

The XRD pattern of TN-900 confirms the presence of broad peaks at 43.9 and 77.5 which are similar to TN-800. The broad peaks represent an amorphous graphite within miller indices (002) and (101) respectively. Broad peaks in TN-900 were consistent that this material is disordered in nature to the extent that it does not exhibit such long-range order **(Rahmawati *et al*., 2024).**

The crystallite size of the synthesised carbon materials SN/TN are calculated using Scherrer formula and tabulated in Table 4.5.

Table 4.5: XRD analysis of SN- 700, SN- 800, SN-900TN- 700, TN- 800, TN-900

Precursors	2θ value	Inference	Nature	Crystallite Size (nm)
SN-700	24.2, 43.8	Broad peak	Amorphous	7.65
SN-800	23.4, 43.2	Broad peak	Amorphous	0.67
SN-900	24.6, 43.1	Broad peak	Amorphous	0.71
TN- 700	43.7, 64 , 77.5	Broad peak	Amorphous	0.85
TN- 800	43.9, 77.5	Broad peak	Amorphous	0.66
TN- 900	43.9, 77.5	Broad peak	Amorphous	0.72

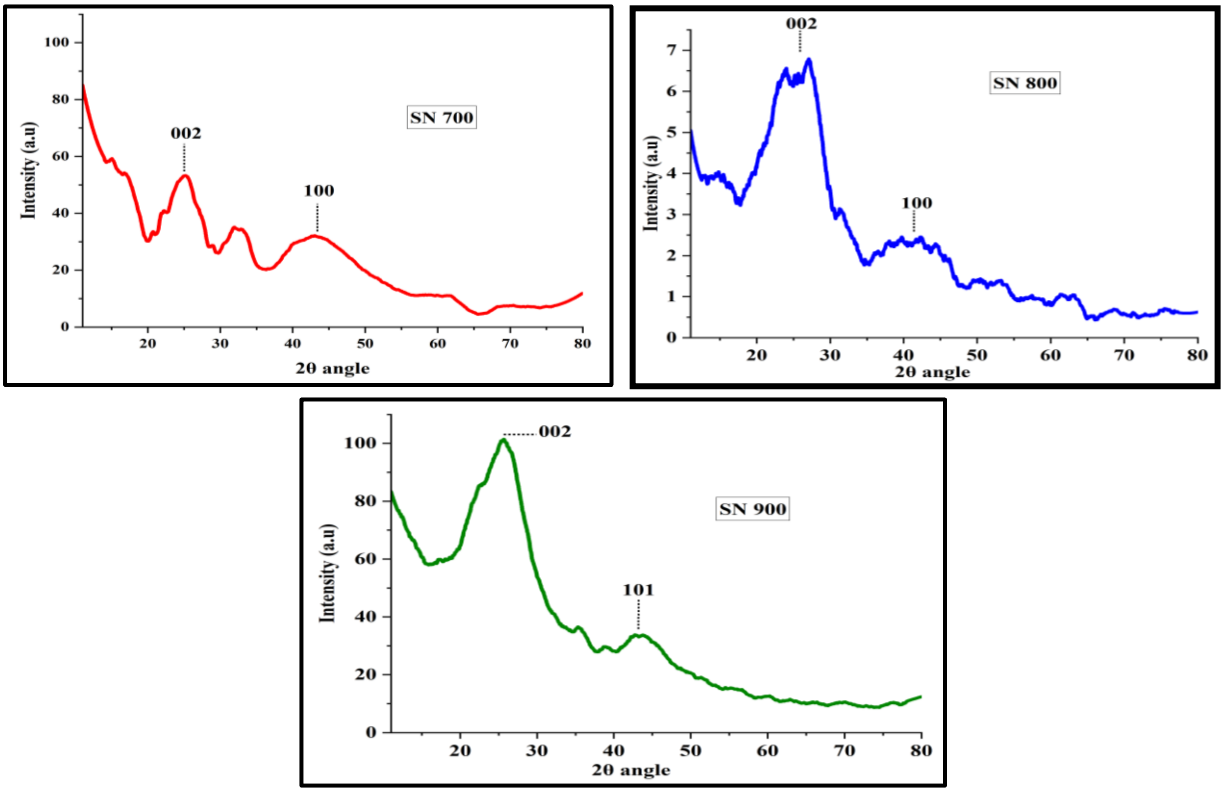

Figure 4.9: XRD Spectra for SN- 700, SN- 800, SN-900

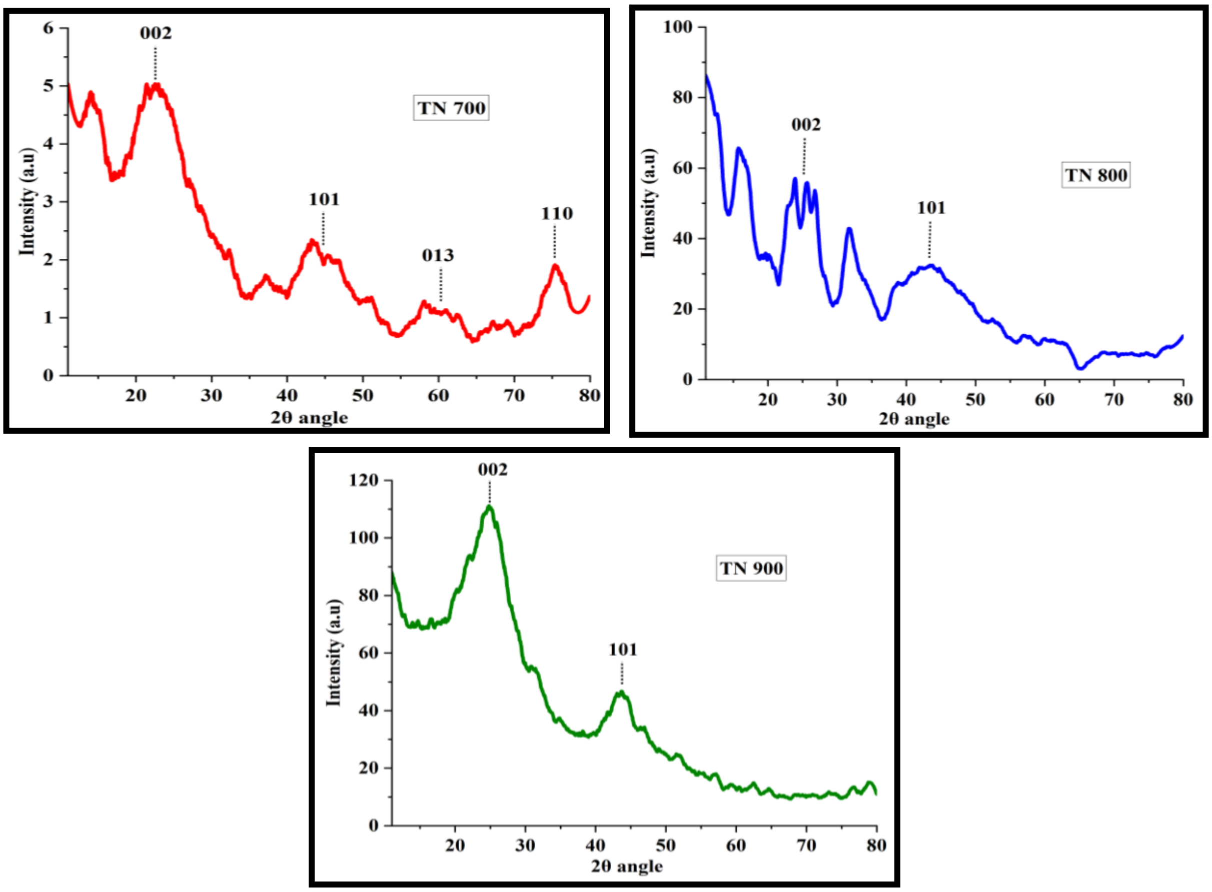

Figure 4.10: XRD Spectra for TN- 700, TN- 800, TN-900

4.2.3 Raman Analysis

4.2.3.1 Raman Analysis of SPL/ TCL

The Raman spectrum of SPL is depicted in Figure 4.11 and G band, D band values tabulated in Table 4.6.

SPL-700/800/900

The Raman spectrum of SPL-700, G position at 1562 cm^{-1} and D position at 1353 cm^{-1} with an I_D/I_G ratio 1.00. This ratio specifies a high degree of graphitization which leads to an ordered graphitic carbon sample. The high R^2 value of 0.94 in the Lorentz-type fit further supports the accuracy of this assessment **(Umeda & Enami, 2020)**. The G band corresponds to the E_2g mode of graphite, which is associated with the stretching of the C-C bond in graphitic materials, while the D band indicates the presence of defects or disorder in the carbon structure **(Nakamura & Akai, 2013)**. 2D band exhibits a lower intensity (I_{2D}/I_G ratio = 0.10) which suggests the presence of a relatively small number of graphene layers or defective graphitic structures, and the crystallite size of 19.2 nm indicates that the material has undergone partial graphitization with a moderate degree of disorder. The I_D/I_G ratio being exactly 1.00 suggests a balanced presence of graphitic and defective carbon structures, highlighting the material's high graphitization degree.

For SPL-800, the Raman spectrum shows a G band at 1593 cm^{-1} and a D band at 1347 cm^{-1}, with an I_D/I_G ratio of 1.01 and a slightly more intense 2D band (I_{2D}/I_G ratio = 0.10) with a crystallite size of 19.0 nm. This slight increase in the I_D/I_G ratio compared to SPL-700 suggests a marginally higher degree of disorder, but still indicates a high degree of graphitization. The small decrease in crystallite size compared to SPL 700 suggests that the material has undergone further graphitization, leading to a slight increase in the degree of order within the carbon structure. The similar $I_{2D}/_{IG}$ ratio implies that there is enhancement in graphitization, the number of graphene layers is maintained in that of multilayer graphene. The R^2 value equals to 0.98 indicates that Lorentzian utilized strong fitting which is consistent with observation **(Jiao *et al.*, 2017)**.

The Raman spectrum of SPL-900 shows G band at 1588cm^{-1} and D band at 1352cm^{-1} with I_D/I_G ratio of 1 .03 with 2D band intensity slightly lowered (I_{2D}/I_G ratio=0.08) and with crystallite size of 18.7nm.This ratio exhibits a marginally higher disorder than SPL-800 but still in the closure range for high graphitization. The lowered I_{2D}/I_G ratio implies a reduction in the stacking of graphene layers which indicates the existence of more imperfect sites that disrupt the development of well-ordered graphene. Even though, a slight decrease in R^2 value of 0.92, still finding a good correlation for the Lorentzian model **(Wang *et al.*, 2019).** High degree of graphitization in SPL-900 is further substantiated by the unshifting position of G band which indicates that the sample has a well-developed graphitic configuration with few defects.

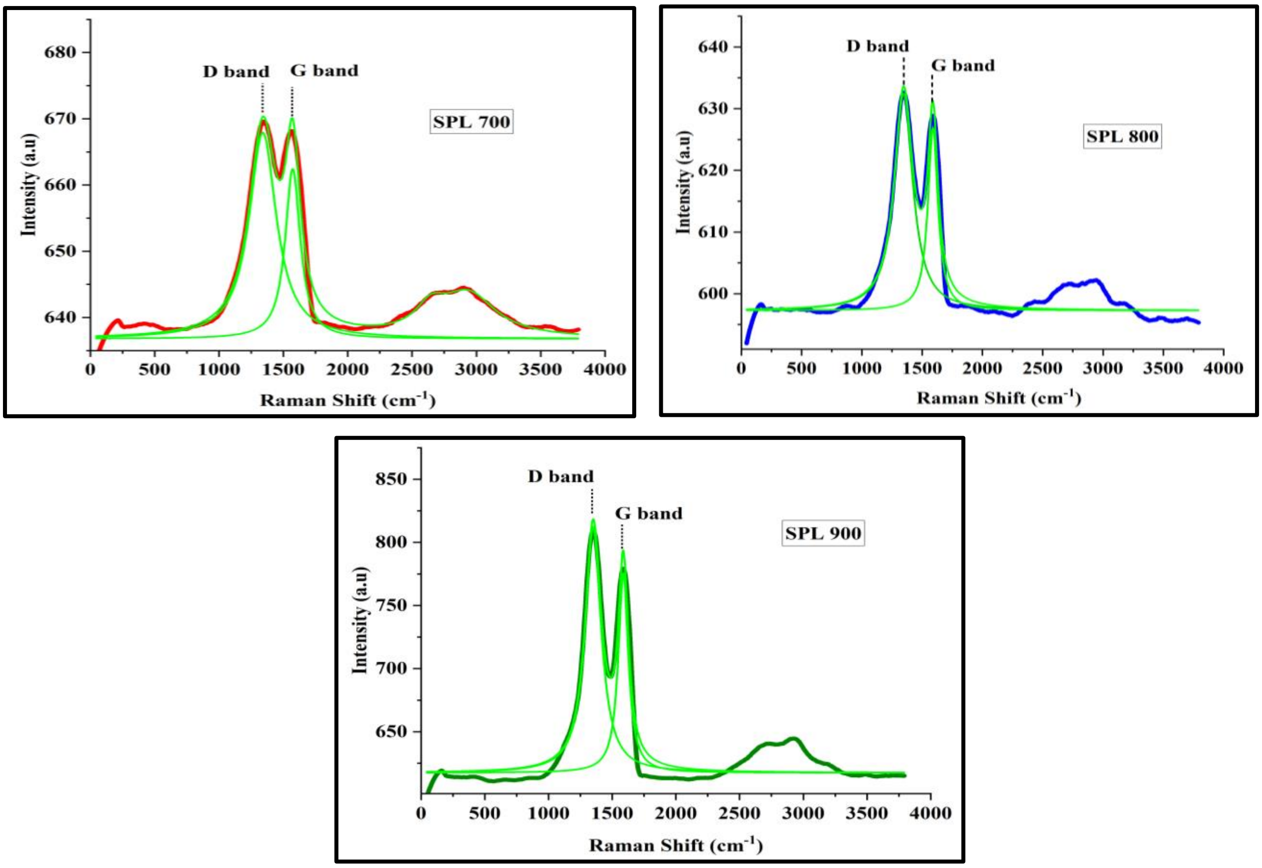

Figure 4.11: Raman Spectra for SPL- 700, SPL- 800, SPL-900

The Raman spectrum of TCL is depicted in Figure 4.12 and G band, D band values tabulated in Table 4.6.

TCL-700/800/900

For TCL-700 demonstrate in Figure 4.12, Raman spectrum shows G band located at 1575 cm^{-1} and D band at 1347 cm^{-1} with I_D/I_G ratio of 0.98, 2D band shows I_{2D}/I_G = 0.08 comparatively low intensity and overall crystallite size of 19.6 nm. This ratio is mostly lower than SPL samples, indicating that TCL 700 has undergone a high degree of graphitization with minimum defects and 2D band indicates that the sample contains a limited number of graphene layers or show disordered structure. From the examined data, R^2 = 0.93 represents consistent Lorentzian fitting supporting better accuracy of the data **(Kuo *et al.*, 2017)**. The I_D /I_G ratio even less than unity indicates a well- ordered structure which is reliable with the high level of graphitization seen in the material.

As shown in Figure 4.12, the Raman spectrum of TCL-800 contains a G band at 1583 cm^{-1} and a D band at 1347 cm^{-1} where I_D /I_G ratio is 1.02 and a similar I_{2D}/I_G ratio = 0.08 was measured with crystallite size of 18.9 nm as in TCL 700 powder. This implies a low degree of disorder related to TCL-700 where high degree of graphitization still persists. This indicates that although the material has been further graphitized compared to TCL 700, the number of graphene layers still remains and enhances the stacking order to a very small extent. The R^2 value of 0.95 indicates strong fit for the Lorentzian model data **(Sha *et al.*, 2018)**.

TCL-900 relates to Raman results as a G band was observed at 1583 cm^{-1} and a D band at 1349 cm^{-1}, I_D/I_G ratio is 1.02, 2D band intensity was slightly lower I_{2D}/I_G ratio = 0.07 and crystallite size of 18.9 nm which is close to samples of TCL 800. Similar to TCL-800, this ratio is also similar and indicates a comparable degree of graphitization. The ratio values are similar to that of TCL-800 which further indicates a comparable degree of graphitization. The R^2 value (0.96) further proves the reliability of the Lorentz fit **(Shin *et al.*, 2020)**. The lesser I_{2D}/I_G ratio discloses that the number of graphene layers which are still low and considered on high disorder materials. Even with increase in carbonization temperatures to 900°C which induce high rates of graphitization, still the low I_{2D}/I_G ratio and high I_D/I_G ratio persist, implying many defects remain within the sample leading to the disruption of the regular stacking of graphene layers. Crystallite size remains constant from TCL 800, implying a high degree of graphitization has been attained; however, this structural order is highly compromised by defects present within the material.

The Crystallite size of the synthesised carbon materials can be calculated using Tuinstra Koenig Relation and tabulated in Table 4.6.

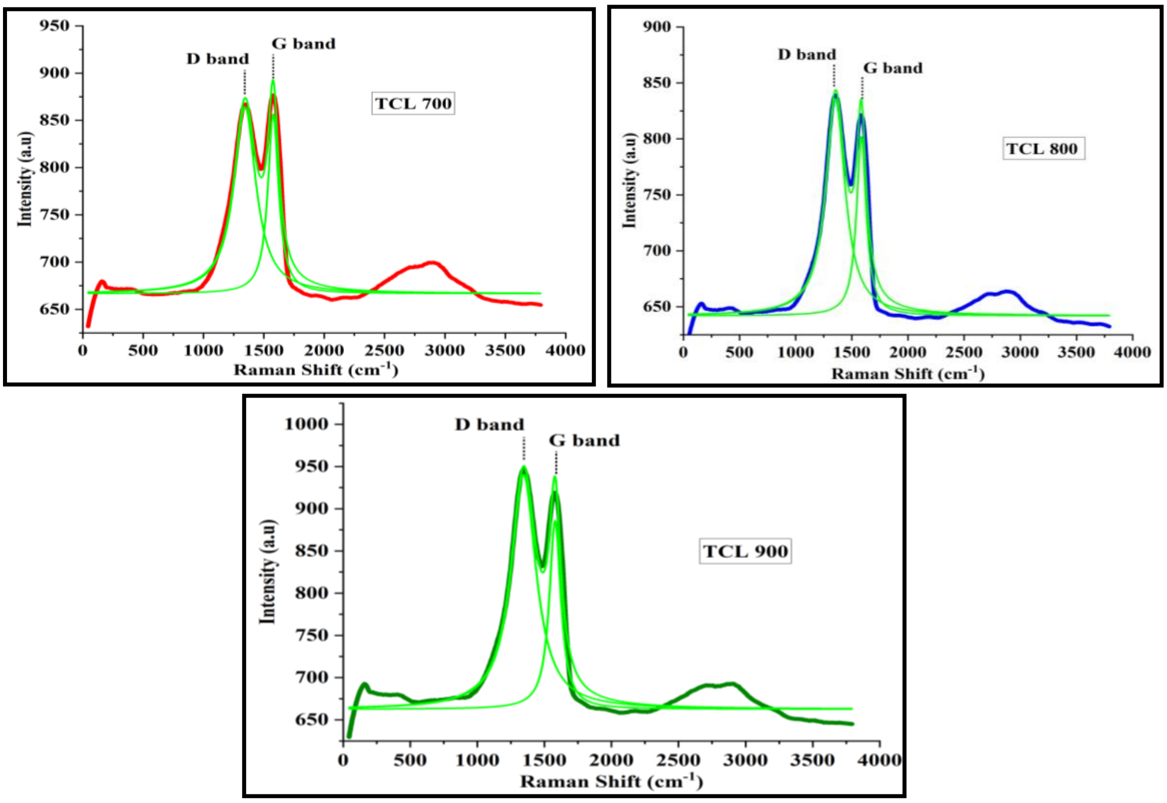

Table 4.6: Raman analysis of TCL- 700, TCL- 800, TCL-900

Figure 4.12: Raman Spectra for TCL- 700, TCL- 800, TCL-900

Samples	**G band**	**D band**	**I_D/I_G ratio**	**I_{2D}/I_G ratio**	**Nature**	**R^2**	**Fit Type**	**Crystallite Size (nm)**
SPL-700	1353	1562	1.00	0.10	High degree of graphitization	0.94	Lorentz	19.2
SPL-800	1347	1593	1.01	0.10	High degree of graphitization	0.98	Lorentz	19.0
SPL-900	1352	1588	1.03	0.08	High degree of graphitization	0.92	Lorentz	18.7
TCL-700	1347	1575	0.98	0.08	High degree of graphitization	0.93	Lorentz	19.6
TCL-800	1347	1583	1.02	0.08	High degree of graphitization	0.95	Lorentz	18.9
TCL-900	1349	1583	1.02	0.07	High degree of graphitization	0.96	Lorentz	18.9

Table 4.7: Raman analysis of SN- 700, SN- 800, SN-900, TN- 700, TN- 800, TN-900

Samples	G band	D band	I_D/I_G ratio	I_{2D}/I_G ratio	Nature	R^2	Fit Type	Crystallite Size (nm)
SN-700	1355	1652	1.00	0.02	High degree of graphitization	0.94	Lorentz	19.2
SN-800	1347	1653	1.01	0.03	High degree of graphitization	0.98	Lorentz	19.0
SN-900	1352	1588	1.05	0.02	High degree of graphitization	0.92	Lorentz	18.3
TN-700	1347	1675	0.98	0.02	High degree of graphitization	0.93	Lorentz	19.6
TN-800	1347	1583	1.02	0.02	High degree of graphitization	0.95	Lorentz	18.9
TN-900	1349	1683	1.02	0.02	High degree of graphitization	0.96	Lorentz	18.9

4.2.3.2 Raman Analysis of SN/TN

The Raman spectrum of SN/TN are depicted in Figure 4.13 & 4.14 and G band, D band values tabulated in Table 4.7.

SN-700/800/900

The Raman spectra for SN-700, Figure 4.13 reveals the presence of a G band at 1562 $cm^{-1}$and the D band at 1353cm^{-1}, I_D/I_G =1.00, with a weak 2D band (I_{2D}/I_G= 0.02). This ratio demonstrates high levels of graphitisation implying proper order of graphite arrangement and absence of defects while 2D band implies that there is less graphene layer formation and high degree of disorder in the carbon. The analysis is considered to be accurate owing to the high R^2 value of 0.94 for the Lorentzian fit **(Wu *et al.*, 2013)**. The G band associated with the E_2g mode of a graphite sustains the stretching of the C-C bond while the D band which is considered a disorder band indicates that nitrogen doping has been relatively efficacious, without prominently distorting a graphitic lattice **(Sharifi *et al.*, 2012)**

As for SN-800, a strong G band (at 1593 cm^{-1}) and a D band (at 1347 cm^{-1}) were recorded where both bands intensities and ID/IG ratios were 1.01 ratio of 2D band intensity remains less(I_{2D}/I_G ratio= 0.03) .The slightly higher ratio compared to SN-700 disorder is most likely as a result of high nitrogen doping levels, still corresponded to high degrees of graphitization and 2D band denoting that enhancement of the carbonization temperature to 800ºC has only improved the graphitization process to a minimal degree. R^2 value of 0.98 for the Lorentzian plot indicated a good fit and further supported the findings **(Wu *et al.*, 2013)**. The G band has shifted upward showing that the graphitic ordering has improved and hence the sp^2 carbon bond has improved due to the nitrogen doping effect.

The Raman spectrum of SN-900 shows a G band at 1588 cm^{-1} and a D band at 1352 cm^{-1}, where the I_D/I_G ratio is 1.05, 2D band intensity remains low (I_{2D}/I_G ratio = 0.02). The increase in ratio suggests that the nitrogen has intercalated the carbon lattice more extensively. TN-900 still retains a strong degree of graphitization and although 2D band intensity is low, and despite high carbonization temperature implies that partial graphitisation process occurs with occurrence of structural defects. Although, lower the R^2 value of 0.92 still provides for a reasonable degree in the Lorentzian fit **(Shi *et al.*, 2018)**. The position of the G band in SN-900, along with its I_D/I_G ratio, reflects the stability of the graphitic order and the development of defects through nitrogen doping.

TN-700

For TN-700, the Raman spectrum is characterized in Figure 4.14, where G band was found at 1575 cm^{-1}, and D band at 1347 cm^{-1} with an I_D/I_G of 0.98 and 2D band which was weak in intensity with I_{2D}/I_G = 0.02. This slightly lower ratio suggests increase in graphitization and less defects compared to SN samples. However, the weak 2D band is still suggesting that the material is mostly disordered in nature with partial development of graphene sheet- like structure formation. The relatively larger crystallite size is suggestive that although the graphitic domains exist, they are not properly ordered structures hence the 2D band intensity is low. The R^2 value of 0.93 was achieved in the Lorentzian fit supporting, a good approach to any statistical analysis **(Achour *et al.*, 2013)**. The G band can be assigned to the E_2g mode of graphite which is due to the C-C bond stretching, and the D band arises defect which is nominal in this sample.

TN-800

The Raman spectrum in TN-800 has a G band at 1583 cm^{-1}, D band at 1347 cm^{-1} with an I_D/I_G ratio of 1.02 and low intensity of the 2D band (I_{2D}/I_G ratio = 0.02). Furthermore, this ratio shows relatively higher disorder as compared to TN-700 but still indicates high graphitization level. The consistent low intensity of the 2D band within these samples confirms that the rise in temperature of carbonization has not appreciably enhanced the orientation of graphene layers such that the material still shows a high level of structural disorder. The R^2 value of 0.95 proves the good Lorentzian fit as a reliable assumption which reinforces the validity of the results obtained **(Wu *et al,* 2013)**. The position of the G band and I_D/I_G ratio imply that the nitrogen doping led to some defects but a predominantly graphitic material structure is retained.

TN-900

For TN-900, the Raman spectrum presents a G band with a peak 1583 cm^{-1}, D band at 1349cm^{-1} with an I_D/I_G of 1.02 and low intensity of the 2D band ($I_{2D}/I_G = 0.02$). This ratio corresponds to TN-800 remarkable, exhibiting a level of graphitization and defects are also similar. The R^2 value of 0.96 represents the reliability of the Lorentzian fit **(Sinelnikova *et al.*, 2023)**.

Discussion

Raman analysis of the biomass carbon samples SPL-700, SPL-800, SPL-900, TCL-700, TCL-800, and TCL-900 demonstrates a considerable degree of graphitisation in all of the samples analyzed, with slight variations in the I_D/I_G ratio indicative of minor difference in disorder level. The good R^2 values arising from the Lorentzian fits substantiate the reliability of these observations.

N-doped Carbon samples SN-700, SN-800, SN-900, TN-700, TN-800 and TN-900 show a high degree of graphitization in all the samples; however, the slight differences in the I_D/I_G ratio indicate differences in defects due to nitrogen doping. The strong R^2 values for the Lorentzian fits confirm the reliability of these observations.

All SPL/TCL/SN/TN samples have low 2D band intensity further illustrates the incapacity of the carbonization process to produce adequately ordered graphene structures. The uniformity in all the samples in respect to even G band position and I_D/I_G ratio suggests that the graphitization process was consistent with the structural properties of the material contributed by the nitrogen doping. These results are also corroborated by XRD results also.

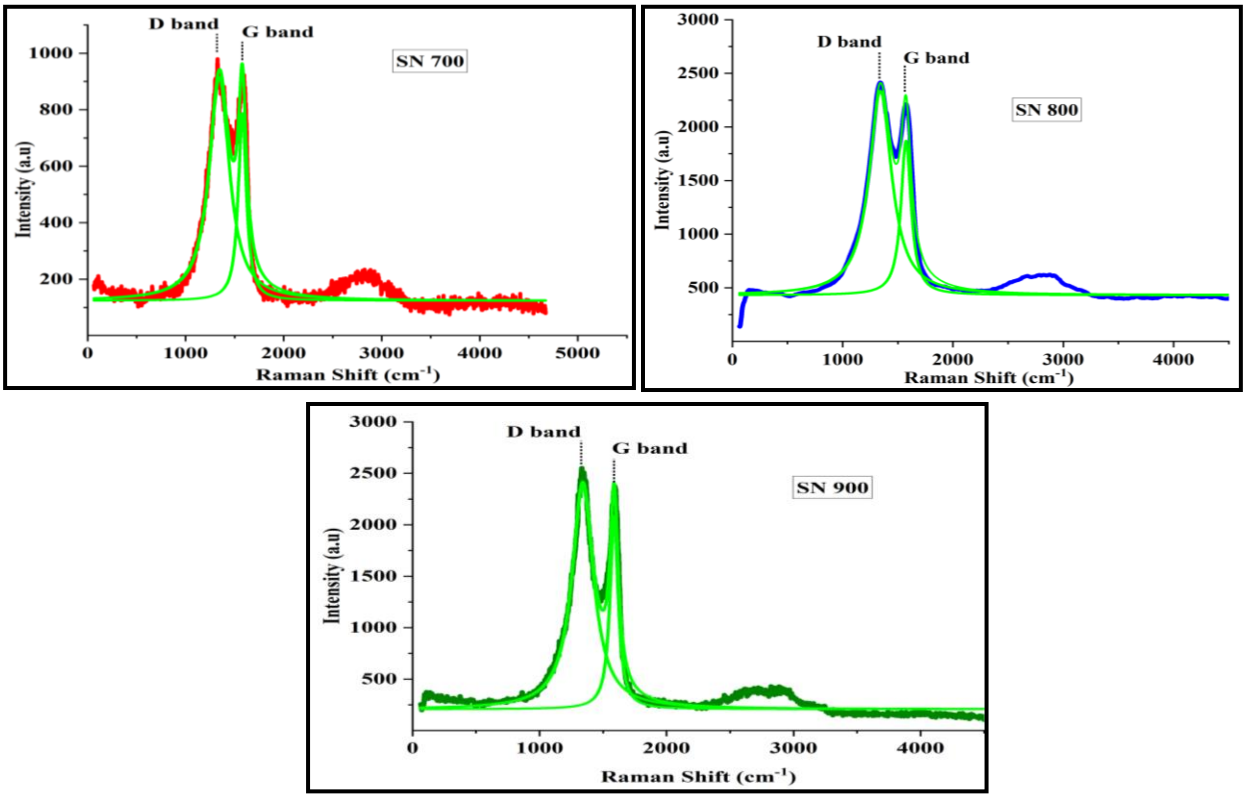

Figure 4.13: Raman Spectra for SN- 700, SN- 800, SN-900

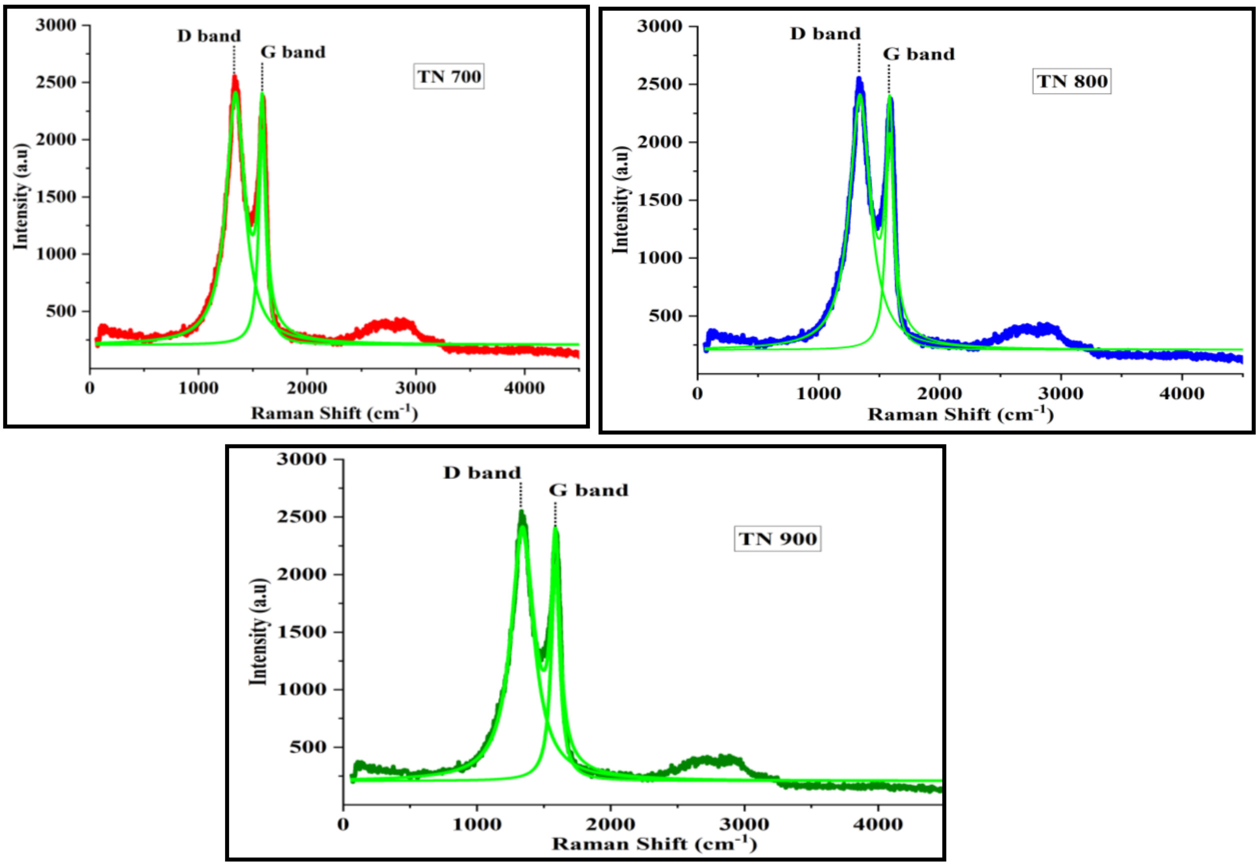

Figure 4.14: Raman Spectra for TN- 700, TN- 800, TN-900

4.2.4. Field Emission Scanning Electron Microscopy

4.2.4.1. FESEM Analysis of SPL/ TCL

The FESEM images of SPL/TCL are depicted in Figure 4.15

SPL 700

SEM image analysis of SPL 700 indicates that the sample demonstrates an intricate connected porous architecture with porosities varying from 15.4 µm to 16.3 µm. This substantial porosity is predominantly useful for supercapacitor applications such as offering large surface area for absorption of electrolyte ions and enhancing ion transport. Through a network of pores, the internal surface becomes more available and a quicker diffusion extent for ions is attained which improves the capacitance. In addition, the moderate heating temperature of 700°C helps in the generation of mesopores, which are needed to enhance energy storage and power delivery in supercapacitors **(Taslim *et al.*, 2022; Fuertes and Sevilla, 2015)**.

SPL 800

From the SEM images of the SPL 800 sample, it can be seen that the material has a developed active porous network with pore size of 5.2µm to 7.2µm. Increase in thermal treatment temperature up to 800°C helps in enhancing the carbonization process which in turn results in the more appropriate and uniform structure of the pore. In addition to this, the presence of pores small in size compared to the SPL 700 sample shows an improvement in the micropore volume which is beneficial in enhancing the specific surface area and the material's energy storage capacity **(Chen *et al.*, 2014)**. Furthermore, the uniformity and interconnectivity of the pores enable fast ion transport, thus making it possible for supercapacitors to accumulate a high-power density.

SPL 900

The SEM image of the SPL 900 sample indicates a complex hierarchical porous structure with pore diameters ranging from 7.0 µm to 7.5 µm. At this elevated heating temperature, the carbonization synthesis process is more progressive, leading to a high extent of graphitisation and more stable carbon structure. The combined effects of micropores and mesopores in the hierarchical porosity aim to improve the energy density and power density of the supercapacitors. Micropores are significantly contributing to high capacitance owing to the improved surface area, whereas mesopores enable ion transport and help in alleviating internal resistance **(Zhu *et al.,* 2011)**. However, the high temperature graphitization at 900°C improves the material's conductivity which increases the performance as a supercapacitor electrode.

TCL 700

SEM images of the biomass carbon TCL 700 demonstrate highly open pore structure with connected pores. The investigated pore sizes were 5.2 µm to 7.1µm. When it comes to applications in supercapacitors, the presence of this well-developed porous network helps in ion transport and charge storage due to enhanced surface area **(Liu *et al.*, 2010).**

TCL 800

The SEM image of the biomass carbon TCL 800 sustains the development in porosity of architecture when compared with that of TCL 700. The pores are well-defined and their size varies from 5.9 µm to 7.7 µm. The enhancement in pores size and surface area at this temperature is advantageous for supercapacitors as it aids in providing more electroactive sites for electrochemical processes **(Zhang *et al.*, 2010).**

TCL 900

The biomass carbon sample TCL 900 SEM image is presented with a structure which is very graphitic and has a highly ordered hierarchical porous network. The pore ranges from 7.0 µm up to 7.9 µm. This hierarchy of porosity including both micropores and mesopores is promising for supercapacitors achieving both high energy density and power density **(Wang *et al.*, 2011).**

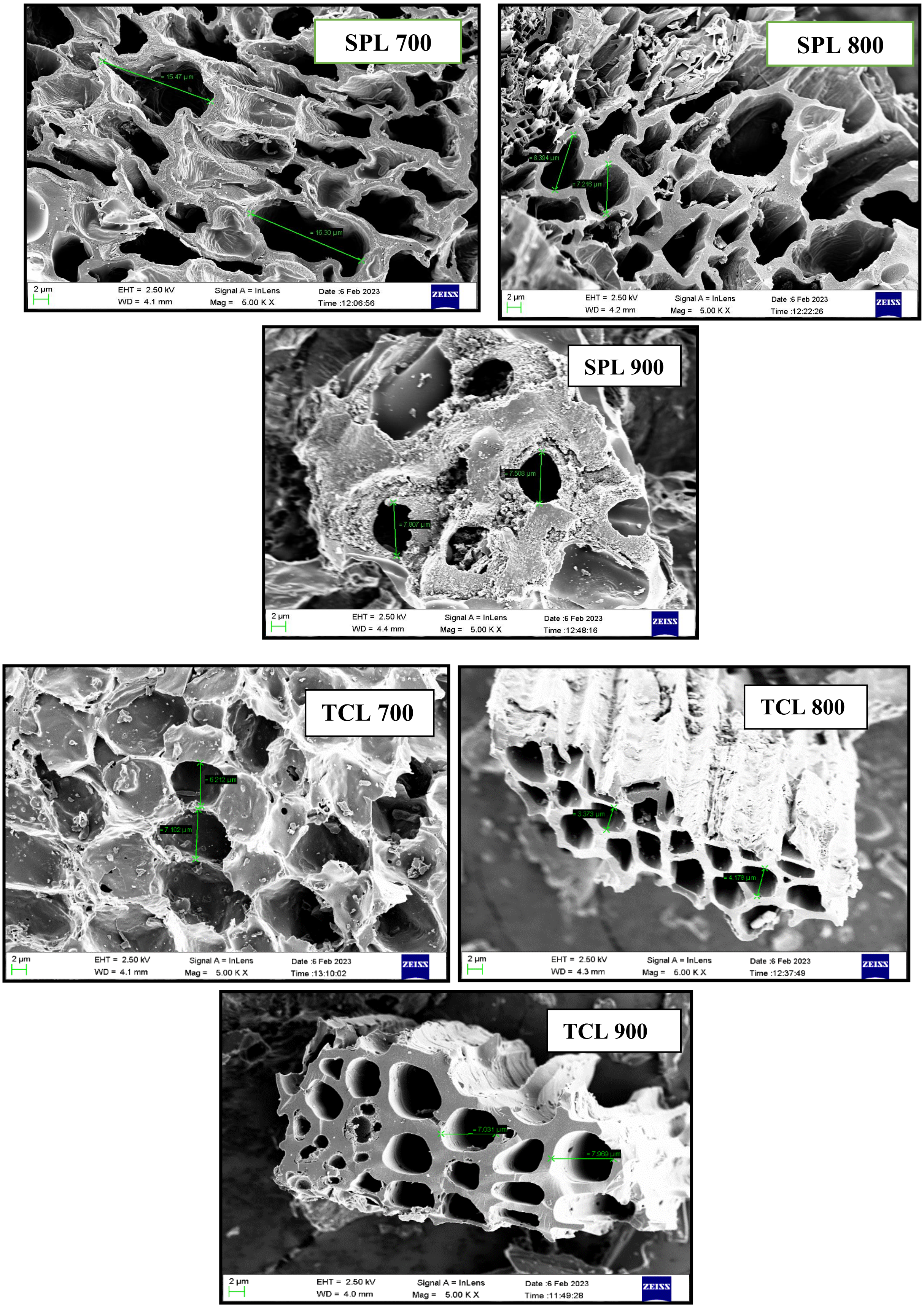

Figure 4.15: FESEM images of SPL- 700, SPL- 800, SPL-900, TCL-700, TCL-800, TCL- 900

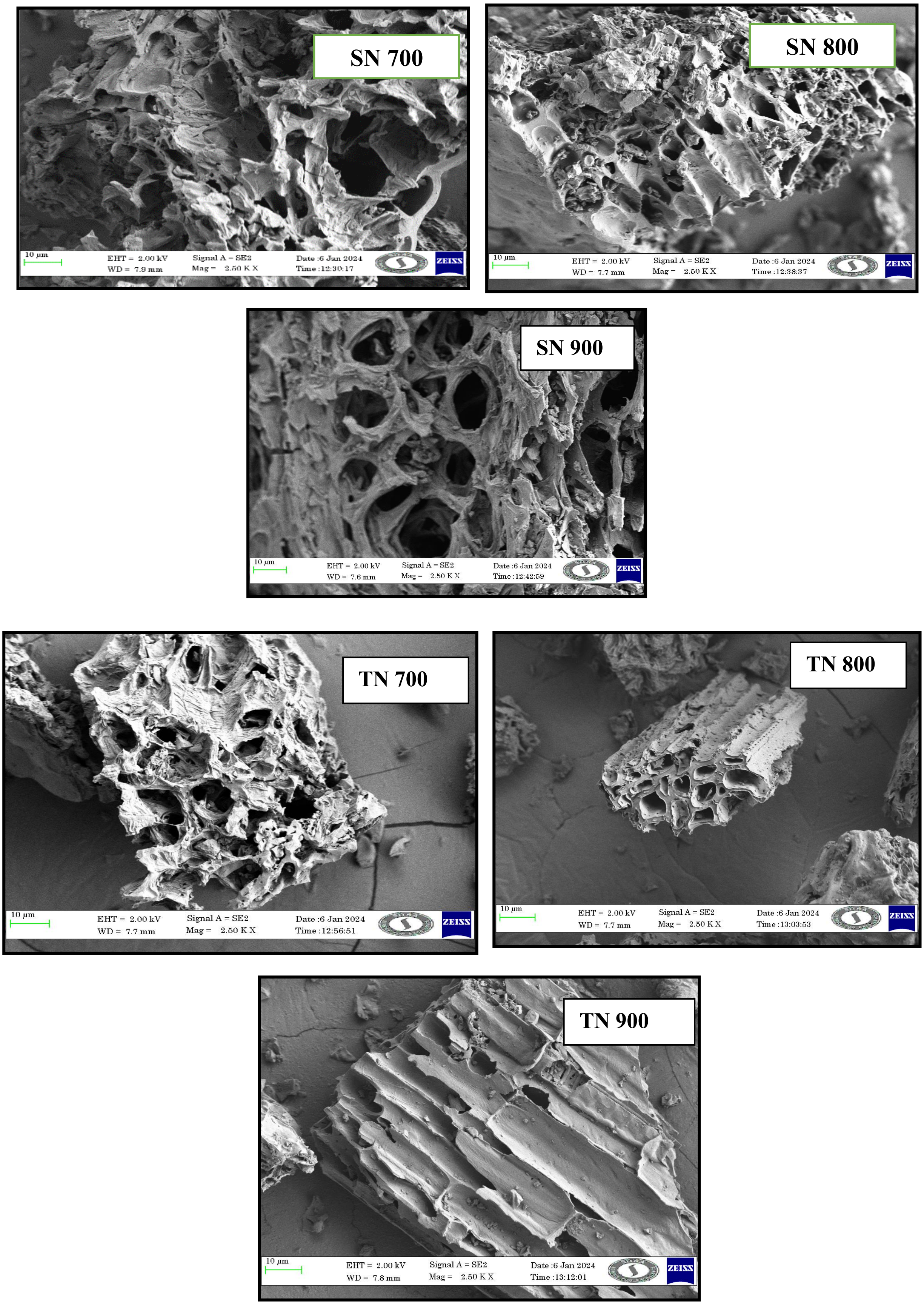

Figure 4.16: FESEM images of SN- 700, SN- 800, SN-900, TN-700, TN-800, TN-900

4.2.4.2. FESEM Analysis of SN/ TN

The FESEM analysis of SN/TN are depicted in Figure 4.16

SN 700

The SEM image of the SN 700 sample clearly indicates the porous structure with extensive surface roughness. This macroporous structure can clearly indicate the improved textural properties on the application of nitrogen doping treatment on the carbon. It is observed that carbonization at 700°C generates well developed porous material for energy storage devices such as supercapacitors, batteries, etc. Such porous structure is beneficial in the transportation of ions and electrons thus improving the electrochemical activity of the material. The pore diameter has a range of 10 – 20 μm affording a high surface area **(Asih *et al.*, 2024, Guo *et al.*, 2017, Qiu *et al.*,2024)**.

SN 800

The SEM image of the SN 800 sample shows a more defined porous structure related to SN 700. A more regular distribution and slightly larger diameters of the pores with a range between 15 μm to 25 μm were observed. This implies that a carbonization temperature of 800°C generates further enhancement and optimization in the pore architecture of the sample. The structural characteristics in this temperature could enhance the adsorption properties of the material making it appropriate in the field of gas storage or filtration. The surface morphology revealed the existence of graphitic areas which is advantageous for electrical conductivity **(Wu *et al.*, 2013)**.

SN 900

The SEM image of the SN 900 has an extensive porous network structure with refined pore sizes averaging between 20 and 30 μm. The carbonized material at 900°C shows improved surface area and pore volume for a carbon material that are useful in energy storage and catalysis applications. The well-defined porous framework promotes effective mass transfer and presents a substantial number of active sites for interactions that promote chemical changes. The increase in carbonisation temperature development of graphitic structures embedded in the carbon matrix enhances the strength and conductivity of the carbon materials **(Kolla *et al.*,2012).**

TN 700

The SEM image of the TN 700 sample shows a porous structure with large macropores. The carbonization process at 700°C enables the incorporation of these porous frames, which are useful for several electrochemical devices. The existence of macro pores ranging between 10 to 15 µm increase its surface area making it ideal for utilization in supercapacitors and catalytic activities. These pores offer sufficient area for electrolyte ions to penetrate the electrode material, which is essential in high-performance energy storage devices **(Gnawali *et al.*, 2023; Qiu *et al.*, 2024)**.

TN 800

The SEM image of TN 800 illustrates a well-organized and complex pore structure than that of TN 700. The pores are greater in size and more uniform, with the diameters lying between 15 and 20 µm. This specifies that carbonization at 800°C results in the further improvement of the porous structure. Such a structure is quite useful where high surface area and rapid mass transport are required such as in gas storage, gas separation as well as in electrochemical capacitors. At this temperature, the increased porosity and surface area notably enhance the quality of the material, which offers effective sites for ion adsorption and charge storage. The presence of graphitic regions in the carbon framework has improved the electrical conductivity of the material which is important for advanced energy storage systems **(Hou *et al.*, 2022; Kalpana & Lee., 2016; Xiong *et al.*, 2022)**.

TN 900

The SEM image for TN 900 sample displays a complex pore structure where the sizes of the pores range from 20 to 25 µm. Carbonization at temperatures of 900°C produces a material that has a remarkable amount of surface area and interconnected porous structure. This structural feature offers benefits in the application of energy devices, catalysis, and adsorption **(Fayanto *et al.*, 2018; Yuan *et al.*, 2024; Fang *et al.*, 2016; Astrakova 2012)**.

Discussion

The SEM images of the biomass carbon heated at 700, 800, and 900°C reveal certain notable morphological features, which are imperative for supercapacitor systems.

All the three temperatures exhibit well- defined porous structures, which help in ion movement and give a large surface area for charge accumulation. Besides, higher temperatures make the biomass carbon possess higher degree of porosity and graphitization thereby improving the electrochemical properties of the biomass carbon materials and making them suitable for supercapacitor electrodes. The increased graphitization at 900°C enhances the electrical conductivity of the carbon material, which is essential for reducing internal resistance and improving the charge-discharge efficiency of supercapacitors therefore we anticipate high specific capacitance for these samples.

The SN/TN sample exhibited a finer distribution of microporous and mesoporous structures on the pore walls. By incorporating urea as a nitrogen source into the SPL/TCL sample, urea decomposes at high temperatures, producing NH_3 and CO_2 gases as indicated by the reaction:

$$CO(NH)_2+H_2O \rightarrow 2NH_3+CO_2$$

As the gas escapes, it forms pores at its original location. The resulting ammonia gas further interacts with the biomass carbon, described by the reaction:

$$C+NH_3 \rightarrow HCN+H_2$$

Additionally, hydroxyl (–OH) and carboxyl (–COOH) groups on the biomass carbon surface react with ammonia gas, leading to the formation of amino functional groups. Consequently, the SN/TN sample demonstrated a more compact and orderly porous structure compared to the SPL and TCL samples. The number of pores within a specific area and the micropores on the pore walls significantly increased compared to those of the SPL and TCL samples. Interestingly, the TN/SN sample porous structure with large pores resembled that of the SPL/TCL sample, enhancing its contact area with electrolyte ions. The compact pore structure of TN/SN facilitated numerous channels for ion transport, thereby improving its ion transport rate. Furthermore, the high degree of graphitization observed in SN 900/TN 900 samples- as already noticed in XRD and Raman results- improve the material's electrical conductivity and mechanical strength, making it a promising candidate for high-performance energy storage devices and as a catalyst support in various chemical reactions **(Yue *et al.*, 2022)**.

4.2.5. EDAX Analysis

4.2.5.1. EDAX Analysis of SPL/TCL

The EDAX analysis of SPL/TCL are illustrated in Figure 4.17 and tabulated in Table 4.8

SPL 700

The Energy Dispersive X-ray Analysis (EDAX) of the SPL 700 sample reveals a carbon content of 69%, indicating a substantial degree of carbonization at 700°C. The oxygen content is 17%, suggesting the presence of oxygenated functional groups. The nitrogen percentage of 12% could be helpful in improving the electronic properties and surface chemistry of the carbon material enhancing its effectiveness in energy storage devices including supercapacitors and batteries. Trace elements like potassium (K) and calcium (Ca) constitute 2% only, which may serve as activation agents during the carbonization process, increasing the porosity of the material as well **(Pothaya *et al.*,2024)**.

SPL 800

In the SPL 800 sample, the EDAX results for the carbon content were 63%, less than SPL 700 but notable increase in 28% of oxygen content. The increase in oxygen because of the high temperature promotes the oxygen containing groups formed to be more stable and therefore improving the wettability of the materials in electrochemical devices. The nitrogen content has also been found to be 18%, suggesting enhanced nitrogen incorporation which will improve the pseudo capacitance. The trace elements have been reduced to 1%, an indication whereby higher temperatures have a purifying effect that would preferably enhance a more graphitic and conductive structure **(Nuradi *et al.*, 2022)**.

SPL 900

The EDAX analysis of SPL 900 shows a very high carbon content of 81% signifying that increase in the carbon content implies higher degree of carbonization at 900°C. The reduction in the oxygen value to 12% indicates loss of oxygenated groups, which increases the graphitic nature and the electrical as well as structural integrity. The nitrogen content drops to 6% suggesting certain nitrogen functionalities might be lost at elevated temperature which may modify the surface activity. The residual nitrogen can still contribute to the electrochemical attributes of the material. The trace constituents remain at 1% affirming contamination for key applications with high purity carbon materials **(Nuradi *et al.*, 2022)**.

TCL 700

The EDAX data for TCL 700 shows carbon content of 70% implying good carbonization at 700°C. The carbon-oxygen ratio is low with the oxygen content being 18% which indicates the existence of surface oxygenated functional groups on the material surface. The nitrogen at 10% which will enable the material to improve its electronic conductivity and surface reactivity. Potassium and calcium are present in trace amounts 2% and their presence could be catalysts in the process of carbonization assisting in producing porous structure **(Periyasamy *et al.*, 2023)**.

TCL 800

For TCL 800, EDAX analysis reveals a carbon content to be 69% similar to the TCL 700 while oxygen content is sustained at 18%. The increase in the oxygen content shows that functional groups that play an important role in the electrochemical features of the material have been retained. The nitrogen content is increased to 11% thus increasing the capacitance and catalytic activity of the material. The minor elements still remain constant in the proportions of 2%, suggesting their effective catalytic activity at this temperature during carbonization **(Xue *et al.*, 2022).**

TCL 900

The EDAX analysis of TCL 900 exhibits that carbon content is about 70%, demonstrating high carbonization efficacy at 900°C. The oxygen level decreases slightly to 17%, supporting decomposition of less stable oxygen groups generating more graphitic layers which improves conductivity. The nitrogen level is kept at 12%, suggesting availability of nitrogen groups that improve the material’s electrochemical activity. The trace elements are diminished to about 1% indicating that high temperatures have some purification effect owing to more crystalline structure for efficient carbons applications **(Kang *et al.*, 2021)**.

4.2.5.2. EDAX Analysis of SN/TN

The EDAX analysis of SN/TN are illustrated in Figure 4.18 and tabulated in Table 4.9

SN 700

The EDAX analysis of SN 700 shows that carbon content to be 57%, oxygen for 23%, nitrogen present at 18% and the trace elements potassium and calcium account for 2%. Relatively high quantity of nitrogen indicates adequate nitrogen doping of the material, which is crucial for improvement of the electrochemical characteristics including electrical conductivity, as well as the active sites of the material. Oxygen and trace elements may facilitate the development of the functional groups, which would enhance the total capacitance and energy storage properties **(Zhao *et al*., 2005)**.

SN 800

For EDS in SN 800, the carbon content slightly reduces to 54%, whereas oxygen content is at 29%, nitrogen is at 16% and trace elements decrease to 1%. The high oxygen content at this temperature of pyrolysis indicates that there is the addition of more oxygen containing functional groups, which promote the penetration as well as the surface area essential in electrochemistry. Although there is an insignificant reduction in nitrogen level, it is still sufficiently high for the retention of better electrochemical properties **(Sarma *et al*., 2022)**.

SN 900

In SN 900, the carbon content is further reduced to 52% with 27% of oxygen, 19% of nitrogen and 2% of trace elements. Compared to the other materials, this carbon content appears to be low, however, the high level of nitrogen incorporation (19%) is remarkably notable, as it can enhance the performance of this material used in supercapacitors and batteries due to the increased pseudo capacitance and charge transfer in the device. The stable presence of trace elements shows the formation of functional groups which is favorable for the stability of the material **(Toprak 2020; Rahaman & Kar 2011).**

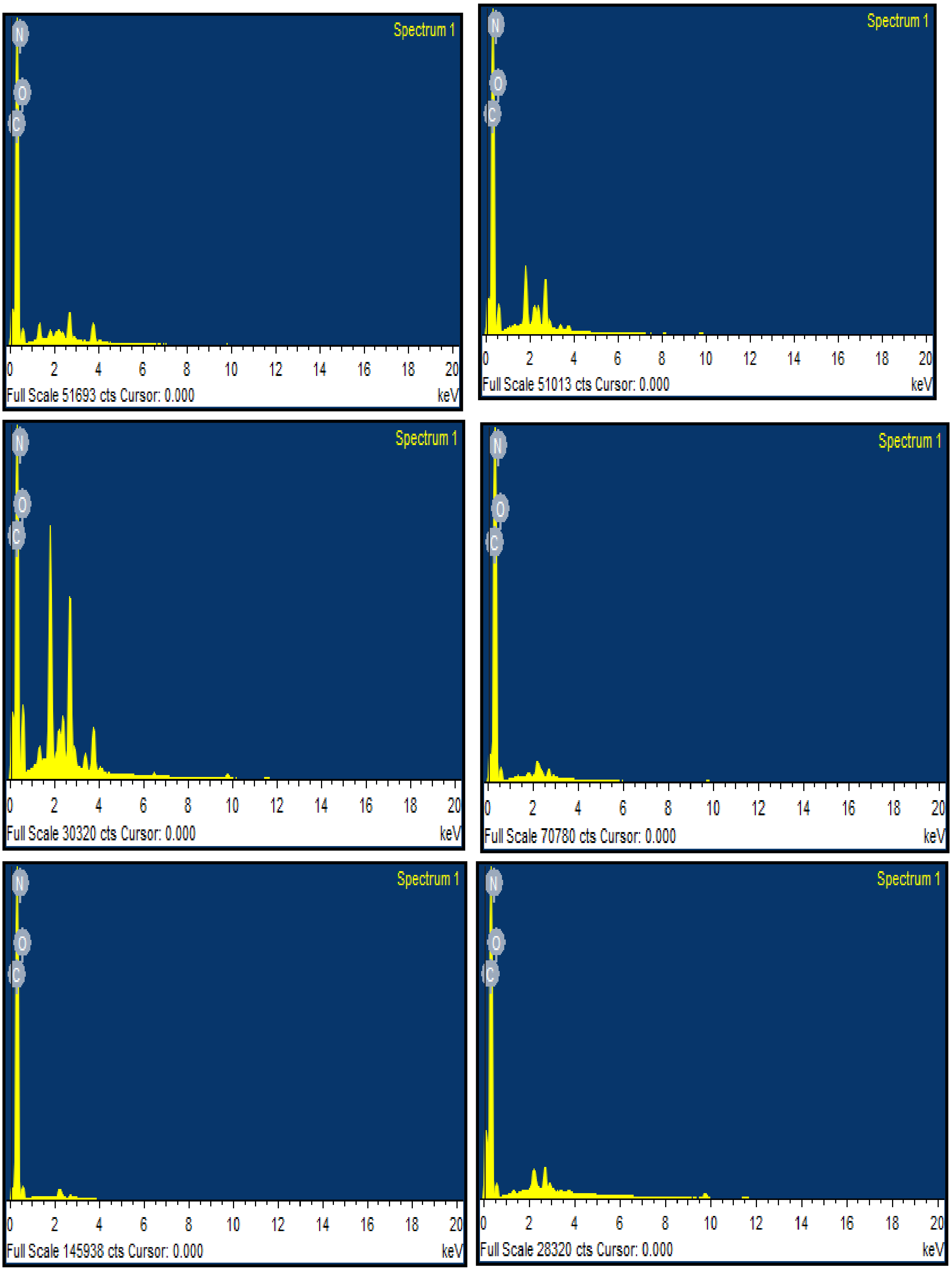

Figure 4.17: EDAX analysis of SPL- 700, SPL- 800, SPL-900, TCL-700, TCL-800, TCL-900

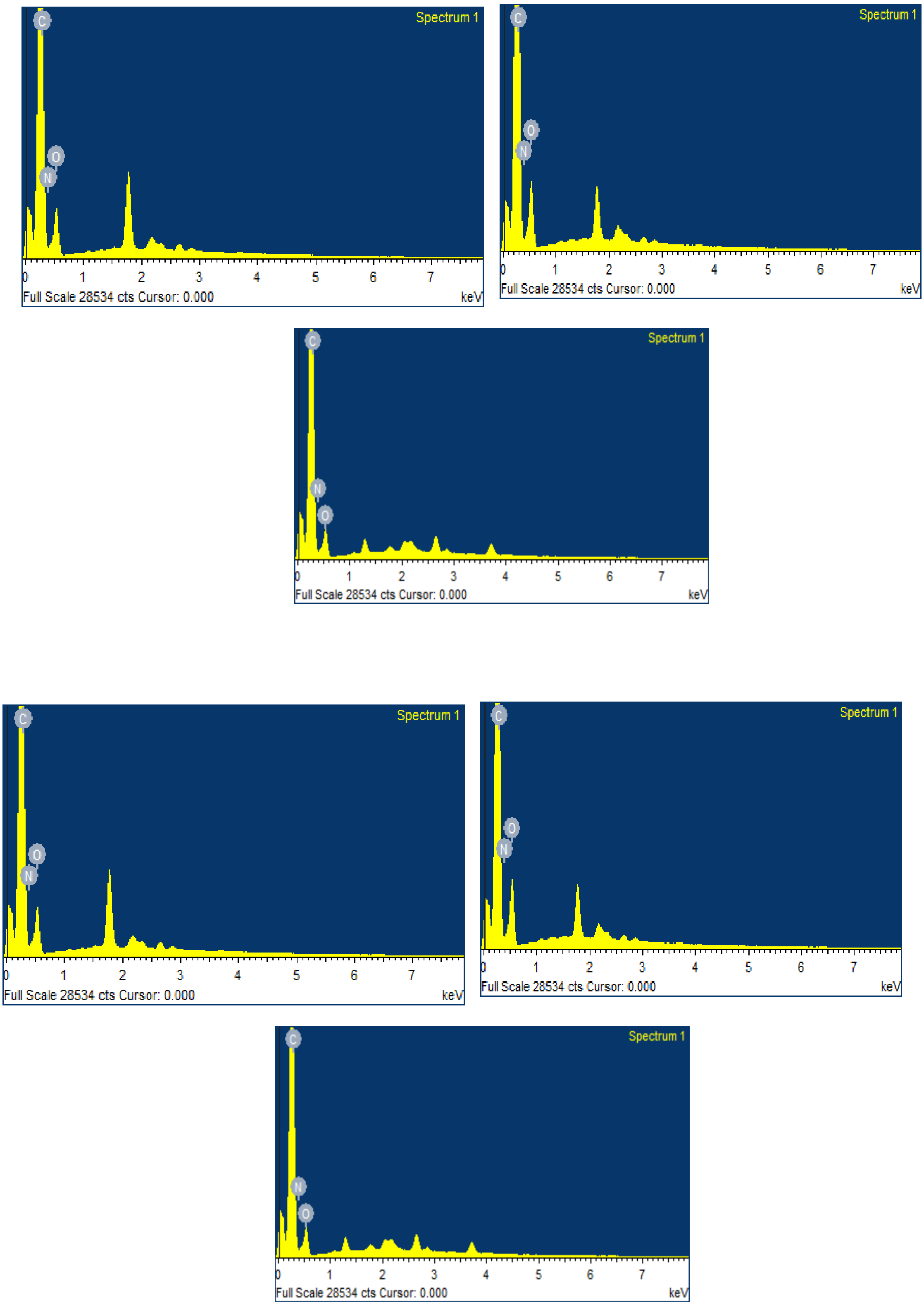

Figure 4.18: EDAX Analysis of SN- 700, SN- 800, SN-900, TN 700, TN 800, TN 900

TN 700

EDAX analysis of TN 700 shows the carbon content is 65%, oxygen 20%, nitrogen 15%, and other elements are 2%. It indicates better formation of the carbon matrix during pyrolysis than in the SN series. The 15% of nitrogen content suggests sufficient doping which can be useful in improving the electronic property and generating defect sites that would be beneficial as a catalyst and for energy storage **(Sarma *et al.*, 2022)**.

TN 800

In TN 800, the carbon content is 60%, oxygen 25%, nitrogen 15%, with 2% as trace elements. The increased oxygen content at this higher temperature suggests that more oxygenated functional groups have been formed which can increase the hydrophilicity and also the electrochemical performance of the material. The nitrogen content in the material remains constant and thereby enabling the material with enhancement in the electrochemical properties **(Sarma *et al.*, 2022)**.

TN 900

For TN 900, the carbon content is 59% oxygen is 23% nitrogen is 17% and other elements are 1%. Since the nitrogen content in this sample 17% is higher than all the other samples in the TN series, this implies that sample may show improved electrochemical performance due to higher pseudo capacitance and conductivity. A slight decrease in the trace elements may indicate a pure carbon matrix which can result in high stability of the material **(Sarma *et al.*, 2022).**

Table 4.8: EDAX Analysis of SPL- 700, SPL- 800, SPL-900, TCL-700, TCL-800, TCL-900

Precursors	C%	O%	N%	K %	Ca%	Mg%	Cu%
SPL 700	69	17	12	0.6	0.8	0.2	0.4
SPL 800	63	18	18	0.55	0.3	-	0.2
SPL 900	81	12	6	0.65	-	-	0.4
TCL 700	70	18	10	0.62	0.63	0.4	0.4
TCL 800	69	18	11	1.9	-	-	0.1
TCL 900	70	17	12	0.7	-	-	0.3

Table 4.9: EDAX Analysis of SN- 700, SN- 800, SN-900, TN-700, TN-800, TN-900

Precursors	C%	O%	N%	K %	Ca%	Mg%	Cu%
SN 700	57	23	18	0.95	0.40	-	0.6
SN 800	54	29	16	0.85	-	-	0.2
SN 900	52	27	19	1.25	-	-	-
TN 700	65	20	15	0.05	-	-	-
TN 800	60	25	15	-	-	-	-
TN 900	59	23	17	0.23	0.53	0.23	0.1

4.2.5.3. Colour Mapping of Nitrogen-Doped Biomass Carbon

The Series of color mapping images of nitrogen-doped biomass carbon (SN 900, TN 900) reveal the elemental distribution of the material. These images show the presence and the arrangement of oxygen (O), carbon (C), and nitrogen (N) within the biomass carbon matrix. This information is vital for better understanding the structural and functional features of the material beneficial in energy storage and catalysts.

The blue color map presents the arrangement of oxygen in the samples of the SN 900, TN 900 series. Over the carbon matrix, the oxygen is distributed consistently, indicating that the biomass carbon has been oxidized or functionalized uniformly. Such uniformity is vital to enhance the surface properties and induce active sites for electrochemical reactions.

The red color map reveals the content of carbon, a major constituent of SN 900, TN 900 sample. The high intensity of red color observed in the sample indicates the carbon content is supposed to be high, which is typical of carbon structures of biomass origin. The continual carbon interface is necessary to provide electrical conductivity and structural support.

The nitrogen dopants are distributed in the green region within the SN 900, TN 900 sample materials represented in color mapping images. The nitrogen doping is relatively even, which is important in improving the electrochemical property. Nitrogen functional groups enhance the electron conductivity, offer active centers for the reactions, and further increase the carbon surface's hydrophobicity.

These color mapping images of nitrogen-doped biomass carbon (SN 900, TN 900) offer significant information of element arrangement of the material. The carbon, oxygen and nitrogen displays a homogeneously dispersed matrix, essential for electrochemical applications. These observations endorse the prospects of SN 900, TN 900 as comprising advanced materials for energy storage and also catalytic applications **(Duarte *et al.,* 2021 & Liu *et al.,* 2020).**

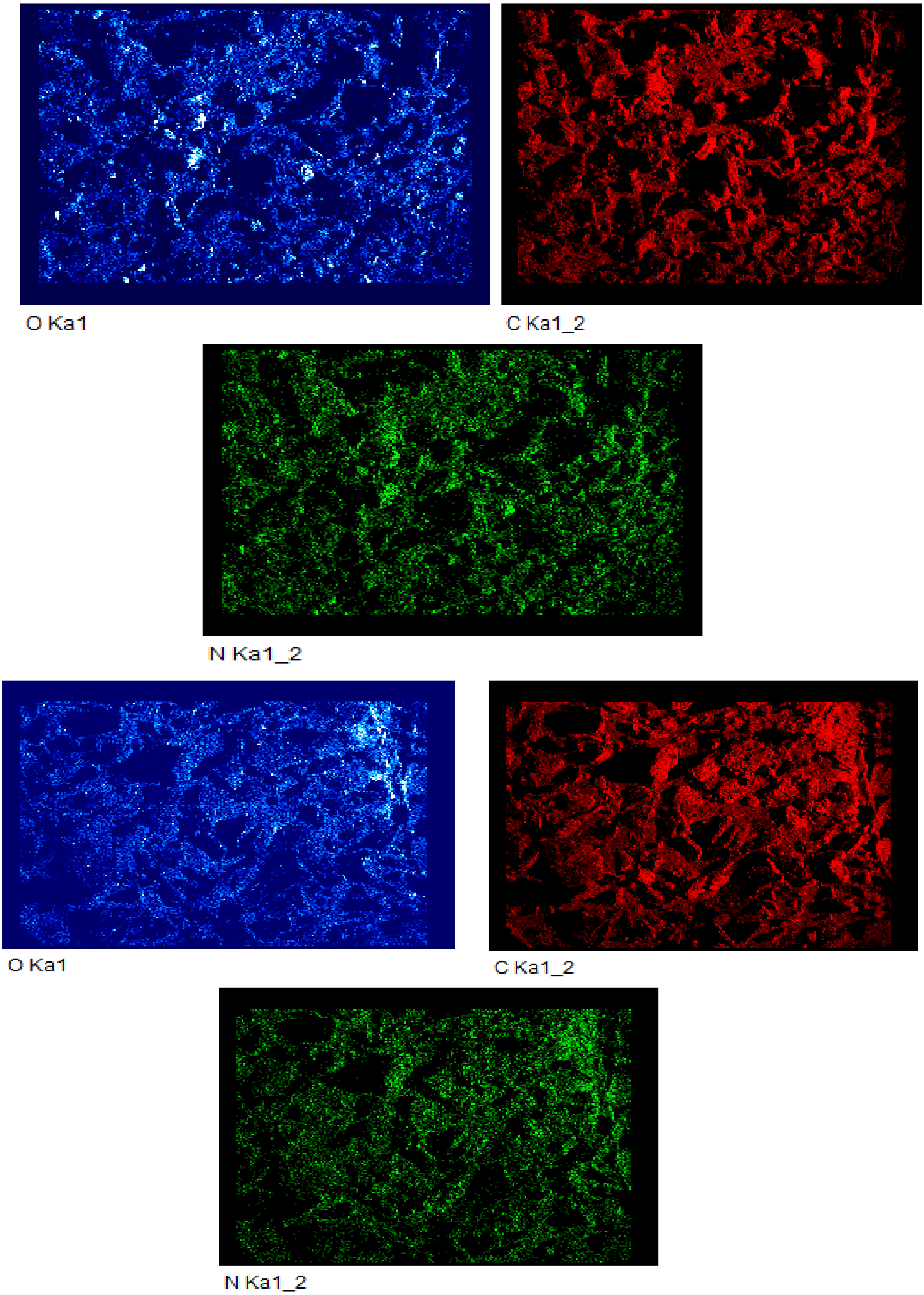

Figure 4.19: Colour mapping images of SN 900, TN 900

4.2.6. TEM Analysis

4.2.6.1. TEM Analysis of SPL:

Carbon structural analysis which was carried out by TEM in regard to SPL carbon in Fig (4.20) reveals a disordered hierarchically porous structure that possesses both mesopores and micropores. The existence of numerous white spots within the disordered carbon sheets confirms that the carbon from SPL leaves consist of many micros and mesopores, which are impregnated with enough nitrogen (**Duc-Luong Vu *et al.*, 2017**).

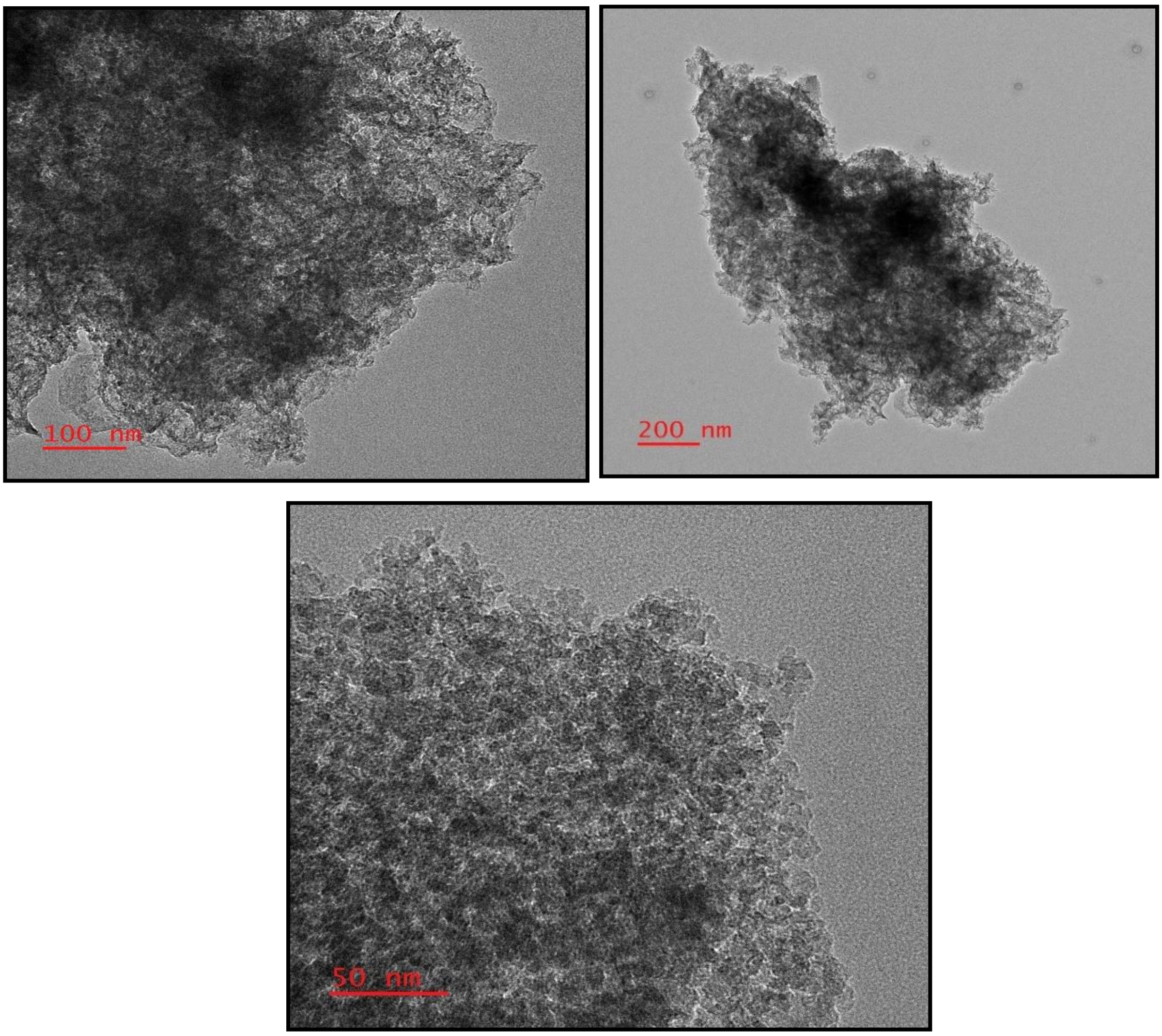

Figure 4.20: TEM images for SPL- 900

4.2.6.2. TEM Analysis of TCL:

The porous structural feature was further confirmed by TEM as shown in Fig.4.21. The graphitic ordered structures with partial amorphous nature which were supposed to assist in providing edge defects/active sites for ion solvation/intercalation or electrolyte adsorption. From the TEM images, it can be seen that the temperature of carbonization and the precursors logically do not influence the porous structures that are relatively evenly distributed with varying sizes of pores. **(Cheng *et al.*, 2018).**

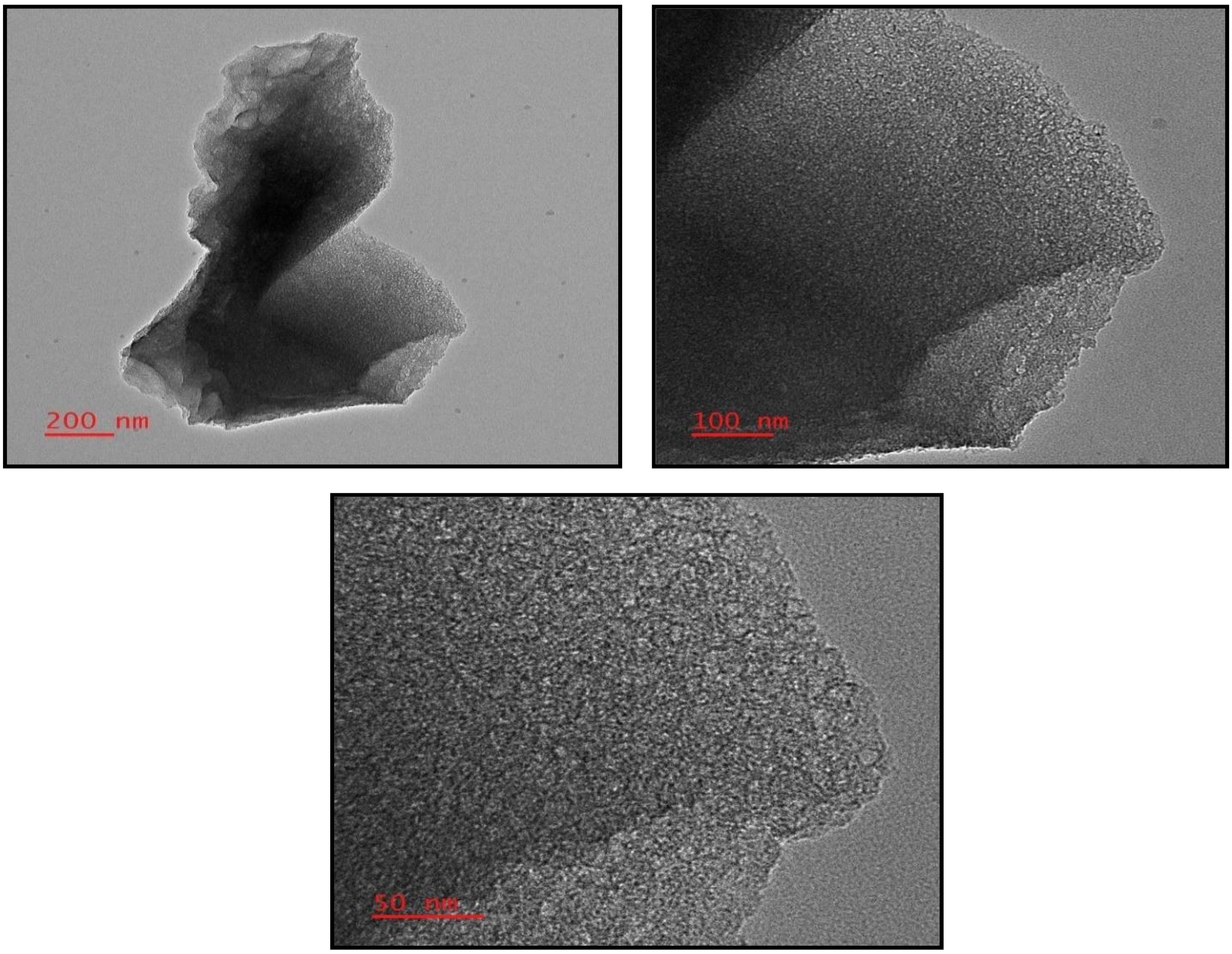

Figure 4.21: TEM images for TCL-900

4.2.6.3. TEM Analysis of SN:

The high-resolution transmission electron microscopy (HRTEM) was employed to evaluate the structure of the SN. Figure 4.22 depicts the clusters of the smallest particles that are about 50 nm in size. It can be seen that the selected area electron diffraction (SAED) ring patterns indicate an amorphous nature of the material. From SEM images, it was shown at various magnification level images displaying rough surface and pores of the carbon materials.

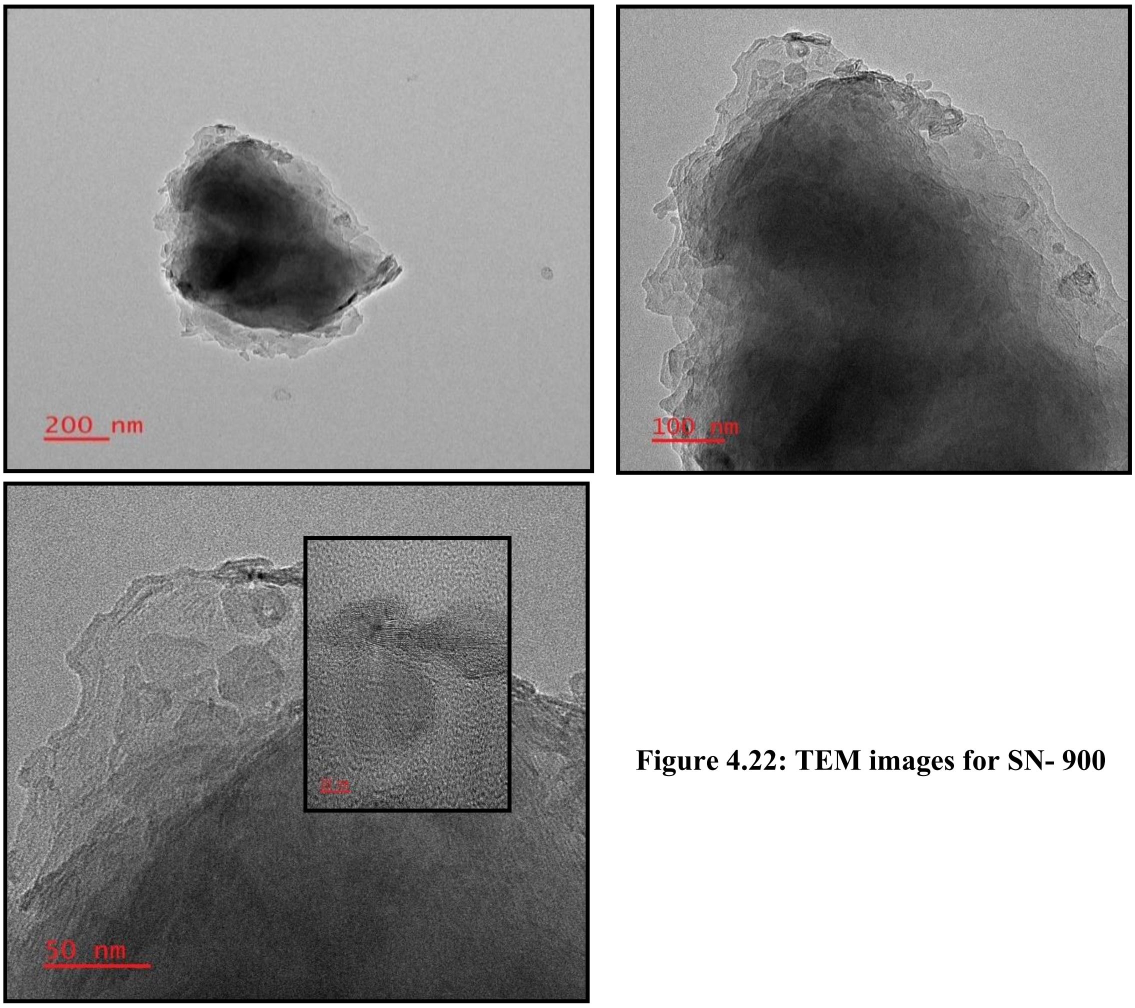

Figure 4.22: TEM images for SN- 900

4.2.6.4. TEM Analysis of TN:

The images (Figure 4.23) show that the TN carbon material has a profusely disordered pore structure, and the tendency of the graphene structure can be distinctly observed at the edge of the carbon material. This architecture ensures that both carbon materials have capacity for charge storage and rapid transfer of ions. (**Zhang *et al.,* 2017**).

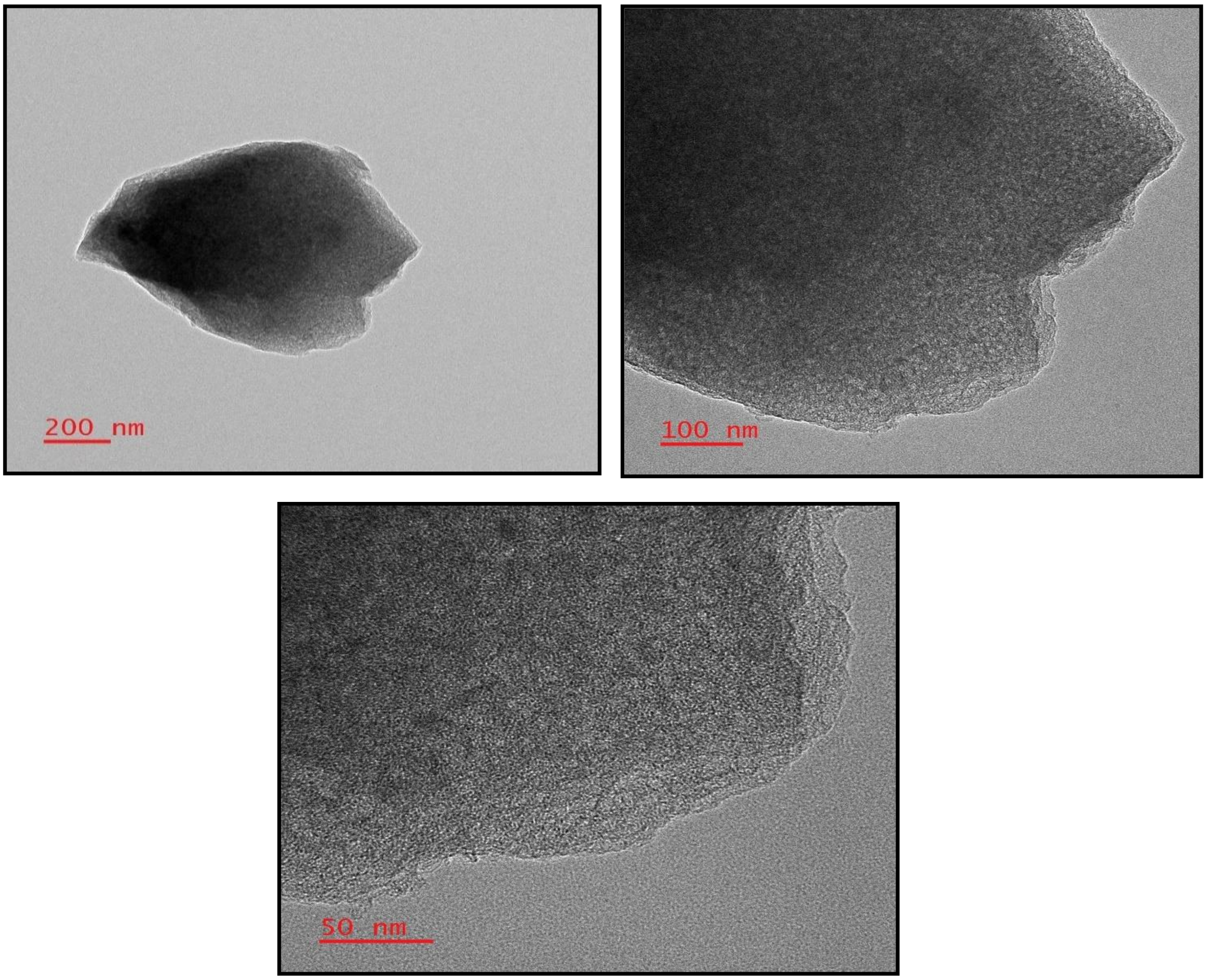

Figure 4.23: TEM images for TN-900

4.2.7. BET Analysis

4.2.7.1. BET Analysis of SPL 900

The BET (Brunauer-Emmett-Teller) studies of the biomass-derived carbon sample (SPL 900) provide valuable insights into the structural characteristics. In addition, Figure 4.24 reveals the adsorption-desorption isotherm of sample SPL 900, which is a type IV isotherm. indicating the presence of mesoporous structures. The specific surface area of 111.8 m^2/g, along with the total pore volume of 0.19 cm^3/g and the average pore diameter of 7.06, aid the efficacy of the materials for modern high performance electrochemical devices.

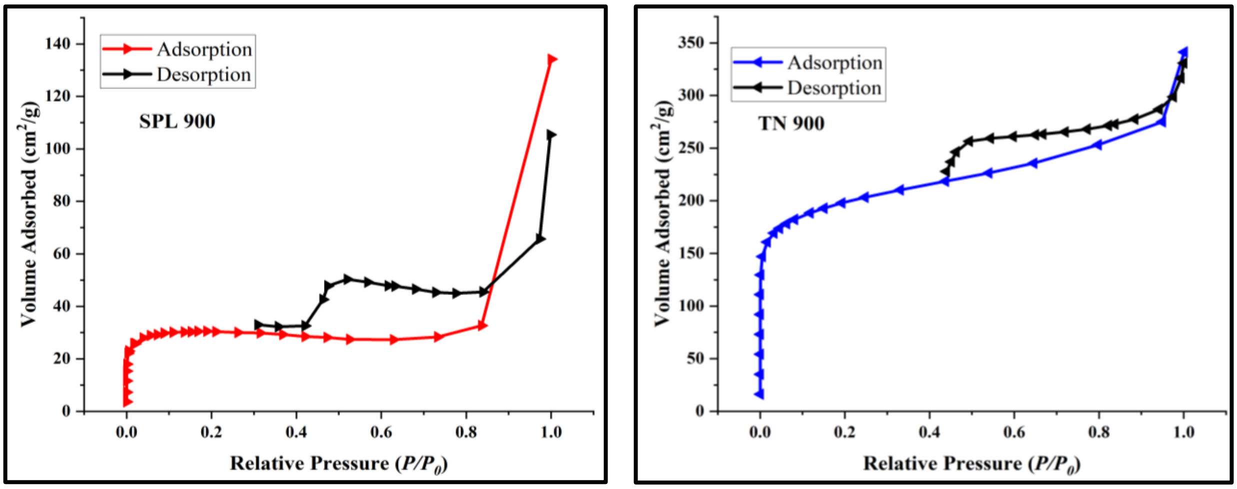

Figure 4.24: Adsorption and Desorption isotherm of SN 900, TN 900

Rapid adsorption occurs within the relative pressure range of ($P/P_0 < 0.1$), indicating the presence of micropores that provide a high surface area to facilitate efficient ion adsorption of an electrolyte. The hysteresis loop in the relative pressure ranges from 0.4 to 1.0 is consistent that the material is mesoporous which assists in ion movement and retards diffusion resistance. The steep increase in the adsorbed volume at high relative pressures shows the presence of larger mesopores or even macropores that will promote the available ions and storage of the material. The micropore and mesopore structures in hierarchical order possessed by SPL 900 allows adequate ion movement and diffusion thus retaining remarkable electrochemical activities **(Negi et al., 2022)**.

4.2.7.2. BET Analysis of TN 900

The BET analysis of nitrogen doped biomass derived carbon (TN 900) suggests comprehensive insights on structural characteristics, which is depicted in the adsorption-desorption isotherm (Fig. 4.24). A type IV isotherm is observed which is characteristic of mesoporous materials. The material possessed surface area 665.8 m²/g, total pore volume 0.50 cm³/g, and average pore diameter of 3.04 nm which confirms its potential for electrochemical applications **(Matsagar *et al.,* 2021; Zhou *et al.,* 2019).**

The rapid adsorption of the gas at low relative pressures (P/P0<0.1) which indicates the presence of micropore for the high surface area and enhances electrolyte ion adsorption. The hysteresis loops of adsorption and desorption at relative pressures from 0.4 to 1.0 enhances the mesoporous nature of the material, aids in ion intercalation and its mobility. The sharp increase at high relative pressure indicates the presence of large mesopores and macropore structures which make ions easier to access and provide more storage capacity. TN 900 material has hierarchical pore structure consisting of micro- and mesopores which allows enhancement of the performance of electrochemical devices through effective diffusion of ions **(Li *et al.,* 2024).** Comparison of BET surface area and specific capacitance of SPL 900&TN 900 with literature (Figure: 4.25) reflects the comparable nature of the synthesised carbon materials.

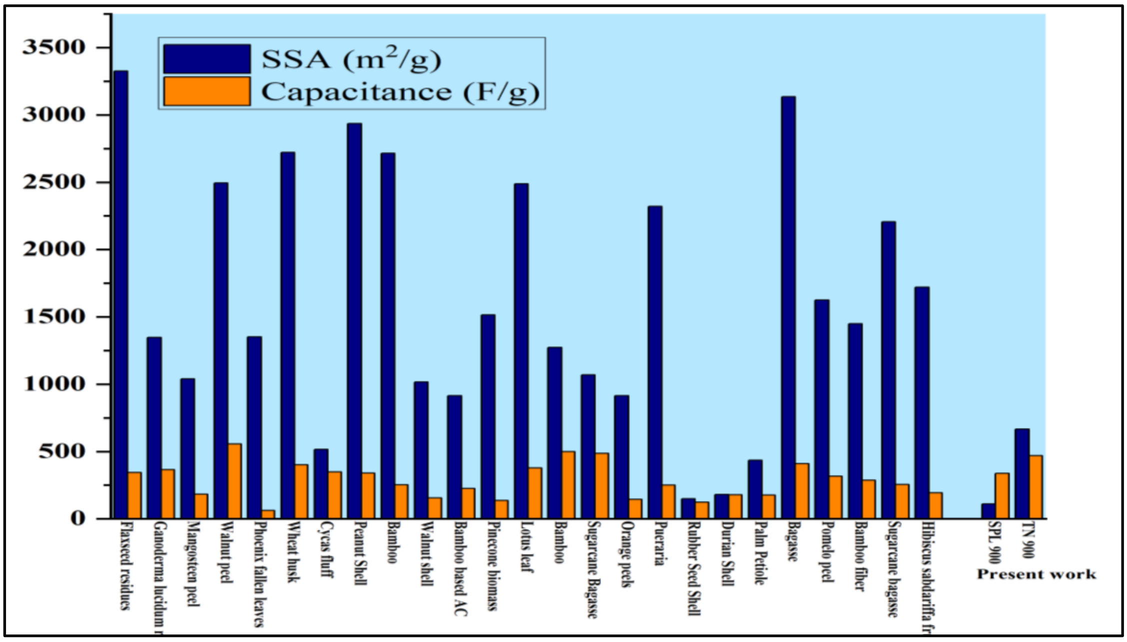

Figure 4.25: Comparison of BET surface area and specific capacitance reported in literature with SPL and TN carbon materials

4.3. PHASE III: Electrochemical characterization of SPL/TCL/SN/TN derived carbon materials for utilization of synthesized carbon materials in supercapacitor electrode applications

The distinctive properties of SPL, TCL, SN and TN suggest effective use in the electrochemical energy storage applications, particularly high-rate super capacitors. Capacitive performance of SPL/TCL/SN/TN has been investigated using three electrode systems in which 1 M sulphuric acid was used as the electrolyte. In this configuration, the electrode is loaded with the active material of about 1 mg which indicates that they are capable of being efficiently used in supercapacitors. The electrochemical behavior of the carbon is determined through the following tests:

- Cyclic Voltammetry
- Galvanostatic Charge and Discharge
- Electrochemical Impedance Analysis

4.3.1. Cyclic Voltammetry

Tests for cyclic voltammetry were performed on SPL/TCL/SN/TN prepared from carbon materials. The experiments are performed by utilizing varying scan rates between 5 to 50mV/s. While conducting this experiment, the potential window is between 0.3 and -0.2V. With this comprehensive approach, it is possible to evaluate the performance and electrochemical characteristics of each carbon material at different scan rates.

4.3.1.1. CV Profile of SPL/TCL

The cyclic voltammograms for SPL/TCL are illustrated in Figure: 4.26& 4.27 and the results are tabulated in Table 4.10.

SPL 700/SPL 800/SPL 900

The Cyclic Voltammetry (CV) curves for SPL 700 have quasi rectangular shapes indicating it exhibits characteristics of both EDLC and Pseudocapacitive nature. The specific capacitance values for SPL 700 at various scan rates (10 mV/s, 20 mV/s, 30 mV/s, 40 mV/s and 50 mV/s) are 241 F/g, 204 F/g, 138 F/g, 106 F/g and 88.3 F/g respectively. The decrease in specific capacitance with the increase of scan rate ascribed to the inadequate time for ion diffusion at higher scan rates which in turn limits the diffusion of the electrolyte ions into the inner pores of the carbon material. The specific capacitance was distinct at lower scan rates indicating that SPL 700 has a high surface area as well as a well-developed porous structure which is essential in effective charge storage **(Kibona., 2019).**

The quasi-rectangular nature of cyclic voltammograms obtained for SPL 800 indicates the presence of ideal capacitive behavior and low resistive losses. At scan rates of 10 mV/s, 20 mV/s, 30 mV/s, 40 mV/s, and 50 mV/s specific capacitance values of 225 F/g, 139 F/g, 229 F/g, 235 F/g and 193 F/g respectively. The reason for the increase in the specific capacitance at higher scan rates (30 mV/s to 50 mV/s) could be the presence of more electroactive sites in the electrode material that become active at higher scan rates. The SPL 800 sample has excellent rate capability indicating its potential for high power applicability **(Muramatsu *et al.*, 2020**).

A quasi-rectangular shape can be seen in the cyclic voltammetry of SPL 900, reflecting considerable pseudo capacitance. The specific capacitance at 10 mV/s, 20 mV/s, 30 mV/s, 40 mV/s and 50 mV/s of various scan rates were recorded as 928 F/g, 451 F/g, 355 F/g, 265 F/g and 196 F/g respectively. The capacitance was also substantial at lower scan rates (928 F/g at 10 mV/s), which implies a high level of redox active sites and effective charge storage. The decrease in specific capacitance with an increased scan rate suggests that the ion diffusion processes are more intense in the SPL 900, probably due to its porous structure and abundant electroactive sites. This distinctive characteristic of SPL 900 seems to be promising for a high capacity and stable energy storage **(*Lv et al.*, 2017 ; Wu *et al.*, 2020).**

TCL 700/TCL 800/TCL 900

The CV plots of TCL-700 sample display the presence of distinct redox peaks which support the pseudo capacitance behavior of biomass carbon due to the minor amount of trace elements (K, Ca, Mg) noticed in EDAX analysis. Incrementing the scan rate from 10 mV/s to 50 mV/s resulted in an increase in current response which is a typical capacitive behavior. The CV shapes are almost rectangular especially at lower scan rates indicating that efficient charge has been stored such that the electrochemical processes are stable. The values of specific capacitance lowers with increased scan rates from 10mV/s = 103F/g and at 50mV/s = 83F/g, this is attributed to low ion diffusion at high scan rates **(Bandaranayake *et al.*, 2016 & Salehifar *et al.*, 2015)**.

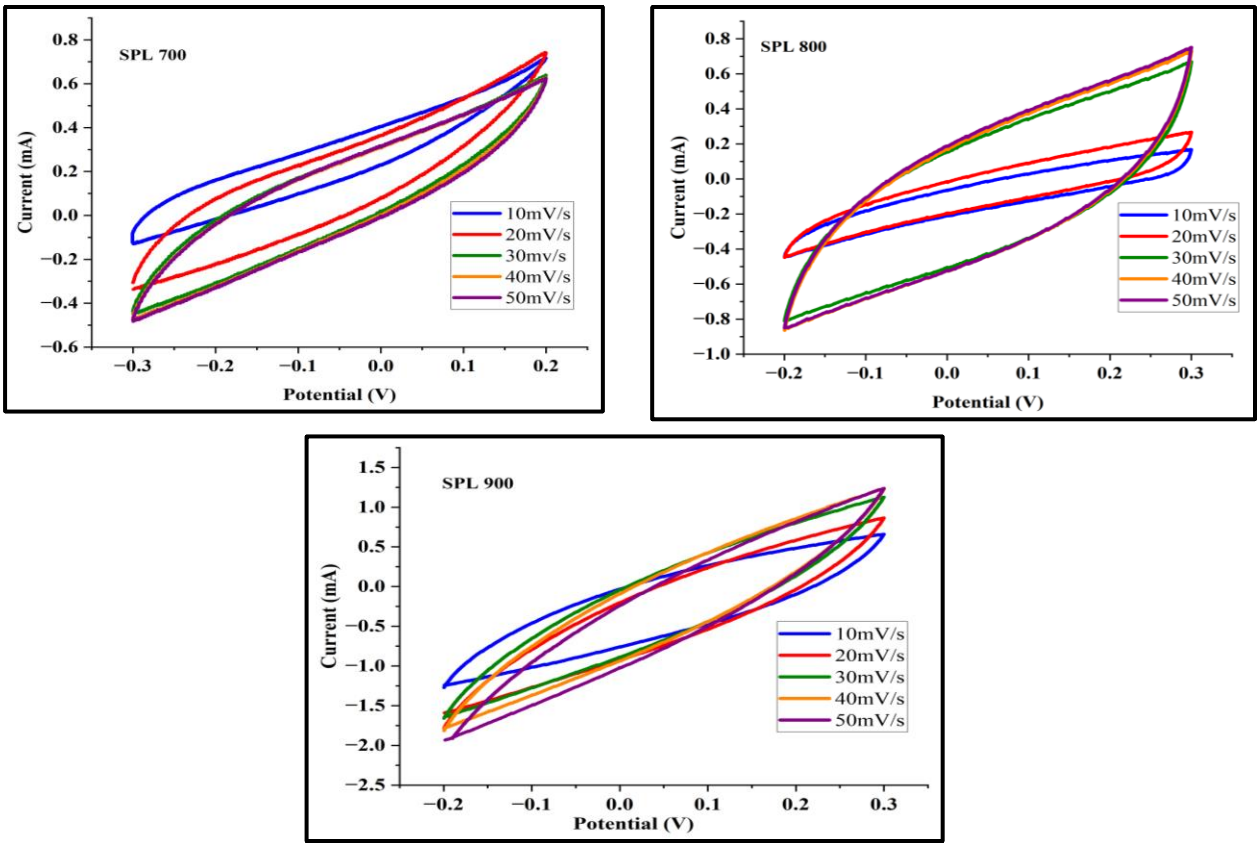

Figure 4.26: Cyclic Voltammetry for SPL- 700, SPL- 800, SPL-900

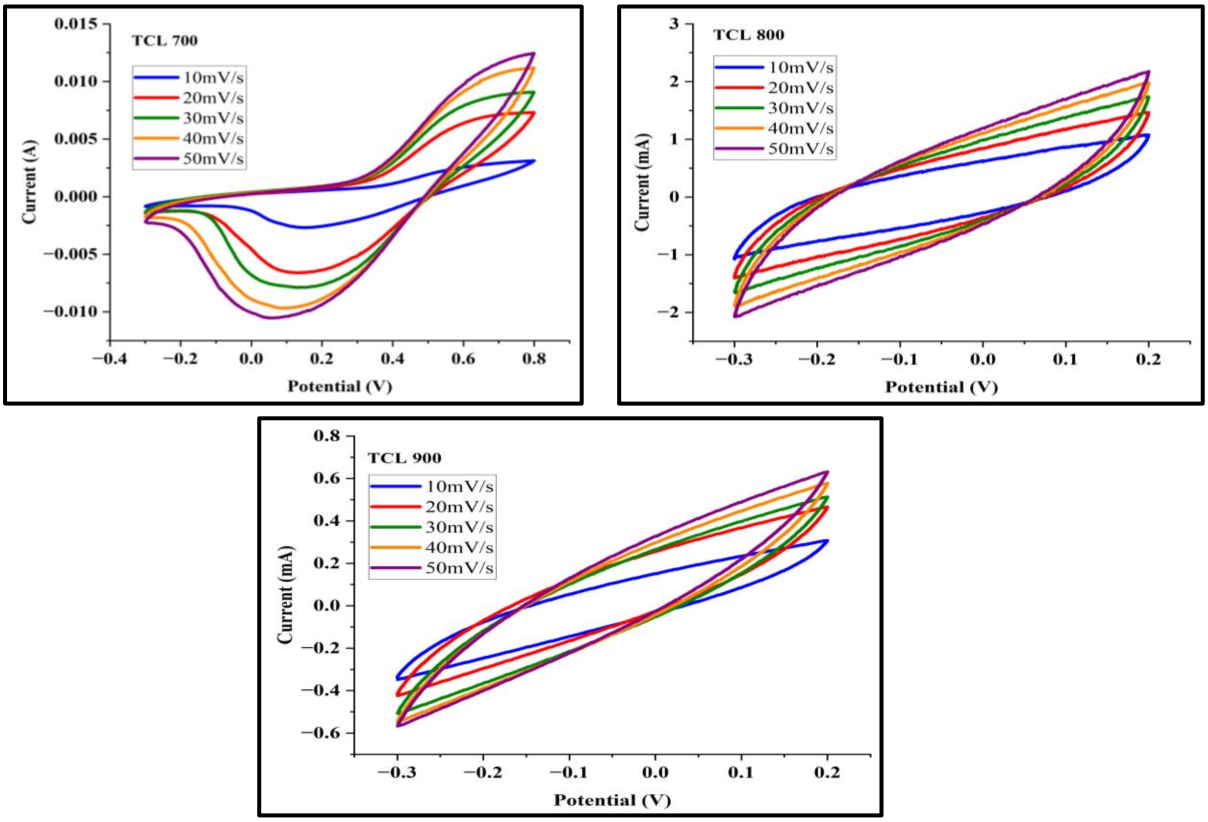

Figure 4.27: Cyclic Voltammetry for TCL- 700, TCL- 800, TCL-900

Regarding the TCL-800 sample, the CV curves exhibit quasi rectangular shapes representing a combination of electric double layer capacitance and pseudo capacitance. The specific capacitance drops from 121F/g under a potential scan rate of 10mV/s to 44 F/g at 50 mV/s suggesting that the sample has high-rate capability. The observed lower specific capacitance values with respect to TCL-700 were ascribed to the high temperature treatment which reduced the surface area and active charged storage sites as well the reduction of heteroatoms or functional groups impacting to provide pseudocapacitive effect **(Pellitero *et al.*, 2021 ; Omar *et al.*, 2016**).

The CV curves of the TCL-900 sample exhibit the largest current response among the three samples, suggesting the higher capacitive performance. The CV curves are nearly rectangular in shape at various scan rates implying predominant EDLC with minimal ion resistance towards diffusion. The specific capacitance at considerable scan rates ranging from 10 mV/s – 255 F/g to 50 mV/s – 89 F/g. These values can be ascribed to the ideal pore structure and conductivity of the treated sample **(Wang *et al.*, 2013 ; Aziz *et al.*, 2019).**

4.3.1.2. Cyclic Profile of SN/TN

The cyclic voltammograms for SN/TN are illustrated in Figure: 4.28& 4.29 and the results are tabulated in Table 4.10.

SN 700/SN 800/SN 900

The CV curves for the SN-700 sample can be characterized as quasi-rectangular shape revealing a pseudo capacitive nature. As the scan rate is increased from 10 mV/s to 50 mV/s, the current response increases, which is common for capacitive materials. The CV profiles show a rectangular shape especially at low scan rates implying enhanced electrochemical stability and excellent charge retention ability. Specific capacitance values also decrease from 309 F/g at 10 mV/s to 57 F/g at 50 mV/s due to the inadequate ion diffusion at high scan-rates. This trend implies that the material has a large number of active sites and surface area for charge storage **(Mir & Shah 2022)**.

For the SN-800 sample, the CV curves are close to quasi rectangular shapes and no redox peak exists indicating the contribution of both electric double layer capacitance and pseudo capacitance. It is observed that specific capacitance values reduce from 252 F/g at

10mV/s to 52 F/g at 50 mV/s, which is an indication of high-rate capability. The decrease in specific capacitance value compared to SN-700 is owing to the further elevated heating temperature which may reduce the surface area and amount of active sites where charge can be stored **(Kibona., 2019)**.

The CV curves for the SN-900 sample show the maximal current response among the other SN series, representing the high capacitive behavior. The CV curves taken at different scan rates are almost rectangular in shape, indicating that ionic diffusion resisted with electric double layer capacitance as the predominant mechanism. The specific capacitance values are notably greater , ranging from 345 F/g at 10 mV/s to 104 F/g at 50 mV/s assigned to the ideal pore architecture and high conduction for SN -900 **(Mir & Shah 2022)**.

TN 700/TN 800/TN 900

The CV curves for the TN-700 sample demonstrate quasi-rectangular shapes, which are pseudocapacitive behavior. The current response is observe to be increase with scan rate, which represents capacitive materials. The specific capacitance value for 10 mV/s is 214 F/g, 80 F/g for 50 mV/s, owing to the limited ion diffusion with increase in scan rate. This trend implies that high surface area with many active sites for storage of charge to be stored in the material (**Chen *et al*., 2021)**.

The CV profile for TN-800 contains rectangular curves with wide redox peaks, showing the existence of both EDLC and pseudo capacitance. The specific capacitance values obtained are highest for the TN series decreasing from 403F/g at 10mV/s to 247 F/g at 50 mV/s. This suggests outstanding rate capability and high surface area with enough active sites for charge storage **(Pellitero *et al*.,2021)**.

The CV graphs of the TN–900 sample present a rectangular profile implies that there is a predominance of electric double-layer capacitance. Specific capacitance values decrease from 201 F/g at 10 mV/s to 146 F/g at 50 mV/s. The specific capacitance values of TN-900 are lower than the values of TN-800 likely due to a higher graphitization for higher temperatures can improve conductivity but will tend to decrease surface area and the extent of active sites for charge storage **(Alimi *et al*., 2022)**.

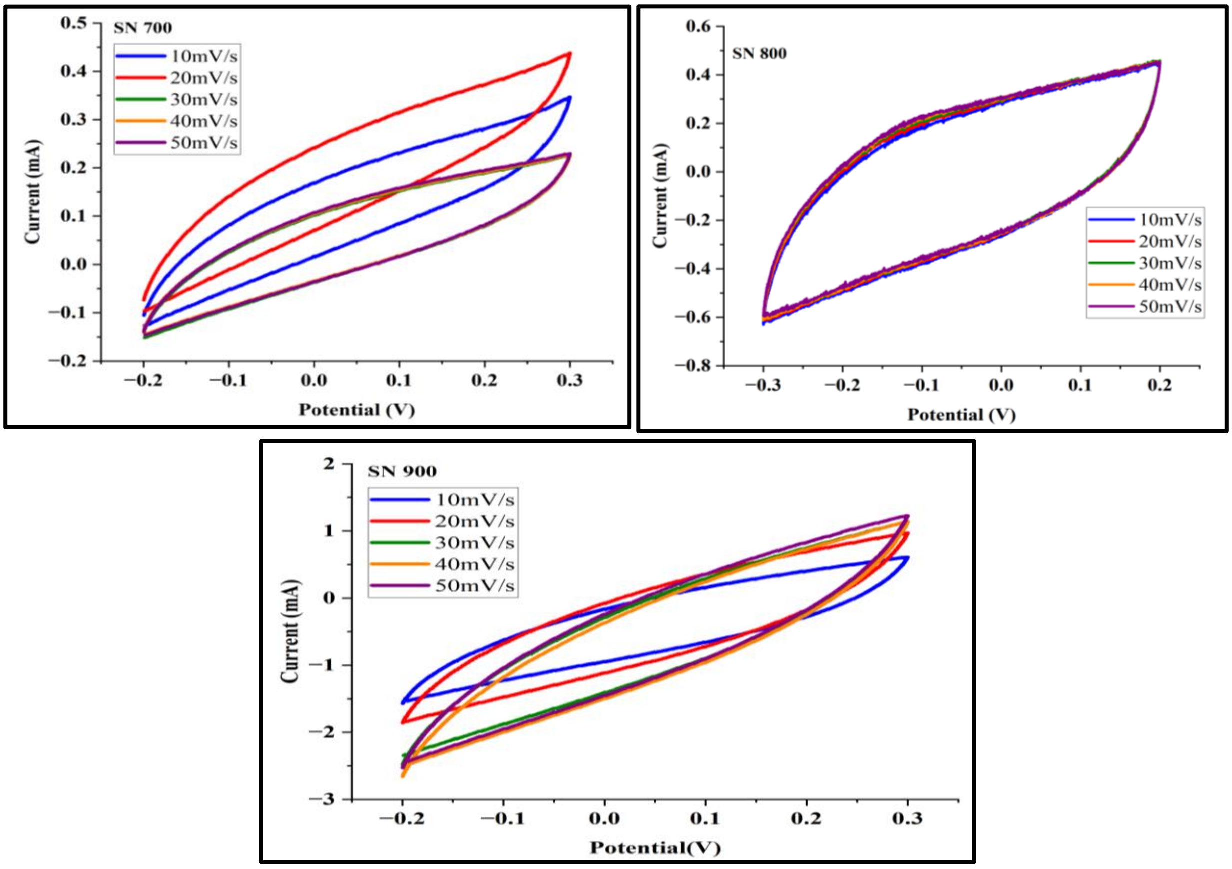

Figure 4.28: Cyclic Voltammetry for SN- 700, SN- 800, SN-900

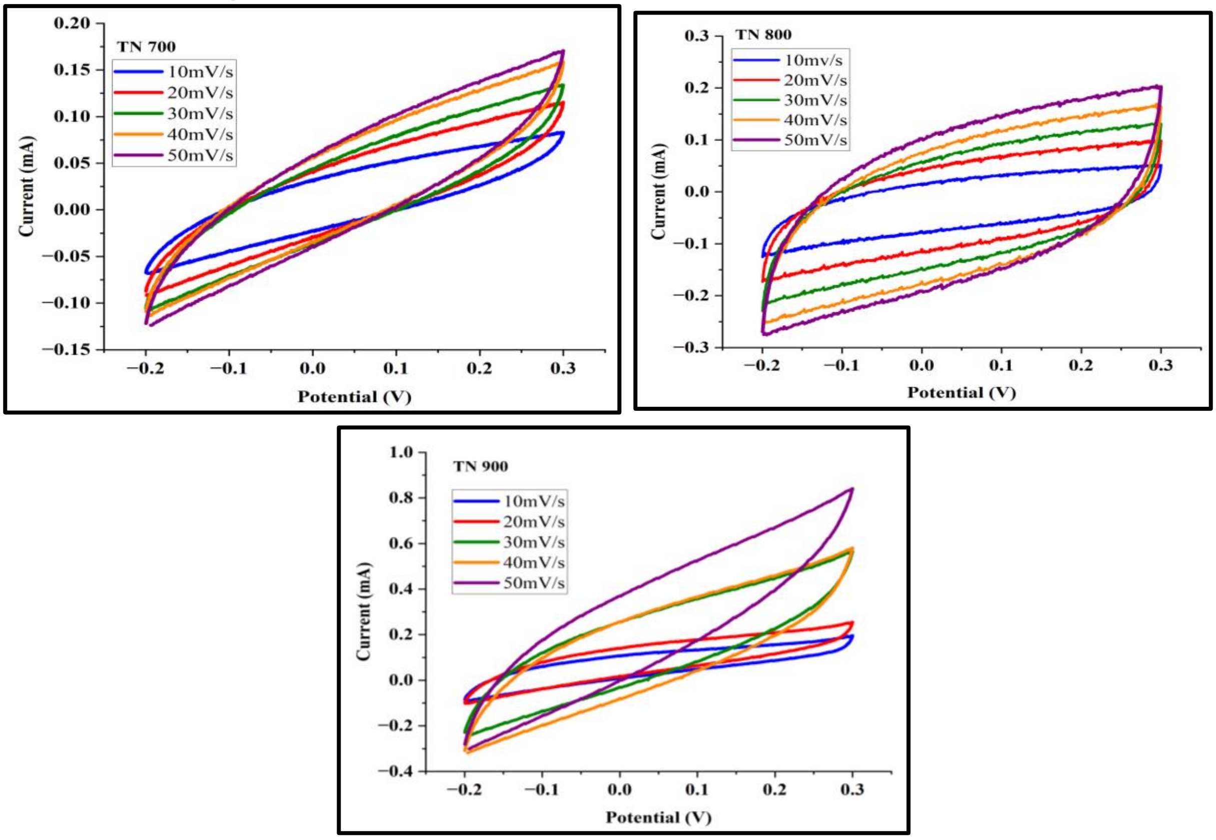

Figure 4.29: Cyclic Voltammetry for TN- 700, TN- 800, TN-900

Discussion

Notably all the CV curves of SPL/TCL/SN/TN except TCL 700 exhibited a symmetric fish- shaped / modified ellipsoid curve- a deviation from the pronounced rectangular shape – due to defects and surface roughness. The overall change of specific capacitance with increase in scan rate is displayed in Figure 4.30 for SPL/TCL/SN/TN (**Tariq *et al*., 2023; Bograchev *et al*., 2023)**

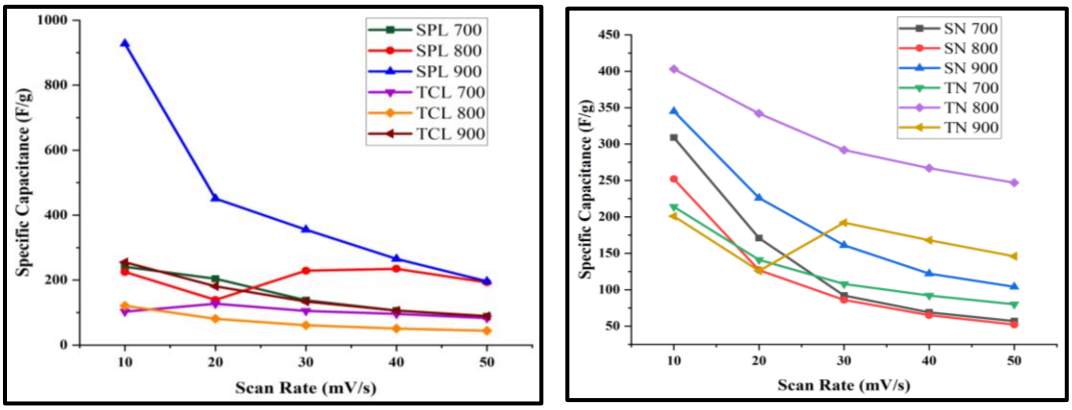

Figure 4.30: Specific Capacitance Vs Scan Rate from Cyclic Voltammetry

Table 4.10: Specific Capacitance obtained from Cyclic Voltammetry

Sample	**Specific Capacitance (F/g) obtained from CV**				
	10mV/s	**20 mV/s**	**30 mV/s**	**40 mV/s**	**50 mV/s**
SPL-700	241	204	138	106	88.3
SPL-800	225	139	229	235	193
SPL-900	**928**	451	355	265	196
TCL-700	103	127	105	96	83
TCL-800	121	81	61	51	44
TCL-900	**255**	181	134	106	89
SN-700	309	171	92	69	57
SN-800	252	127	86	65	52
SN-900	**345**	226	161	122	104
TN-700	214	141	108	92	80
TN-800	**403**	342	292	267	247
TN-900	201	126	192	168	146

4.3.2. Galvanostatic Charge and Discharge Analysis (GCD)

The GCD profile for all the prepared carbon at current densities of 200 µA/g and 250 µA/g are discussed below. The rest of the profile for current densities (75 µA/g, 100 µA/g and 125 µA/g) are presented in Annexure II

4.3.2.1. GCD Profile of SPL/TCL

The GCD profiles of SPL/TCL are displayed in Figure 4.31 &4.32 and Tabulated in Table 4.11

SPL-700/SPL 800/SPL 900

The galvanostatic charge-discharge (GCD) profiles for SPL-700 at current densities of 200 and 250 µA/g disclose the behavior of the material electrochemically. The observed potential vs time curves indicate the charge storage capacity and efficiency of this biomass carbon. At 200 µA/g, SPL-700 displays a specific capacitance of 38.8 F/g that declines to 30.66 F/g when the current density is increased to 250 µA/g. This reduction can be attributed to the increased current density, which reduces the time available for ion diffusion into the porous structure of the carbon material. The IR drop during the preliminary discharge process is indicated on the GCD curves. This drop suggests the internal resistance offered by the electrode materials as well as the internal electrolyte. The presence of IR drop suggests that there are inherent resistive components within the system for performance optimization **(Men *et al.*, 2022).**

For SPL-800, at 200 µA/g and 250 µA/g GCD curves depict higher specific capacitance values than the values for SPL-700. In particular, SPL-800 at 200 µA/g has a specific capacitance of 100 F/g and this value goes up to 125 F/g at 250 µA/g. This appreciable increase indicates that the pore structure of SPL-800 is well developed with a larger surface area, suggests this material holds more charge and ion transport. SPL-800 shows less IR drop, which implies that internal resistance is less. This can arise from better ionic transport, enhanced conduction in the carbon framework and system as a whole this improvement in conductivity promotes the electrochemical performance **(Luo *et al.*, 2017; Iqbal *et al.*, 2022)**.

SPL-900 produced the highest specific capacitances in the SPL series with values of 271.2 F/g and 338.9 F/g at 200 and 250 µA/g respectively. SPL-900 is characterized by GCD profiles that demonstrates excellent charge storage capability and stability performance of this biomass carbon. The more dependence of the capacitance on the current density implies the presence of good porous structure and ion transport. In the case of SPL-900, the IR drop is minimal signifying very good conductivity as well as low internal resistance. This minimal IR drop contributes to the high specific capacitance and general performance of SPL-900 **(Liu *et al.*, 2022; Ganesh *et al.*, 2022)**.

TCL-700/TCL 800/TCL 900

At 200 µA/g and 250 µA/g, the GCD curves for TCL-700 show capacitance values of 34.04 F/g and 17.75 F/g, respectively. The lower capacitance at higher current density suggests limited diffusion of ions and charge storage efficiency. The IR drop in TCL-700 is quite visible and hence higher internal resistance exists with respect to the SPL series. This high resistance could result from a poorly formed pore matrix or a lower degree of electrical conductivity which will affect the general electrochemical activity **(Chandrashekhar & Yadav 2023)**.

As for TCL-800, it has been noted that the specific capacitance values at 200 µA/g and 250 µA/g are 96.8 F/g and 122.25 F/g respectively. It indicates improved charge storage mechanisms and ion transport capabilities. The IR drop in TCL-800 is less than that of TCL-700, which means that the internal resistance is lower, and the conductivity is higher than that in TCL-700. This enhancement in performance says the usefulness of TCL-800 for high-performance energy storage applications **(Chandrashekhar & Yadav 2023)**.

As for TCL-900, at specific current densities of 200 µA/g and 250 µA/g the specific capacitance values are 53.3 F / g and 48.9 F / g respectively. The GCD profiles show modest charge retention and stability. The dependence of capacitance on the current density indicates poor ion diffusion and charge storage incapacity. Internal resistance (IR drop) of TCL-900 is evident which compromises the performance characteristics. Improvement of the pore structure and electrical conductivity of TCL900 could increase the electrochemical properties **(Nivetha *et al.*, 2023).**

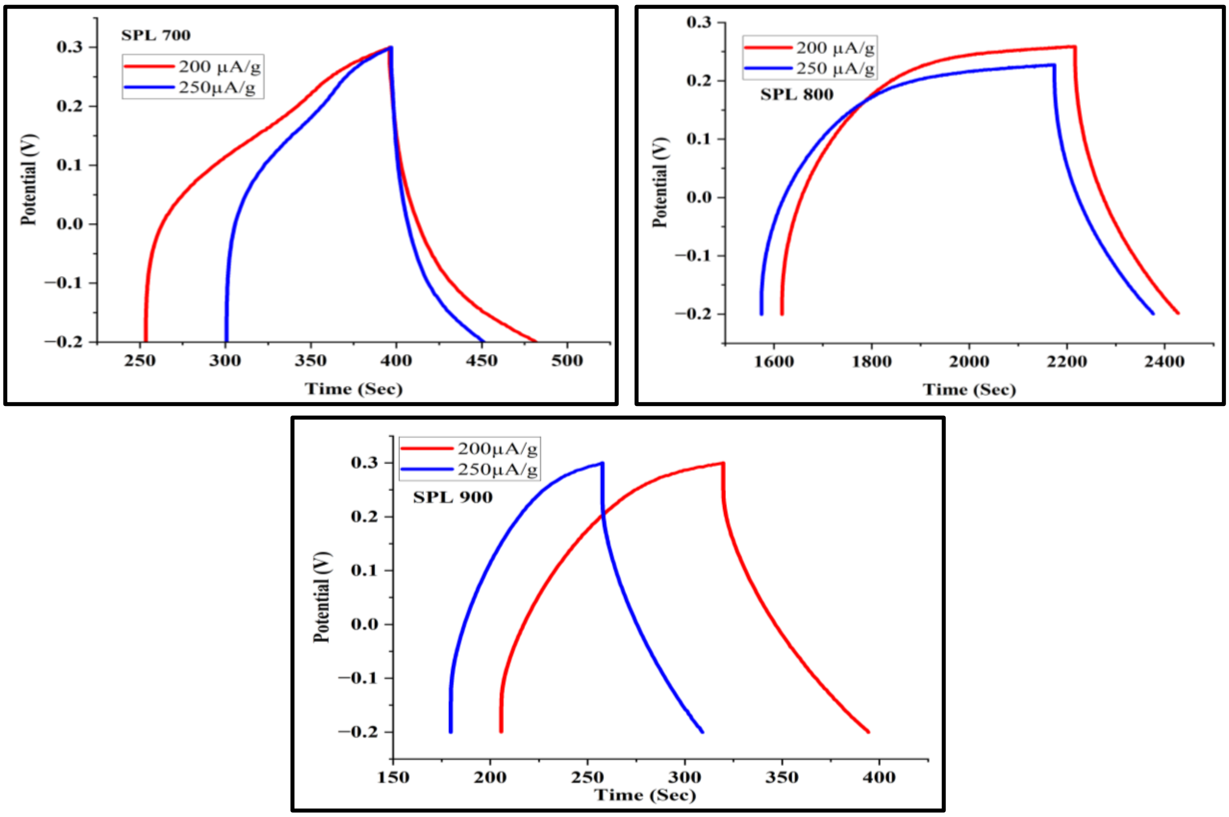

Figure 4.31: GCD Profile for SPL- 700, SPL- 800, SPL-900

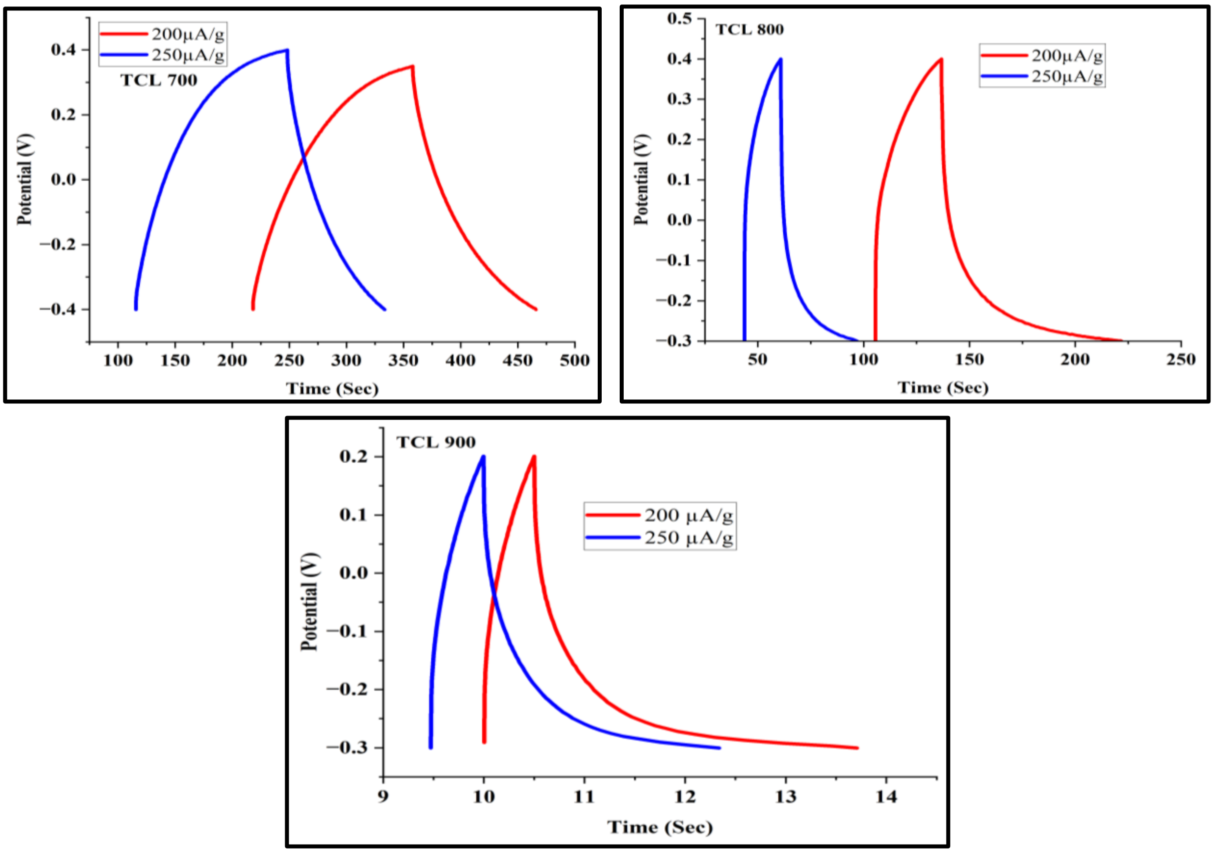

Figure 4.32: GCD Profile for TCL- 700, TCL- 800, TCL-900

4.3.2.2. GCD Profile of SN/TN

The GCD profiles of SN/TN are displayed in Figure 4.33 &4.34 and tabulated in Table 4.11

SN-700/SN-800/SN-900

The galvanostatic charge-discharge (GCD) of SN-700 displays a specific capacitance of 29 F/g at a current density of 200 A/g, which drops to 16.87 F/g at 250 A/g. This decrease in capacitance with increase of current density can further ascribed to the limited ion diffusion in the carbon porous structure due to high current densities. IR drop seen in the GCD curves of SN-700 is substantial indicating high internal resistance in the material. This is owing to the below ideal conductivity and less pore development which limits ion transport and declines charge retention capability **(Ragavan & Pandurangan 2017).**

Regarding the effect of increasing the current density, it is clear that the specific capacitance of SN-800 is considerably higher than that of SN-700, with values of 141 F/g at 200 µA/g and 124 F/g at 250 µA/g respectively. The performance elucidated above also indicates that SN-800 possesses a more elaborated pore structure and higher surface area, which is advantageous in terms of ionic transport and the ability to store charge. Compared to that of SN-700, the IR drop in SN-800 is considerably lower. This increase in current flow improves the electrochemical properties and thus SN-800 can be considered for high storage performance **(Li *et al.*, 2023).**

SN-900 shows highest specific capacitance 383.2 F/g at 200 µA/g to 355 F/g at 250 µA/g amongst the SN series. The GCD profiles measure the standards of efficiency on storage and retention of charge. The sharp increase in capacitance with current density suggests the highly porous formation of SN-900 with effective ion transport. The GCD profiles measure up to the standards of efficiency on storage and retention of charge. The minimal IR drop seen in the GCD for SN-900 depicts that better conductivity and minimal internal resistance, thus attributing to their excellent performance. This low resistance is vital for attaining high specific capacitance for these materials **(Hao *et al.*, 2020)**.

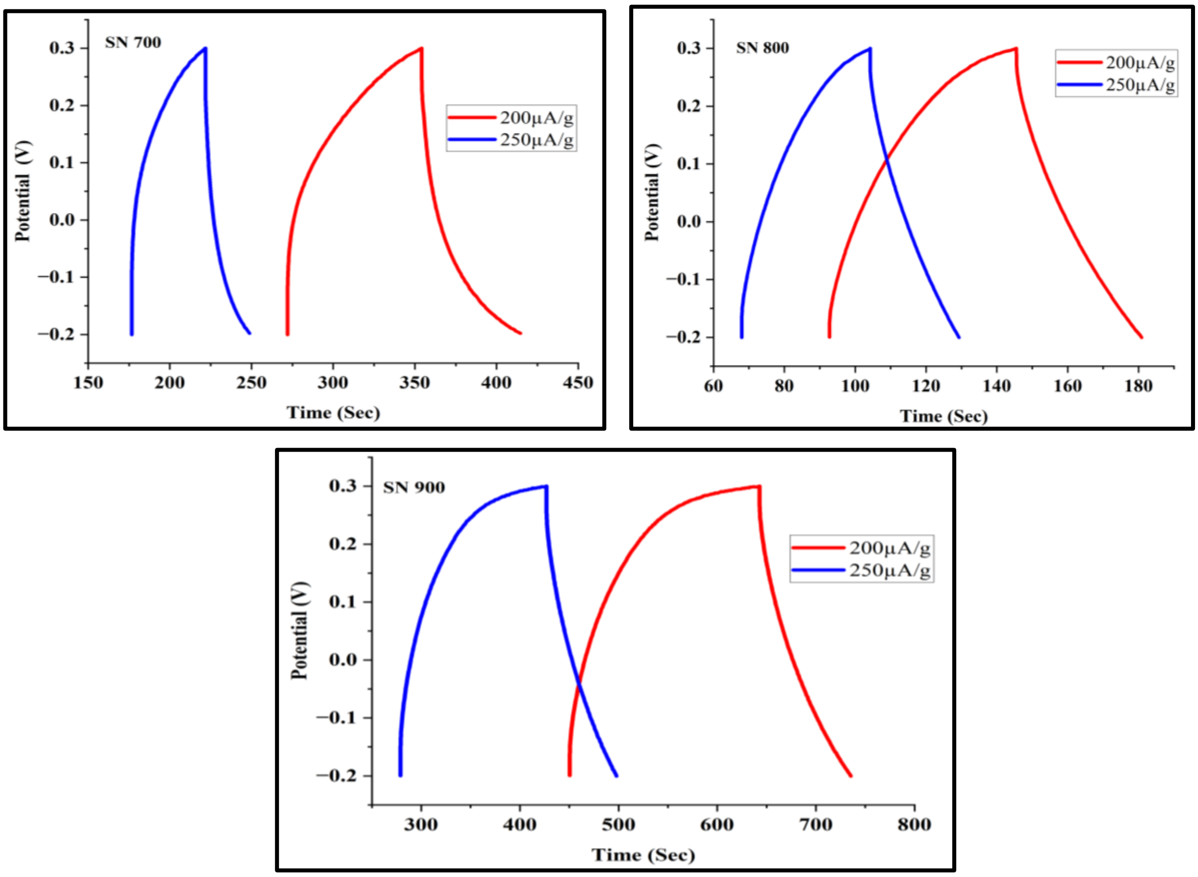

Figure 4.33: GCD Profile for SN- 700, SN- 800, SN-900

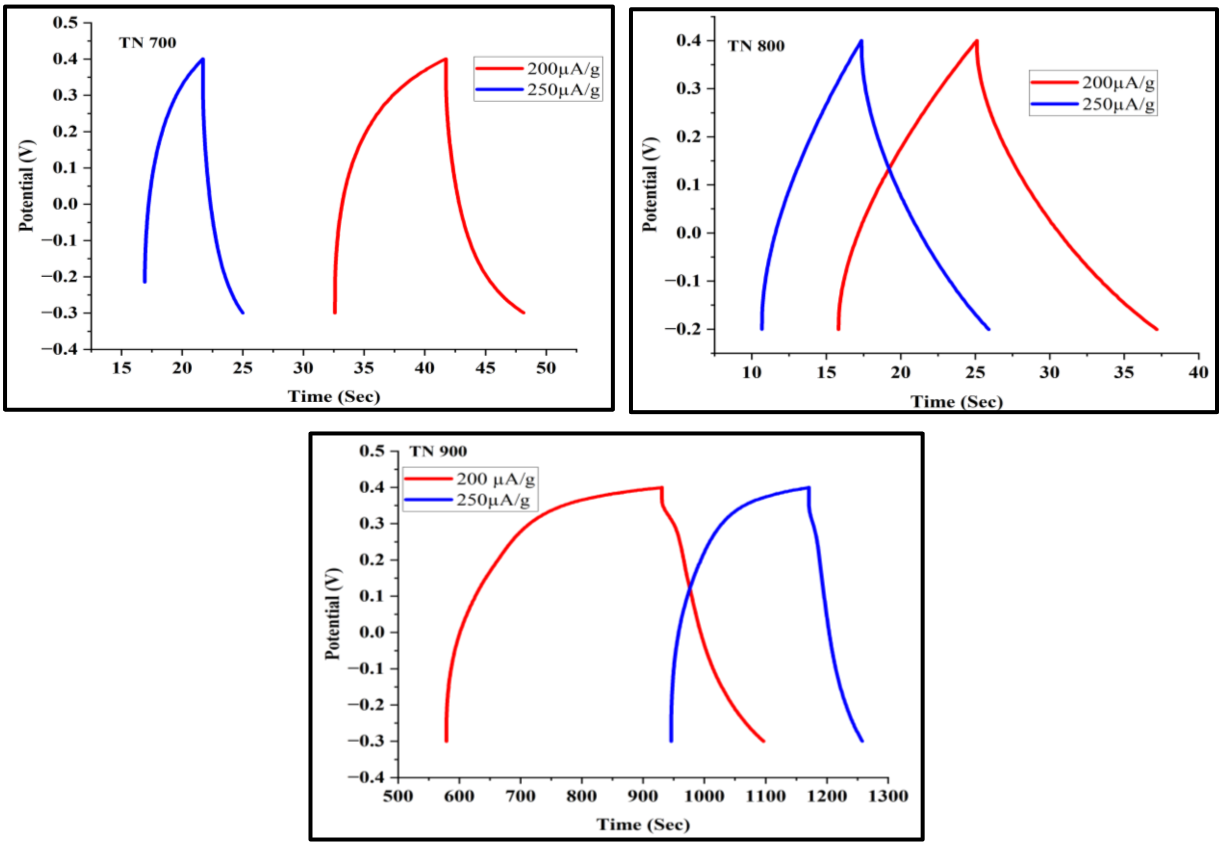

Figure 4.34: GCD Profile for TN- 700, TN- 800, TN-900

TN-700/TN-800/TN-900

The GCD curves for TN-700 at current densities of 200 µA/g and 250 µA/g exhibit values of specific capacitance of 9.84 F/g and 5.96 F/g respectively. The increase in the current density also brings a decrease in the capacitance values which indicates that there will be poor ion diffusion and efficiency in charge storage at high current densities. The obvious IR drop in TN-700 indicates that higher internal resistance, this can be due to poorly developed pore structure or lower conductivity. This higher resistance adversely affects the overall electrochemical performance **(Ali *et al.*, 2021)**.

TN-800 shows improved performance than TN-700, at nearly the same current densities, the specific capacitance value is 59 F/g at 200 µA/g and 52.1 F/g at 250 µA/g. There was notable increase in ion accumulation as well as their transport in TN-800. The IR drop in TN-800 was less prominent with TN-700, signifying low internal resistance and electrical conductivity was higher. This enhancement in performance suggests TN-800 can be utilized for energy storage to operate on a higher energy **(Ragavan & Pandurangan 2017)**.

TN-900 provides high specific capacitance with 257 F/g at 200 µA/g and 171.2 F/g at 250 µA/g. The GCD curves suggest moderate levels of charge storage capacity and performance reliability. The deficiency of ion diffusion and charge storage effectiveness as evidenced that capacitance decreases with increasing current density. IR drop value in TN-900 is quite significant, suggesting internal resistance that has effects on efficiency. Enhancing pore structure and electrical conductivity of TN-900 could improve its electrochemical characteristics **(Thirumal *et al.*, 2024)**.

Discussion

Comparison of GCD results of biomass-derived carbons SPL series and TCL series shows significant differences in specific capacitance and internal resistance. Generally, SPL-900 provides the highest capacitance and least IR drop suggesting improved performance. At the same time, TCL-700 and TCL-900 show high internal resistance and lower capacitance, and in order to enhance their performance. All these findings emphasize the influence of material structure and conductivity on the performance of energy storage systems.

The GCD analysis of the nitrogen-doped biomass-derived carbons (SN and TN series) highlights the relative change in specific capacitance and internal resistance. As for SN-materials, SN-900 is the most efficient due to high capacitance values, small IR drop. TN-900 shows high capacitance (Figure:4.35). In general, these results emphasize the critical nature of material architecture and conductivity in delivering high energy storage systems.

The GCD profiles for all the prepared carbon samples exhibited pseudo capacitance dominant curves as noticed in CV results. **(Sheng *et al*., 2021) (Okhay *et al*., 2021)**

Table 4.11: Specific capacitance obtained for prepared carbon materials from GCD

Sample	**Specific Capacitance (F/g) obtained from GCD**				
	75µA/g	**100µA/g**	**125µA/g**	**200µA/g**	**250µA/g**
SPL-700	16.0	20.64	25.33	38.8	30.66
SPL-800	37.2	50.2	62.5	100	125
SPL-900	101.4	133.7	168.7	271.2	**338.9**
TCL-700	21.6	28.46	32.42	34.04	17.75
TCL-800	36.37	45.55	64.5	96.8	**122.25**
TCL-900	13.3	18.5	22.5	53.3	48.9
SN-700	111.75	150.25	96.87	29	16.87
SN-800	157.2	202.6	182.25	141	124
SN-900	381.75	416	**450**	383.2	355
TN-700	110.1	46.8	34.13	9.84	5.96
TN-800	165.5	103.7	86.2	59	52.1
TN-900	352	**470**	302	257	171.2

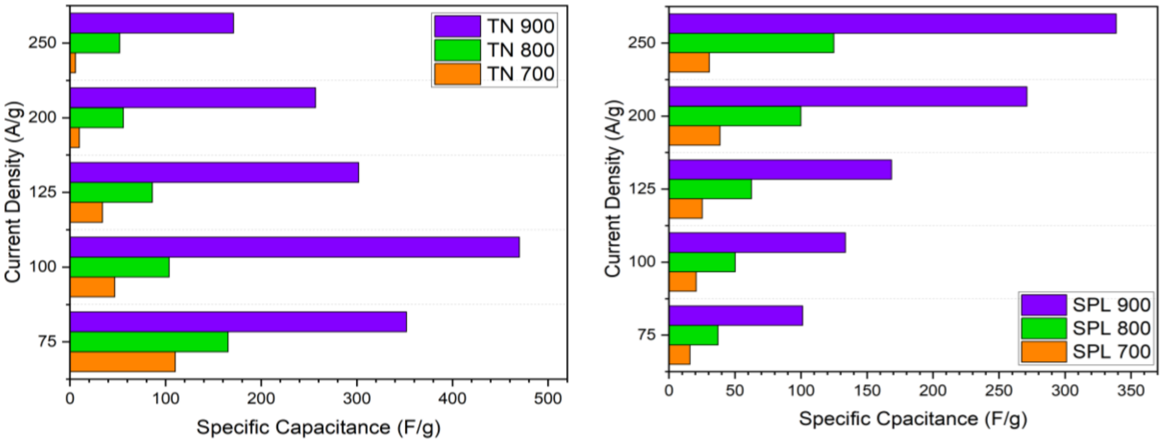

Figure 4.35: Specific capacitance Profile for Synthesised carbon materials

4.3.3. Electrochemical Impedance Spectroscopy

4.3.3.1. EIS Analysis of SPL/TCL

The EIS spectrum of SPL/TCL are depicted in Figure 4.36 & 4.37 and the results are tabulated in Table 4.12

SPL-700

In SPL-700, Nyquist plot indicates the high value of real part of impedance (Zr) and imaginary part (Zi), indicating significant charge transfer resistances and higher Warburg impedance, owing to diffusion limitations. The values of Rs (9.4 Ω) and Rct (33.2 Ω) show that the material has average amounts of electronic and ionic conduction characteristics. The moderate value of charge transfer resistance suggests that the electrochemical process taking place at the interface of the electrode and the electrolyte is quite favorable. The higher impedance is likely to be due to poor carbonization of the material at 700ºC, since this results in lower graphitic and higher non-graphitic content which will contain functional groups that obstruct electron transport **(Akter *et al.*, 2023)**.

SPL-800

On the contrary, better electrochemical performance can be inferred from the SPL-800 with a reduced imaginary part of reactance as compared to SPL-700. Comparing SPL-800 with SPL-700, the latter type of SPL-800 increases both Rs (23.1 Ω) and Rct (43.6 Ω) resistance greater. This may be due to some functional groups exerting an enhancing effect on overall conductivity while giving rise to a moderate resistance. The difference in impedance compared to SPL-700 can be ascribed to restructuring carbon atoms to a more ordered graphite structure but with some remaining defects, which add to the impedance **(Bhujel *et al*., 2019)**

SPL 900

SPL-900 possesses the minimum imaginary impedance and as a result the electrochemical properties are improved. The Rs (47.8Ω) and a much lower Rct (22Ω) shows improved charge transfer capabilities. The lower impedance values are caused by high pyrolysis temperature, which enhances the extent of graphitization and reduces the portion of amorphous carbon leading to high electronic conductivity and low charge transfer resistance **(Souza 2013)**.

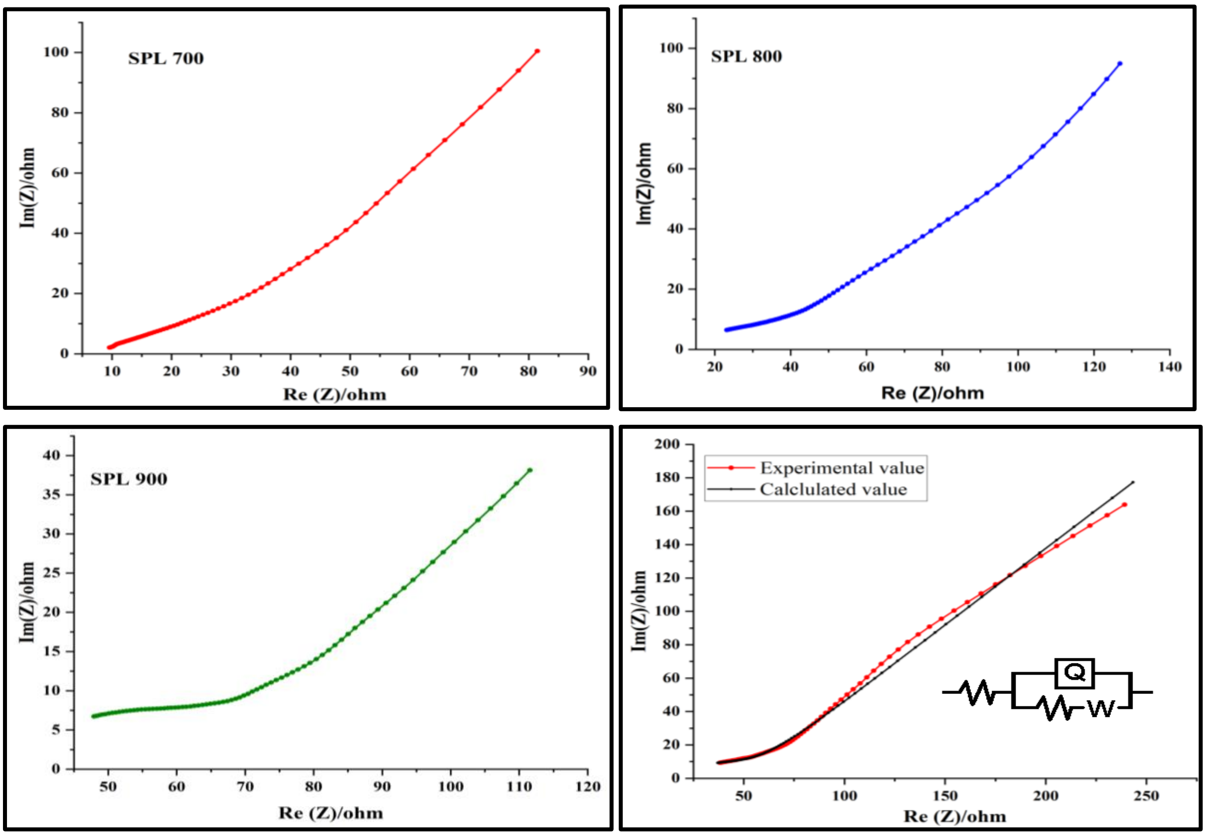

Figure 4.36: EIS spectra for SPL- 700, SPL- 800, SPL-900

TCL-700

The Nyquist plot for TCL-700 has a fair amount of impedance in both the real and imaginary components. Considering Rs (14.2 Ω) and Rct (15.5 Ω), the material can be considered as low in charge transfer resistance, which is a sign of good electrochemical performance. The moderate impedance implies that, at 700°C, the carbon structure retains some surface functional groups which allow for the transfer of electrons without compromising the carbon structure integrity **(Akter *et al.*, 2023)**.

TCL-800

TCL-800, on the other hand, has a higher value of impedance, especially in the real part. In comparison to TCL-700, the Rs (6.6Ω) and Rct (27.8Ω) values demonstrate a reduction in electronic resistance but an escalation in charge transfer resistance. The reason for the increase in charge transfer resistance is probably because there is partial graphitization caused by the removal of some functional groups which normally should be there to assist the ion transfer but enhance electronic conductivity **(Bhujel *et al.*, 2019)**.

TCL-900

Among the TCL samples, TCL-900 has the highest impedance with respect to all other samples and shows higher when real and imaginary components of the impedance are taken into account. There is also a dramatic increase of the two Rs (108.7 Ω) and Rct (72.3Ω) which are considered to be high and hence imply low electrochemical activity. The high impedance is perhaps attributed to extensive graphitization at 900°C, where this condition would improve electronic conductivity and, at the same time, decrease the number of active sites furnished by ion transfer functional groups **(Souza 2013)**.

4.3.3.2. EIS Analysis of SN/TN

The EIS spectrum of SN/TN are depicted in Figure 4.38 & 4.39 and the results are tabulated in Table 4.12

SN-700

The Nyquist plot for SN-700 shows Zr/ Zi values which are primarily real and imaginary impedance respectively. The Rs (54.2 Ω) and Rct (88.9 Ω) shows that there is a lot of resistance and charge transfer resistance. The reason for these high impedance values is likely due to the fact that carbonization has not been completed and nitrogen doping is low at 700°C leading to a structure with little conductive paths and high resistance to electron transfer **(Akter *et al.*, 2023)**.

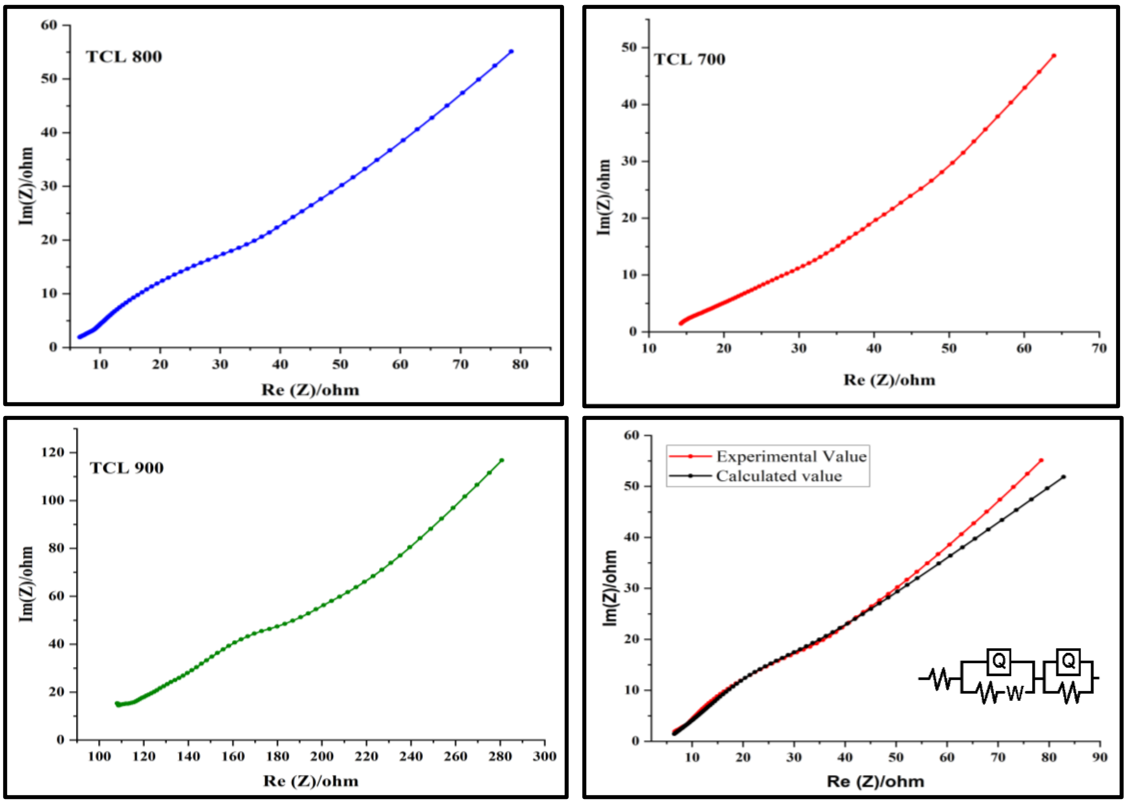

Figure 4.37: EIS spectra for TCL- 700, TCL- 800, TCL-900

SN-800

SN-800 demonstrates the minimum electrical impedance compared to SN-700 because of improved electrochemical properties of the sample carbon structure. The Rs (13.1 Ω) and Rct (16.5 Ω) on the other hand are extremely low hence reinforcing the electronic-ionic conductivity. The enhancement of performance is linked to better carbonization and nitrogen doping at 800°C, which enhances the conduction band and reduction of charge transfer resistance **(Bhujel *et al*., 2019)**.

SN-900

The Nyquist plot for SN-900 shows a little increase in impedance over that of SN-800 but lesser than that of SN-700. The Rs (31.7 Ω) and Rct (19 Ω) are acceptable for resistance and charge transfer capabilities. This increase in impedance at 900°C thermal treatment was mostly ascribed to excessive graphitization, which decreases the amount of active sites for nitrogen incorporation and hence increases the resistance rather slightly while good electrochemical properties are still achieved **(Akter *et al.*, 2023)**.

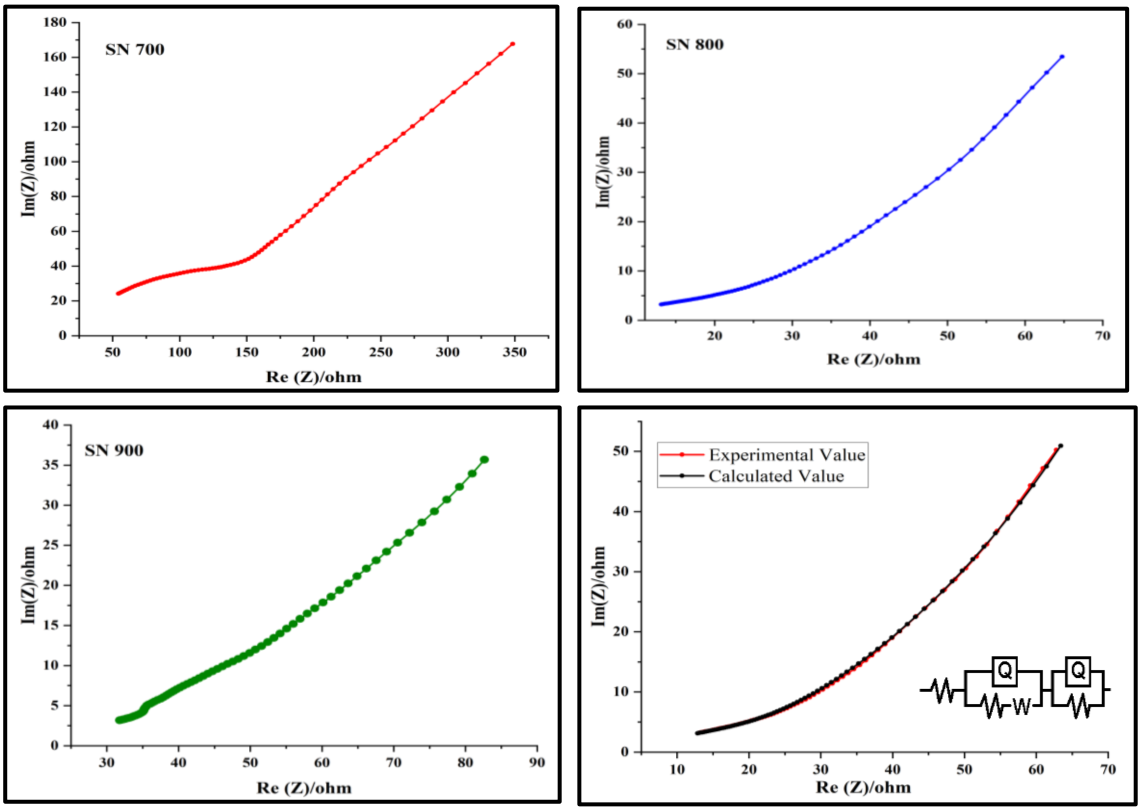

Figure 4.38: EIS spectra for SN- 700, SN- 800, SN-900

TN-700

Among all the analyzed samples, TN-700 demonstrates the largest values of impedance, as well as the lowest real and imaginary parts. The Rs (0.07 kΩ) and Rct (0.23 kΩ) infer excellent ionic and electronic conductivity. The exceptionally high impedance at 700 °C can be due to poor nitrogen incorporation into the material which decreases the overall utilized conductivity and electrochemical efficacy of the material **(Akter *et al.*, 2023)**.

TN-800

In comparison to TN-700, TN-800 recorded higher impedance values thus decrease in the electrochemical performance. Rs (20.2 Ω) and Rct (45.7 Ω) values are comparatively higher implying more the resistance. The increase in impedance at 800°C can be due to over-carbonization, which might lead to a decrease in the number of nitrogen active sites and, consequently, higher resistance **(Akter *et al.*, 2023)**.

TN-900

The Nyquist plot for TN-900 shows impedance values higher than TN-700 but lower than TN-800. The Rs (40.3 Ω) and Rct (29.9 Ω) indicate moderate resistance and charge transfer capabilities. The moderate impedance at 900°C could be due to optimal graphitization and nitrogen doping, which balance the material's conductive network and active sites for electrochemical reactions **(Souza 2013)**.

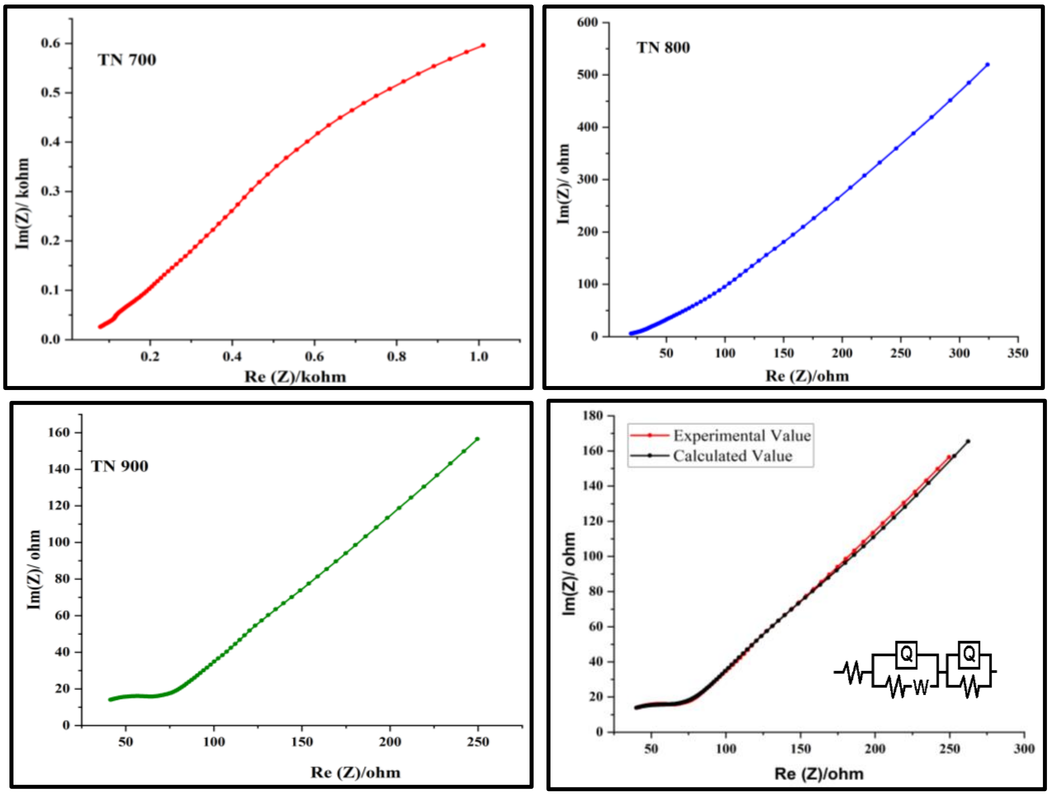

Figure 4.39: EIS spectra for TN -700, TN-800, TN-900

Discussion

The impedance spectra of SPL and TCL samples illustrate the impact of pyrolysis temperature on the electrochemical properties of biomass-derived carbons. Higher temperatures generally enhance graphitization, reducing charge transfer resistance but can lead to increased overall resistance due to the loss of functional groups necessary for ion transfer. The balance between graphitization and functional group retention is critical for optimizing the electrochemical performance of biomass-derived carbon materials.

Table 4.12: Rs &Rct values obtained for prepared carbon materials

Sample	Rs (Ω)	Rct(Ω)	R1	R2	CPE	Warburg
SPL-700	9.4	33.2	13.69	51.2	0.01079	0.1241
SPL-800	23.1	43.6	0.001253	48.89	0.0138	0.2219
SPL-900	47.8	22	18.19	75.04	0.01365	0.467
TCL-700	14.2	15.5	0.0433	0.5941	0.03029	1.81
TCL-800	6.6	27.8	0.6909	21.99	0.862	0.5194
TCL-900	108.7	72.3	0.04573	144	0.07572	0.211
SN-700	54.2	88.9	0.034	212.1	0.006846	0.114
SN-800	13.1	16.5	2.016	0.01	0.06319	0.003071
SN-900	31.7	19	0.01	49.4	0.00076	0.5209
TN-700	0.07k	0.23k	0.05107	7.762	16.18	2.341
TN-800	20.2	45.7	1.876	2.08	0.275	1.246
TN-900	40.3	29.9	15.19	63.65	0.0087	0.1685

4.4. Energy Density and Power Density

The Ragone plot compares the power (P) versus energy (E) density for different electrode materials SPL/TCL/SN/TN, as depicted in Figure 4.40, 4.41 and tabulated in Table 4.13 &4.14. As the current density (c.d) increases, it is observed that the energy density decreases while the power density increases. This phenomenon can be attributed to the accessibility of pores within the electrode material to the electrolyte. At higher current densities, only a limited portion of the surface pores is accessible to the electrolyte. This limited accessibility results in a quick discharge, leading to a decrease in energy density but an increase in power density. Conversely, at lower current densities, all pores near the surfaces become accessible to the electrolyte, allowing for a slower discharge and thus higher energy density but lower power density.

SPL 900 displays a high energy density of 11.06 Wh/kg at 780.7 W/kg, TCL-900 shows high energy density of 1.29 Wh/kg at 2588 W/kg, SN-900 reveals high energy density of 12.32 Wh/kg at 624.6 W/kg, TN-900 based electrode material exhibits a high energy density of 11.06 Wh/kg at 482 W/kg, in 1M H_2SO_4, which is significant for supercapacitor applications. These results suggest that the prepared electrode materials, particularly TN-900, exhibit promising energy and power density characteristics, making them suitable for applications in supercapacitors. Comparison of energy density with reported biomass-based functional carbon materials indicate the comparable performance of the carbon materials prepared in the current study and signify their potential in energy storage applications (Figure:4.42).

Table 4.13: Energy Density obtained from prepared carbon materials

Material	Energy density (Wh/kg)				
	250µA/g	200 µA/g	125 µA/g	100 µA/g	75 µA/g
SPL 700	0.55	0.71	0.87	1.34	1.06
SPL 800	3.58	4.19	4.52	4.16	4.93
SPL 900	4.74	6.51	7.81	12.84	11.06
TCL 700	0.75	0.98	1.12	1.18	0.61
TCL 800	1.26	1.58	2.23	3.36	4.2
TCL 900	0.46	0.64	0.78	1.85	1.69
SN 700	0.58	1.00	3.36	5.21	3.88
SN 800	4.3	4.91	6.32	7.03	5.4
SN 900	12.32	13.30	15.62	14.4	13.2
TN 700	0.40	0.66	2.32	3.18	7.48
TN 800	3.54	4.01	5.86	7.05	11.26
TN 900	11.05	17.49	20.55	31.98	23.95

Table 4.14: Power Density obtained from prepared carbon materials

Material	Power density (W/kg)				
	250µA/g	200 µA/g	125 µA/g	100 µA/g	75 µA/g
SPL 700	20.9	28.08	35.32	56.5	70.65
SPL 800	25.62	34.20	42.70	68.38	85.32
SPL 900	230.59	312.48	390.5	624.6	780.7
TCL 700	18.52	24.78	31.22	49.95	62.46
TCL 800	467.6	624	777	1249	1546
TCL 900	773	1037	1300	2081	2588
SN 700	77.33	62.06	39.01	31.2	23.43
SN 800	624.19	499.32	312	249.83	185.49
SN 900	624.6	499.7	312.4	249.2	186.7
TN 700	464.5	371.2	235.2	187.9	140.9
TN 800	1528	1223	764.6	611.4	459
TN 900	482	385	240.9	192.8	144.4

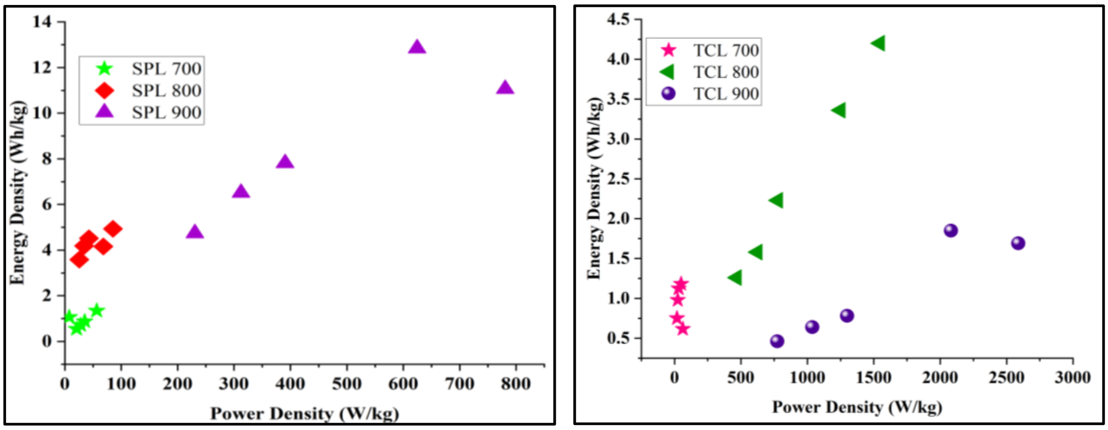

Figure 4.40: Ragone plot for SPL- 700, SPL- 800, SPL-900, TCL -700, TCL-800, TCL-900

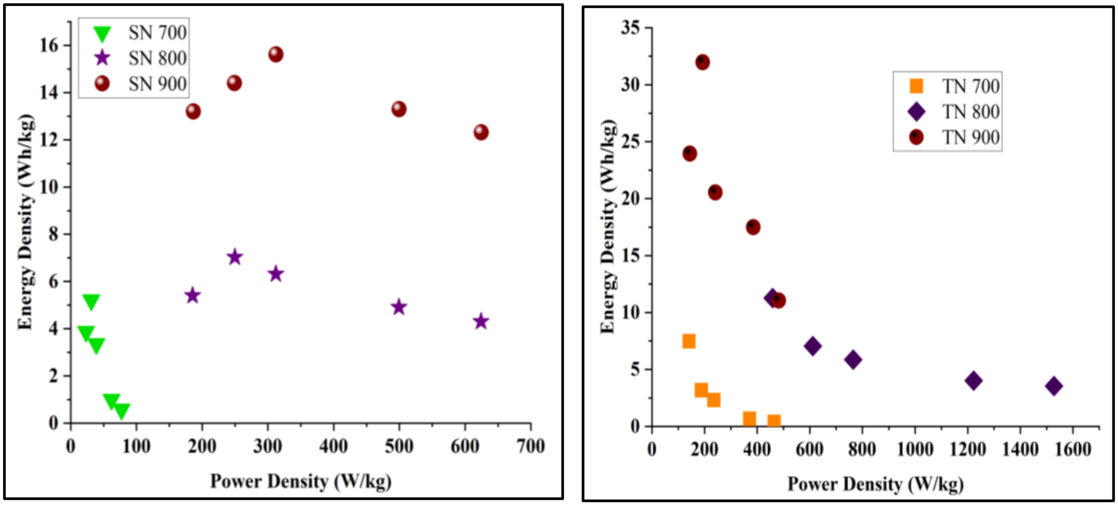

Figure 4.41: Ragone plot for SN- 700, SN- 800, SN-900, TN -700, TN-800, TN-900

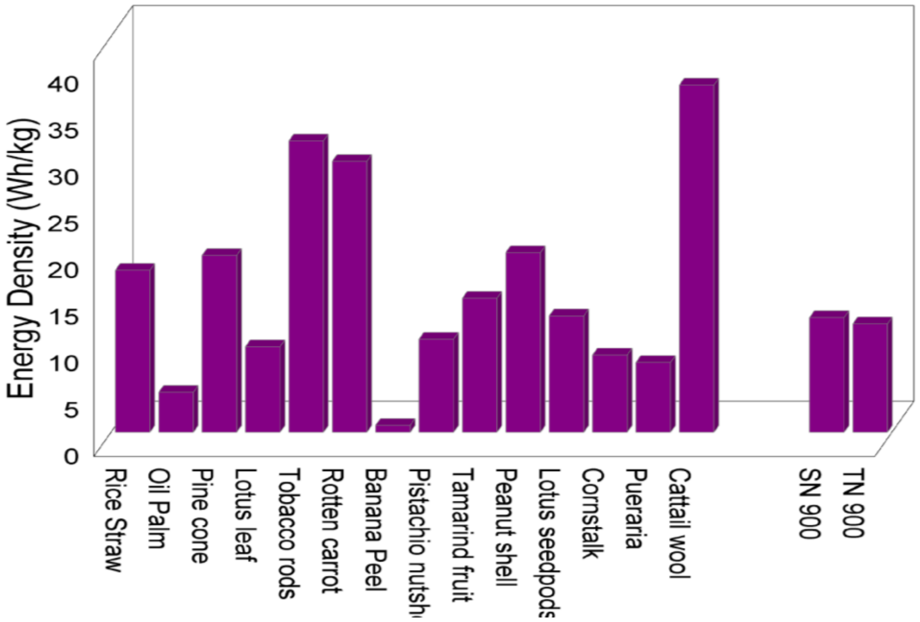

Figure 4.42: Comparison of Energy density reported in literature with SN and TN carbon materials

4.5. Cycle Stability Analysis

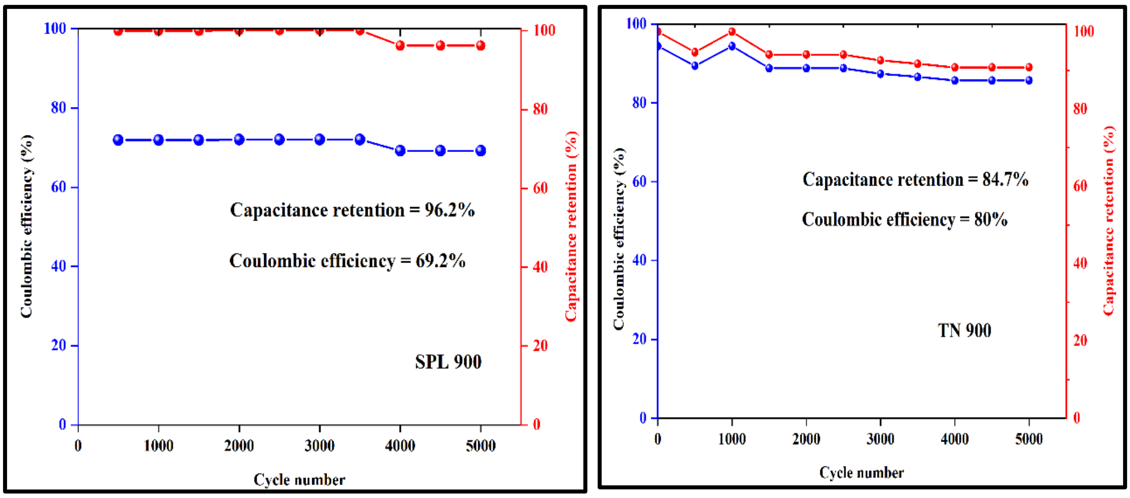

Figure 4.43: Cyclic stability of SPL-900, TN- 900

Cyclic stability is a critical parameter for evaluating the long-term performance and practical applicability of supercapacitor electrodes. The cycling performance of SPL-900 and TN-900 electrodes, as presented in Figure 4.43, was assessed over 5000 continuous charge–discharge cycles. The SPL-900 electrode demonstrated excellent stability, retaining 96.2% of its initial capacitance, while the TN-900 electrode maintained 84.7%. These results indicate that both materials exhibit outstanding electrochemical durability, confirming their potential candidates for high-performance supercapacitor applications.

Table 4.15: Comparing biocarbon materials documented in literature Vs present work

Source	**Electrolyte**	**Capacitance F/g**	**Electrochemical measurements**	**References**
Petroleum pitch	6 M KOH	20	GCD	**Wang *et al.*, 2018**
Carbon nanotubes	6M KOH	29	CV	**Aria *et al.*, 2012**
Graphene based supercapacitors	Ionic liquids	20	CV	**Bondavalli *et al.*, 2018**
Fluid coke derived activated carbon	Aqueous KOH	10-20	CV	**Hu *et al.*, 2008**
Marabu wood	1M TEABF$_4$	20	GCD	**Farm *et al.*, 2020**
Oil palm empty fruit ACM10s ACM30s ACM50s ACM70s	1M H$_2$SO$_4$	 23.024 17.556 8.472 1.866 2.780	CV	**Awitdrus *et al.*, 2015**

Camellia oleifera residue	2M H_2SO_4	367	CV	**Bo. X *et al.*, 2019**
(waste) cumin plant HCl washed cumin plant HF washed cumin plant	1M H_2SO_4	117 127 155	GCD	**Inal. I. I. G *et al.*, 2018**
Sakura flower	6 M KOH	265.8	GCD	**Ma, F *et al.*, 2019**
Coconut shell	6 M KOH	141	GCD	**Divyashree, A *et al.*, 2016**
Rice husk	6 M KOH	176	GCD	**Wu, M *et al.*, 2015**
Commercially available AC (M15B)	Aqueous KOH	249	GCD	**Shi,1996**
SACF25	Aqueous KOH	207	GCD	**Shi, 1996**
SPL 900	1M H_2SO_4	338	GCD	**This work**
TCL 800	1M H_2SO_4	122	GCD	**This work**
SN 900	1M H_2SO_4	450	GCD	**This work**
TN 900	1M H_2SO_4	470	GCD	**This work**

Commercially available activated carbon materials (AC) are used as the electrodes for charge storage supercapacitor systems. Researchers have carried out the electrochemical studies by incorporating the commercially available AC materials. These AC carbon furnishes the specific capacitance which are comparable with the biomass precursors SPL/TCL.

Table 4.16 presents a comprehensive summary of the characterization of all synthesized carbon materials. From the analysis of the SPL, TCL, SN, and TN series (comprising 12 electrodes), it was observed that the samples SPL 900, TCL 800, SN 900, and TN 900 exhibited the highest capacitance values as measured by galvanostatic charge-discharge (GCD) tests. These electrochemical results were further corroborated by extensive physicochemical and morphological studies. The CV and GCD performances of the electrode are well in agreement with each other, although the calculated specific capacitances differ due to the different measurement procedures **(Pattanayak *et al.*, 2022).** Notably, within the TCL series, the performance of TCL 800 deviated from the general trend. This discrepancy may be attributed to the presence of potassium trace elements, as revealed by EDAX analysis, or potential inconsistencies in the synthesis of active materials, which could have compromised the quality of the fabricated electrode.

Table 4.16: Major results from different characterization of the present work

Characterisation	SPL 700	SPL 800	SPL 900	TCL 700	TCL 800	TCL 900	SN 700	SN 800	SN 900	TN 700	TN 800	TN 900
XRD	Amorphous	Amorphous	Amorphous	Crystalline	Crystalline	Crystalline	Amorphous	Amorphous	Amorphous	Amorphous	Amorphous	Amorphous
FTIR	O-H stretching, N-O Stretching, N-H bending, C=C bending	O-H stretching, N-O Stretching, N-H bending C=C bending	O-H stretching, N-O Stretching, N-H bending C=C bending	O-H stretching, N-O Stretching, N-H bending C=C bending	O-H stretching, N-O Stretching, N-H bending C=C bending	O-H stretching, N-O Stretching, N-H bending C=C bending	O-H bond, N-O bond, C=C bending	O-H bond, N-O bond, C=C bending	O-H bond, N-O bond, C=C bending	O-H bond, N-O bond, C=C bending	O-H bond, N-O bond, C=C bending	O-H bond, N-O bond, C=C bending
Raman (I_D/I_G)	1.00	1.01	1.03	0.98	1.02	1.02	1.00	1.01	1.05	0.98	1.02	1.02
EDAX	C, N, O, Ca, K	C, N, O, Ca, K	C, N, O, Ca, K	C, N, O, Ca, K	C, N, O, Ca, K	C, N, O, Ca, K	C, N, O, Ca, K	C, N, O, Ca, K	C, N, O, Ca, K	C, N, O, Ca, K	C, N, O, Ca, K	C, N, O, Ca, K
FESEM	interconnected pores	uniform pore structure	uniform pore structure	interconnected pores	well-developed hierarchical porous network	well-developed hierarchical porous network	well-defined pores	more uniform and slightly larger	well-developed porous network	interconnected macropores	more ordered and intricate pore structure	highly developed and intricate pore network
CV	EDLC and pseudo capacitance	EDLC	pseudo capacitance	pseudo capacitance	EDLC and pseudo capacitance	EDLC	pseudocapacitive	EDLC and pseudo capacitance	EDLC	pseudocapacitive	EDLC and pseudo capacitance	EDLC
GCD (Csp)	38.8	125	338.9	34.04	122.25	53.3	150.25	202.6	450	110.1	165.5	470